

## Physical Models for the Early Evolution of Cell Membranes

The Harvard community has made this article openly available.  
[Please share](#) how this access benefits you. Your story matters.

<b>Citation</b>	No citation.
<b>Accessed</b>	February 19, 2015 10:42:38 AM EST
<b>Citable Link</b>	<a href="http://nrs.harvard.edu/urn-3:HUL.InstRepos:9904006">http://nrs.harvard.edu/urn-3:HUL.InstRepos:9904006</a>
<b>Terms of Use</b>	This article was downloaded from Harvard University's DASH repository, and is made available under the terms and conditions applicable to Other Posted Material, as set forth at <a href="http://nrs.harvard.edu/urn-3:HUL.InstRepos:dash.current.terms-of-use#LAA">http://nrs.harvard.edu/urn-3:HUL.InstRepos:dash.current.terms-of-use#LAA</a>

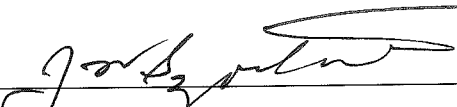
*(Article begins on next page)*

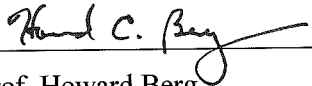
HARVARD UNIVERSITY  
Graduate School of Arts and Sciences

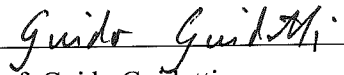


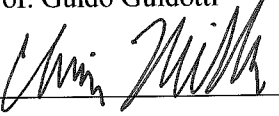
DISSERTATION ACCEPTANCE CERTIFICATE

The undersigned, appointed by the  
Department of Molecular and Cellular Biology  
have examined a dissertation entitled  
"Physical models for the early evolution of cell membranes"  
presented by Itay Budin,  
candidate for the degree of Doctor of Philosophy and hereby  
certify that it is worthy of acceptance.

Signature   
Typed name: Prof. Jack Szostak

Signature   
Typed name: Prof. Howard Berg

Signature   
Typed name: Prof. Guido Guidotti

Signature   
Typed name: Prof. Chris Miller, Brandeis University

Date: May 17, 2012

# **Physical models for the early evolution of cell membranes**

A dissertation presented

by

Itay Budin

to

The Department of Molecular and Cellular Biology

in partial fulfillment of the requirements

for the degree of

Doctor of Philosophy

in the subject of

Biochemistry

Harvard University

Cambridge, Massachusetts

May 2012

© 2012 – Itay Budin

All rights reserved.



Advisor  
Professor Jack W. Szostak

Author  
Itay Budin

## **Physical models for the early evolution of cell membranes**

Cells use lipid membranes to organize and define their chemical environments. All cell membranes are based on a common structure: bilayers composed of phospholipids with two hydrocarbon chains. How did biology converge on this particular solution for cellular encapsulation? The first cell membranes are proposed to have assembled from simple, single-chain lipids, such as fatty acids and their derivatives, which would have been available in the prebiotic environment. Here we argue that the physical properties of fatty acid membranes would have made them well suited for a role as primitive cell membranes and predisposed their evolution to modern, phospholipid-based membranes.

We first considered models for primitive membrane self-assembly, which faces significant concentration barriers due to the entropic cost of aggregation and the solubility of single-chain lipids. We therefore identified two physical mechanisms by which fatty acid membrane assembly can proceed from dilute solutions. Thermal diffusion columns, a proposed prebiotic concentration method, drive the formation of fatty acid vesicles by concentrating an initially isotropic solution past the critical concentration necessary for aggregation. Alternatively, mixtures of fatty acids with varying chain lengths, the expected products of abiotic lipid synthesis, intrinsically reduce the concentration barrier to aggregation through their polydispersity. These results motivated us to better understand the phase behavior of fatty acids in solutions. We found that the composition of fatty acid aggregates, whether vesicles or micelles, is also determined by concentration. Fatty acid vesicles feature significant amounts of coexisting

micelles, whose abundance is enriched in low concentration solutions. We utilized this micelle-vesicle equilibrium to drive the growth of pre-existing fatty acid vesicles by changing amphiphile concentration.

We next considered the evolution of phospholipid membranes, which was a critical and necessary step for the early evolution of cells. We found that the incorporation of even small amounts of phospholipids drives the growth of fatty acid vesicles by competition for monomers with neighboring vesicles lacking phospholipids. This competitive growth would have provided a strong selective advantage for primitive cells to evolve the catalytic machinery needed to synthesize phospholipids from their single-chain precursors. Growth is caused by any relative difference in phospholipid content, suggesting an evolutionary arms race among primitive cells for increasingly phospholipid membranes. What would have been the consequences for early cells of such a transition in membrane composition? We found that increasing phospholipid content inhibits the permeability of fatty acid membranes through changes in bilayer fluidity. For early heterotrophic cells, the emergence of increasingly phospholipid membranes would have therefore imposed new selective pressures for the evolution of membrane transport machinery and metabolism.

Our model for early membrane evolution led us to develop prebiotic models for phospholipid chemistry. The assembly of phospholipids from single-chain substrates requires a single reaction: the acyltransfer of an activated fatty acid onto a glycerol monoester or lysophospholipid. We developed a synthetic model for this reaction that incorporates a copper-catalyzed azide-alkyne cycloaddition and showed that it drives de novo vesicle assembly.

# Contents

Preface	vi
Chapter 1.	
Introduction: Models for cell membranes, their origin, and their early evolution	1-45
1.1 Models and approaches for studying the origin of life	1
1.2 Physical and dynamic properties of lipid membranes	7
1.3 Models for the origin of cell membranes	14
1.4 Fatty acid membrane dynamics	23
1.5 Models for the function of early cell membranes	25
1.6 Models for the early evolution of cell membranes	31
1.7 Implications for early cellular evolution	35
1.8 Overview	36
1.9 References	37
Chapter 2.	
Formation of protocell-like vesicles in a thermal diffusion column	46-68
Chapter 3.	
Heterogeneity in fatty acid chain-length drives membrane assembly	67-87
Chapter 4.	
Multi-phase coexistence allows for the concentration-driven growth of protocell membranes	88-115
Appendix: Structural kinetics of the fatty acid micelle to vesicle transition	116-120
Chapter 5.	
Physical effects underlying the adoption of phospholipid membranes by early cells	121-153
Chapter 6.	
Membrane assembly driven by a biomimetic coupling reaction	154-168

## **Preface**

Much like the assembly of molecules, a scientist's body of work is rarely accomplished individually. My advisor, Jack Szostak, has provided me with equal amounts of intellectual stimulation and freedom, a potent recipe for a young scientist. To say that my time in his lab has been an enjoyable one is an understatement of the highest order. This is in no small part due to my fortune in working with fantastic lab mates. I would especially like to acknowledge Raphael Bruckner, who mentored me early on and whose excitement for science has always been especially infectious. Simon Trevino, Sylvia Tobé, Alonso Ricardo, Noam Prwyes, Doug Treco, Na Zhang, and Craig Blain similarly provided constant help and diversions, both in and out of lab. My committee members, Howard Berg, Howard Stone, and Guido Guidotti, have contributed great advice and even better stories. I have also benefited tremendously through collaborating directly with Anik Debnath, who spent a fruitful summer working with me, and Neal Devaraj. My companions outside the lab, especially Brett Goshe, Chris Rogacz, and Andrew Olive, have provided critical encouragement and entertainment. Most importantly, this work would not have been possible without an amazing family, especially my wonderfully supportive parents, Dan and Alina, and my remarkable sister, Meytal.

## **Chapter 1: Introduction**

### **Models for cell membranes, their origin, and their early evolution**

**Abstract:** The origin of life required a complex interplay between molecular and environmental phenomena in order to allow for the self-assembly and replication of the first cells. Because compartmentalization is a prerequisite for Darwinian evolution, membranes were likely an essential component of the earliest cells. Modern cell membranes are based on phospholipid bilayers, whose structural and dynamic properties I review. In contrast, the first cell membranes could have self-assembled from simple, single-chain lipids that were available in the prebiotic environment. Laboratory models for primitive cell membranes have demonstrated how their intrinsic physical and chemical properties allow for essential functions of early cells, including growth, division, and solute transport. While these processes support a role for single-chain lipids as primitive membrane components, the adoption of phospholipid membranes would have been a critical step in the early evolution of life and must have preceded the emergence of cellular complexity. I therefore discuss models for the origins of biological membranes and the basis for their early evolution.

### **Models and approaches for studying the origin of cells**

In his various musings, Darwin spent fittingly little effort trying to explain life's beginnings. While Darwin recognized that biology is an evolutionary phenomenon, its origin was an event

harkening back to antiquated notions of spontaneous generation. Nevertheless, in the 150 years since *The Origin of Species*<sup>1</sup>, the topic of the origin and early evolution of life has fascinated both scientists and the general public alike. It has become an increasingly broad field, with topics ranging from interstellar chemistry to the population dynamics of evolving systems. Central to these efforts remains the question of how life could have first arisen and evolved on the early earth. At its most basic, this problem is a historical one: reconstructing events that are truly ancient, even on cosmological timescales, and dramatically altered the planet on which they occurred. However, it is also a fundamental question on the conditions necessary for the emergence of evolution in molecular systems. How does chemistry transition into biology?

Geology and paleontology of the early earth have provided broad constraints on the timeline for early life. Hospitable conditions for life are thought to have arisen as recently as ~ 3.8 billion years ago (Ga), before which constant heavy projectile bombardment would have made life unlikely [1]. Meanwhile, the earliest microfossils date to 4 Ga [2] and debated isotopic evidence goes even further [3]. Even this date is restricted by the lack of older sedimentary rocks and it is possible that the origin of life significantly preceded it. The 'end point' for biology's early evolution can be deduced from phylogenetics, which shows a universal common ancestry for machinery involved replication, transcription/translation, protein secretion, glycolysis/respiration, membrane synthesis, and membrane transport [4]. Though the divergence of the archaeal and bacterial lineages of life is thought to have occurred very early, the last common ancestor had clearly already evolved complexity characteristic of a modern cell.

---

<sup>1</sup> Full title: *On the Origin of Species by Means of Natural Selection, or the Preservation of Favoured Races in the Struggle for Life*

Beyond these general parameters, direct evidence on the origin and early history of life is very limited. The lack of evidence has led to an experimental (or synthetic) approach to the problem in which the laboratory synthesis and function of biological components defines plausible pathways for similar processes on the early earth. This approach was begun by the pioneering work of Stanley Miller on amino acid synthesis under electrical discharge [5], which launched the field of prebiotic chemistry. A great deal of progress has been made defining the pool of available molecules on the early earth using two synthetic approaches: (1) experimental simulations (e.g. the Miller experiment) where the basic chemical inputs and local environment are defined, but the possible products are unknown and (2) rational synthesis, where a desired product of prebiotic interest (e.g. a mononucleotide) is defined but the conditions and reactions to obtain it are sought out. Using these approaches, plausible prebiotic mechanisms for the synthesis of carbohydrates [6], amino acids [7], lipids [8-10], and mononucleotides [11] have been reported and explored. A third, non-synthetic approach is the identification of organic compounds in extra-terrestrial bodies, such as carbonaceous chondrite meteorites [12], or in circumstellar and interstellar clouds [13, 14] with the presumption that such molecules could have also been readily available during the earth's formation. Advances in spectroscopic arrays will make these studies increasingly informative in the future [15].

Of course, biology is not simply a pooled mixture of its constituent chemicals, but rather exists as highly organized structures whose functions are coordinated for the exceedingly complex task of replication. Understanding how chemical building blocks (nucleotides, amino acids, lipids, metabolic intermediates etc.) can spontaneously organize and function as primitive biological

systems remains fundamentally unknown. At this point, it is useful to have a working definition for what constitutes a biological system, which I define<sup>2</sup> here as a physiochemical system capable of replication and Darwinian evolution. Extant biology provides a more specific model: it is universally cellular, with a nucleic acid (DNA) genome encoding for protein and RNA machinery that carries out catalysis needed for cellular replication. At its simplest, evolution occurs through of random mutations that occur during genome copying. These mutations correspond to selectable variations in functional polymers (e.g. proteins) that carry out tasks involved in propagation. While non-cellular models of early life have been proposed, the emergence of the first cell-like structures was certainly a very early transition in the origin of life.

Modern cells have become exceptionally efficient at both replication and adaptation. They are also remarkably complex; estimates on the minimal number of genes (encoding proteins and RNA) to sustain replication and protein synthesis *in vitro* range from 150 and up [16]. Transposon-based deletion screens on *Mycoplasma genitalium*, an especially simple bacterium<sup>3</sup>, indicate a minimum of ~380 genes for complete cellular division in a rich media [17]. This complexity is problematic because the overriding physical constraint for the origin of life is one of self-assembly; the spontaneous organization of chemical species into larger organized structures faces large kinetic and entropic barriers. The other constraint is one of historical continuity: given long time scales, primitive cells, by definition, had to be capable of evolving

---

<sup>2</sup> This mimics the definition of life used by NASA, which originated from Gerald Joyce.

<sup>3</sup> This obligate parasite takes in many essential building blocks from its environment and has thus dispensed of the machinery needed to synthesize them. As we will see below, this could have been a reasonable cellular strategy for primitive cells.



the biochemical complexity that defines modern cells. Although it is certainly possible, even likely, that biological systems bearing no biochemical resemblance to modern cells once existed, the lack of plausible pathways for them to evolve into extant systems would relegate them as evolutionary dead ends.

A spontaneous origin of cellular life thus requires cellular systems simple enough to self-assemble but be complex enough to replicate and evolve into the biology that followed. This paradox presents an obvious set of questions: What components are absolutely necessary for a primitive cell to replicate? Are there prebiotically plausible routes for the assembly of these components? And how do these primitive components evolve into the ubiquitous features of extant cells? These questions can be addressed synthetically by efforts to generate primitive cellular system, or protocells, in the laboratory [18]. The goals of this approach are to experimentally test proposed models for primitive cells and identify potential mechanisms for their assembly, function, and evolution. It also aids prebiotic chemistry by identifying potentially useful chemical components whose abiotic synthesis can then be further explored.

The central challenge of building a protocell is identifying minimal chemical components that can result in self-replication. This problem was first contemplated in regards to the universal redundancy of informational polymers in modern cells: genetic polymers (nucleic acids), which are responsible for heredity, are dependent on a separate class of functional polymers (proteins) for their replication and most other cellular functions. The RNA world hypothesis [19] proposes that nucleic acids, specifically RNA, served as both the primary genetic and functional polymer during an early stage of life, thus simplifying this redundancy. The concept gained experimental

credence with the discovery of extant RNA enzymes (ribozymes) [20, 21] and, later, with the structural confirmation that RNA composes the active site for ribosomal peptidyl-transferase [22]. Using in vitro selection techniques, in which libraries of random sequences undergo rounds of selection and amplification, a myriad of synthetic ribozymes have been discovered [23]. These often originated from completely random sequence space [24], indicating the potential for complex RNA catalysis arising spontaneously from abiotically-generated RNA. A remaining, and significant, experimental hurdle is the demonstration of RNA self-replication, unaided by coded proteins. However, there has been significant progress on this front, both through the in vitro selection of RNA-dependent RNA polymerase ribozymes [25-27] and through chemical systems that allow for non-enzymatic RNA copying [28-30].

The ability of nucleic acids to act as both a genetic and catalytic polymer has often led to proclamations that the problem of the origin of life was essentially one of the origin of RNA [31]. This is overly simplistic, since a collection of replicating nucleic acids is not sufficient to act as a primitive biological system, no matter how catalytically proficient. The problem is one of compartmentalization: for natural selection to take hold, genotype (e.g. nucleic acid polymer) and phenotype (e.g. chemical microenvironments generated by catalysis) must be physically linked [18]. Free in solution, prebiotic ribozymes would have performed catalysis indiscriminately on highly diffusive substrates, preventing any specific benefits to themselves. A separation between self and other thus constitutes a strict prerequisite for evolution, and therefore biology [32] (Figure 1). The first serious publications on the origin of life proposed the role of emulsion droplets to perform this essential task [33]. While a variety of such diffusive barriers

could have initially served as compartments, all cells use lipid membranes to compartmentalize and organize themselves.

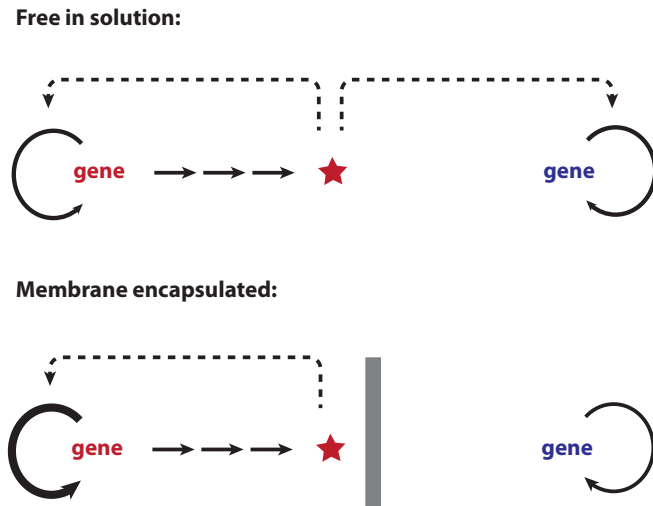


**Figure 1:** Natural selection requires a physical link between replicating genes (e.g. DNA, RNA) and the products they code for (e.g. proteins, functional RNA, metabolites). Free in solution, advantageous products (red star) assist replication of all genes indiscriminately, thus preventing any selective advantage for the genes that code for them. Once membrane encapsulated, products increase replication fitness of their respective genes, thus allowing for a selective advantage over other genes in the solution (blue).

## Physical and dynamic properties of lipid membranes

The fundamental structure of cell membranes was contested for much of the 20<sup>th</sup> century, until high-resolution electron micrographs [34] and X-ray diffraction data [35] provided convincing evidence for a bilayer model [36]. Bilayers are two-molecular thick sheets (each sheet referred to as a leaflet) of lipids with a oily inner region [37, 38]. This model was based on pioneering work in the early 20<sup>th</sup> century by Irving Langmuir on the orientation of lipids in surface monolayers [39]. Bilayers are liquid crystals<sup>4</sup> that assemble due to the energetic cost of exposing non-polar molecules (such as hydrocarbons) to polar molecules (such as water), and vice versa. This

<sup>4</sup> Bilayers can be classified as smectic mesophases: liquid crystals that exist as layers with translational order in one direction.

phenomena, termed the hydrophobic effect [40], is similarly responsible for a range of physical phenomena. Lipid molecules contain one or multiple hydrocarbons moieties (referred to as ‘chains’ or ‘tails’), as well as a polar ‘head’ group whose exposure to non-polar environments is disfavored. This amphiphilicity drives the aggregation of lipids into structures that minimize the exposure of their non-polar tails to water and polar head groups to the tails of other lipids (Figure 2). The structure of the aggregate resulting assemblies depends on temperature, hydration level, and the lipids’ molecular geometries, with cellular lipids generally favoring a bilayer arrangement in dilute solutions [41].

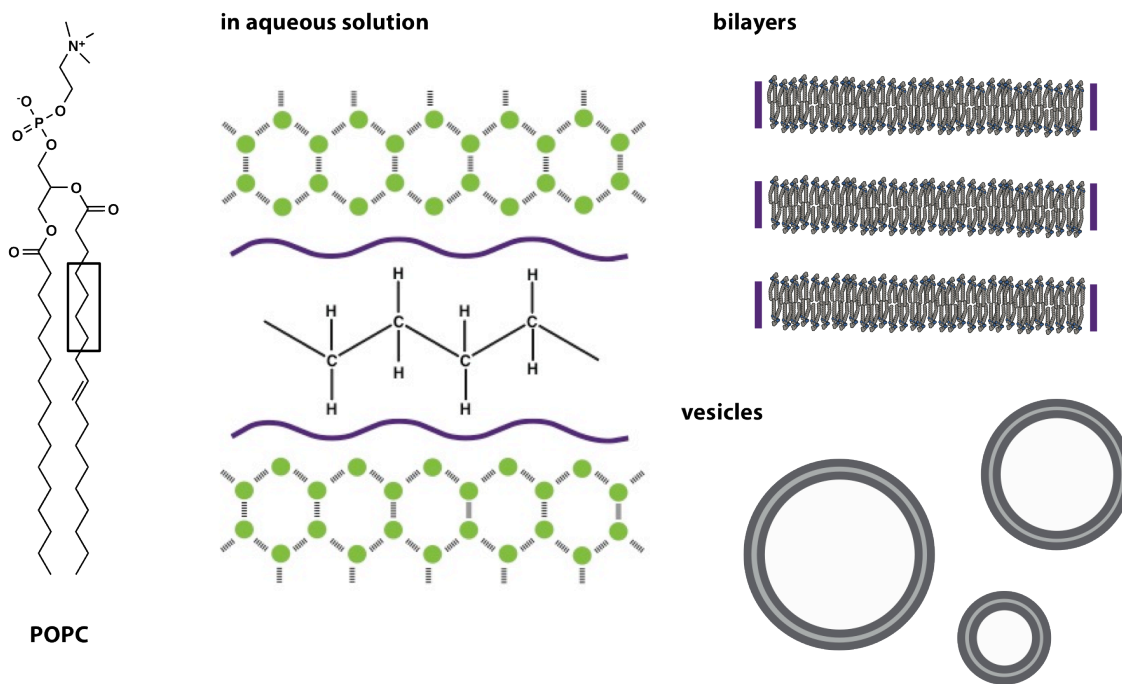


**Figure 2:** Lipid membrane self-assembly. Lipids (e.g. POPC, a phospholipid) feature non-polar hydrocarbon chains. In aqueous solutions, these hydrocarbons (box) drive aggregation through their disruption of water’s (green) inter-molecular hydrogen-bonding network. Aggregation can occur as planar bilayers, which fold up into spherical vesicles to avoid exposure of hydrocarbons at the edges.

The ability of lipid membranes to act as cellular compartments results from their bilayer structure, which effectively allows a thin (~ 3-4 nm) layer of hydrocarbons to be suspended in solution. Because of the polar nature of most biochemical building blocks, the bilayer can effectively separate distinct chemical microenvironments. Ernest Overton and Hans Meyer were the first to observe that the permeability of molecules into cells was predicted by their solubility in non-polar solvents<sup>5</sup> [42, 43]. An expression for passive<sup>6</sup> flux of a solute across a membrane is thus known as Overton's rule and can be obtained from an adaptation of Fick's law for diffusion:

$$J = P_M \Delta c \quad (1)$$

$$P_M = \frac{K_P D_M}{h} \quad (2)$$

Where  $J$  is the flux across the membrane,  $P_M$  is the characteristic permeability coefficient (generally expressed in units of cm/s),  $\Delta c$  is the difference in solute concentration across the membrane,  $h$  is the membrane thickness,  $D_M$  is the solute's diffusion coefficient across the membrane, and  $K_P$  is the hydrocarbon to water partition coefficient of the solute. This simple expression of membrane permeability is empirical, with partition coefficients generally measured in model systems, such as *n*-octanol to water, that mimic the partition into the membrane. Nonetheless, it has proven remarkably resilient, with very few examples of molecules whose

---

<sup>5</sup> These findings were the first evidence that membranes were composed of lipids, with Overton (correctly) surmising that cholesterol and phospholipid were membrane components.

<sup>6</sup> Passive refers to the absence of any protein transporters or pump and generally means permeation by diffusion through the membrane.

passive permeation do not obey the relationship [44]. Because  $K_P$  is very small<sup>7</sup> for almost all biomolecules, lipid membranes pose formidable permeability barriers, allowing cells to control transport through membrane protein transporters.

As has often been true of molecular biology, the chemical composition of many cellular lipids preceded any knowledge of their structural role. Theodore Gobley first characterized the structure of phospholipids when he observed that lipid extracts from egg yolk yielded glycerophosphoric acid and fatty acids upon hydrolysis. Phospholipids are the ubiquitous building block of biological membranes and feature a common basic structure: two hydrocarbons chains of variable length and unsaturation that are linked to a glycerol-phosphate, onto which a variety of functional groups are esterified (Figure 3). From an evolutionary perspective, phospholipids can be classified into two classes. Diacyl phospholipids are found in all bacteria and eukaryotes, and feature fatty acid chains esterified onto the 1 and 2 positions of *sn*-glycerol 3-phosphate. In contrast, archaeal (dialkyl) phospholipids feature isoprenoid chains that are attached via ether linkages to the 2 and 3 positions of *sn*-glycerol 1-phosphate. These two lipid classes were found in the last common ancestors of bacteria/eukaryotes, and of archaea, respectively, and thus define the two most fundamental lineages of biology<sup>8</sup>. Importantly, archaeal and bacterial phospholipids share a common set of head group moieties (choline, ethanolamine, glycerol, and serine, all esterified to phosphate), strongly suggesting that their last

---

<sup>7</sup> Examples of octanol to water partition values: tryptophan  $7 \times 10^{-2}$ , glycine  $1 \times 10^{-3}$ , sucrose  $2 \times 10^{-4}$ , arginine  $8 \times 10^{-5}$ ; values for nucleic acids and most metabolites are too small to be measured experimentally.

<sup>8</sup> The opposing chirality of glycerol-phosphate in archaeal versus bacterial phospholipid synthesis pathways would have provided a mechanism for their parallel function in an early cell. This was a likely requirement for the emergence of the novel pathway, whichever it was.

common ancestor did indeed have phospholipids. Cells, especially eukaryotes, have also evolved a diverse variety of other lipid types, such as sterols and sphingolipids, but the presence of phospholipids as a major membrane component is universal<sup>9,10</sup>.

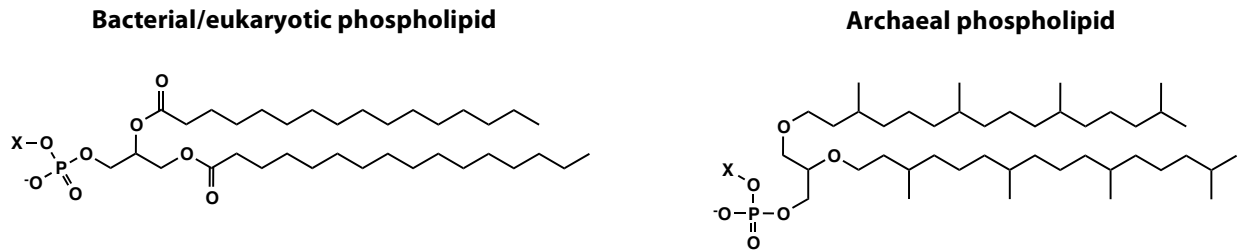


**Figure 3:** Phospholipid structure. Bacteria and eukaryotes synthesize diacyl phospholipids, while archaea feature dialkyl ether phospholipids. X represents a variable head group moiety.

Paramount to the function of cell membranes is the underlying basis of the hydrophobic effect. The disaffinity of lipids for water is not mediated through lipid-lipid attractions, but rather by the strong hydrogen-bonding network of liquid water and other polar solvents<sup>11</sup>. Non-polar (hydrophobic) molecules disrupt this network, resulting in a large energetic cost for their solubilization (Figure 2). Under biological temperatures, water molecules form ordered, solvation shells around non-polar surfaces to maintain maximum hydrogen bonding, which is

---

<sup>9</sup> An interesting exception to this is marine cyanobacteria that have evolved sulfolipids to adapt to phosphate-poor environments (reference 47).

<sup>10</sup> In addition, cell membranes are densely packed with proteins, e.g. 23% of membrane area in reference 48. Membranes are effectively very valuable real estate for cells.

<sup>11</sup> An excellent example in reference 49: the solvent formamide, which allows for 3 hydrogen bonds per molecule, has been shown to support the formation of phospholipid vesicles, but dimethyl formamide, which is incapable of hydrogen bonding due to methyl substitutions, does not. Methyl formamide, with limited hydrogen bonding, allows for vesicles at only a narrow concentration range.

entropically costly for the system. At higher temperatures, when entropy dominates free energy, these solvation shells no longer form, but there is an enthalpic penalty for the reduced number of hydrogen bonds [50]. Because of the switch in its thermodynamic basis, the hydrophobic effect remains largely constant throughout a wide temperature range [51]<sup>12</sup>, which renders membranes effective organizing structures in the wide variety of thermal environments that can sustain life<sup>13</sup>.

Because membranes do not depend on strong inter-lipid adhesions for structural integrity, they can exist as rather dynamic assemblies, with Brownian motion of the component molecules in the plane of the membrane. The influential fluid mosaic model describes cell membranes as supporting fluid motion in two dimensions, with membrane proteins freely diffusing in a fluid of lipids [52]. In a classic set of experiments using spin-labeled phospholipids, Harden McConnell and colleagues confirmed the fluidity of membranes and the rapid diffusion of lipids within them [52, 53]. The translational diffusion of lipids and proteins is a hallmark of biological membranes and has a fundamental role in cellular metabolism and signaling, among other processes<sup>14</sup>. What physical parameters influence membrane diffusivity? Saffman and Delbrück provided a hydrodynamic solution to the diffusion of membrane components by adapting the Stokes-

---

<sup>12</sup> An exception is at cold temperatures, which is responsible for the cold denaturation phenomena in proteins. However, low temperature also increase van der Waals attractions between acyl chains in membranes, resulting in more ordered membranes at low temperature.

<sup>13</sup> This is not to say cells have not needed to adapt their membrane lipid composition to maintain viability; thermophiles feature a variety of exotic lipid modifications relative to mesophiles.

<sup>14</sup> The importance of membrane dynamics also argues against a role for seemingly analogous shell-like aggregates, which assemble as a result of direct covalent or non-covalent interactions, and has implications for the prospect of exobiology in non-polar solvents (e.g. liquid hydrocarbons).



Einstein equation to the diffusion of a cylinder (a geometric model of a lipid or protein) in a membrane [54]:

$$D_T = \frac{k_B T}{4\pi\mu_M} \left( \log \frac{\mu_M h}{\mu_W r} - \gamma \right) \quad (3)$$

where  $D_T$  is the translation diffusion coefficient,  $k_B$  is Boltzmann's constant,  $T$  is temperature in Kelvin,  $\mu_M$  is the viscosity of the membrane,  $\mu_W$  is the viscosity of the aqueous solution surrounding the membrane,  $h$  is the thickness of the membrane,  $r$  is the radius of the protein/lipid, and  $\gamma$  is Euler's constant ( $\sim 0.5772$ ). Membrane diffusion therefore inversely scales with the viscosity of the membrane, which is generally  $\sim 100$  times that of water, but can vary greatly depending on lipid composition and temperature. Membrane fluidity, which is simply the inverse of viscosity, is thus a commonly used to describe the physical state of the bilayer. Fluidity is therefore homeostatically maintained in cells in response to changes in temperature or chemical environments through changes in lipid compositions<sup>15</sup> [57].

McConnell and colleagues were also first to report that the translocation of phospholipids from one leaflet of the bilayer to another, a process colloquially termed “flip-flop”, is much slower than diffusion, with half-times of hours for their spin-labeled phospholipids [58]. This has been confirmed in several other studies [59-61], though exact flip-flop rates reported vary significantly depending on the assay used. The slow flip-flop rate of phospholipids can be explained in the context of Overton's rule (equation 2): For a lipid to flip across the bilayer, its

---

<sup>15</sup> The homeostatic membrane fluidity can vary dramatically between different cell types, tissues, or even organelles. The least fluid membranes are found in extremophiles, especially archaeal tetraether membranes (55), while the most fluid are in central nervous tissue of animal cells, such as in the retina (56).

head group must effectively permeate across the hydrophobic interior of the membrane. Since phospholipid head groups are either negatively charged or are zwitterionic, their partition into the membrane is rate limiting for this process.

### **Models for the origin of cell membranes**

Pioneering work by Alec Bangham and colleagues first demonstrated that suspensions of purified phospholipids self-assemble into bilayer membranes when hydrated [62]. The energy of exposed bilayer edges resulted in membranes folding up into ‘bubbles’<sup>16</sup> termed vesicles or liposomes (as in Figure 2). These vesicles, as is the case for most methods of preparation, were heterogenous and multilamellar in structure, although subsequent techniques allowed for easy production of small, unilamellar samples. Besides launching the field of membrane biophysics, which utilizes such vesicles to study membrane properties, these experiments showed that cell-like structures can assemble without any pre-existing biological machinery<sup>17</sup>. Such membrane self-assembly is now assumed to be a necessary step for the origin of life. Were the first cell membranes similarly composed of phospholipids? Prebiotic syntheses for phospholipids have been explored [64, 65], but the purification of trace quantities of products from their similarly hydrophobic substrates is challenging. More importantly, the extreme insolubility (~ nM) of phospholipids causes large kinetic barriers to their assembly into vesicles (extensive sonication

---

<sup>16</sup> This is only a visual analogy; membranes differ significantly from bubbles in that they carry negligible interfacial energy and generally permit water across them, both of which allows for their deformation into non-spherical morphologies.

<sup>17</sup> The significant of this was apparently not lost on Bangham, who titled a talk “Membranes Came First!” (63)

was required in Bangham's experiments) and the subsequent growth of those vesicles. Primitive cells would have almost certainly required the addition of lipids from the environment to grow their membranes and such insolubility would have prevented this exchange<sup>18</sup>. Finally, the functional properties of phospholipid membranes make them ill-suited for the role of early cell membranes, as they require extensive protein machinery to divide and to transport molecules across them (discussed further below).

Membranes composed of simple, single chain amphiphiles, such as fatty acids and their derivatives, provide a potential solution to the problem of early cell membrane composition. A component of phospholipids, fatty acids are synthesized by almost all bacteria and eukaryotes but are also likely to have been abundant on the early earth. There are two well-explored prebiotic mechanisms for hydrocarbon synthesis, both producing acids and alcohols as oxygenated alkane derivatives. Spark discharges, similar to those used by Miller, can drive the production of short, branched alkanes up to C<sub>12</sub> in methane/water [10, 66] or methane/carbon dioxide [67]. Fischer-Tropsch-type processes generate large varieties of straight-chain fatty acids up to C<sub>33</sub> [8, 68]. These reactions involve the condensation of hydrogen gas and carbon monoxide at high temperatures and/or pressures and utilize metal catalysts. The latter mechanism is especially of interest because of its longer length products and the possibility that large quantities of such products could have been generated in areas of hydrothermal activity or during impact collisions. Fatty acids are also chemically very stable, in contrast to many other prebiotic molecules of interest [69, 70], and could have accumulated over long time periods on the early earth. The discovery of significant amounts of fatty acids (up to C<sub>12</sub>) in several carbonaceous

---

<sup>18</sup> Phospholipid synthesis in cells occurs in the membrane, negating this problem.

chondrite meteorites provides direct evidence for the abiotic abundance of these molecules [71, 72].

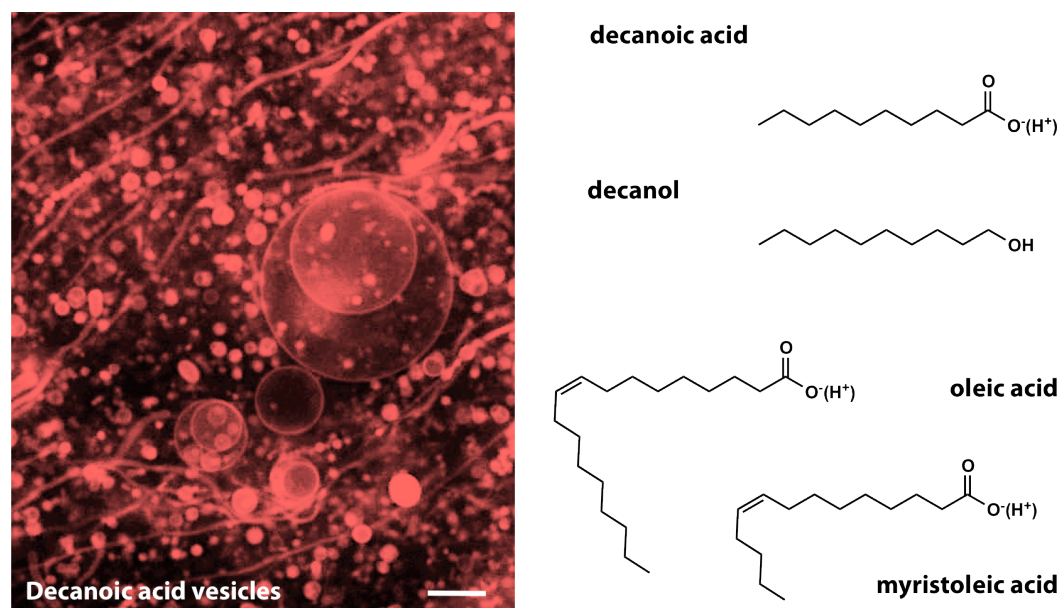


**Figure 4:** Fatty acid membranes. Short chain fatty acids and alcohol, such as decanoic acid and decanol, are products of abiotic lipid synthesis and self-assemble into vesicles (left, scale bar  $5 \mu$ ). Longer chain, unsaturated fatty acids, such as oleic acid and myristoleic acid, serve as additional laboratory models for primitive membrane lipids.

Fatty acid membrane assembly was first reported by Gebicki and Hicks, who showed that oleic acid, a long-chain (C18), unsaturated fatty acid common to cells, forms vesicles with similar morphology and osmotic properties as phospholipids [73, 74]. Follow-up work by Hargreaves and Deamer established that shorter, saturated fatty acids (down to C8), which are predominant species generated by Fischer-Tropsch reactions, can similarly form vesicles [75]. Deamer went on to demonstrate that non-polar extract from the Murchison meteorite, likely containing similar molecules, could also form vesicles when hydrated [76]. While prebiotically implausible, long,

unsaturated fatty acids remain a useful laboratory model because of their lower melting temperatures and effective working concentrations<sup>19</sup>.

Fatty acid aggregation depends on the protonation state of the carboxyl head group and thus the pH of the solution. Fatty acids spontaneously assemble into bilayer membranes when the solution pH is near the pKa of the membrane-incorporated acid (~ 7 - 9), which is elevated considerably from the pKa of the free monomer (~ 4 - 5). Fatty acid membranes are therefore composed of approximately equal portions of protonated and deprotonated fatty acids, the latter of which exist as salts (soaps) with cations in solution. Fatty acid membranes thus feature a net negative charge density of 0.5 per lipid, which is destabilizing, but overcome this through a hydrogen-bonding network between protonated and anionic monomers [77, 78]. The incorporation of fatty alcohols and glycerol monoesters further stabilizes fatty acid membranes [79], likely through a combination of reduction in charge density and increasing hydrogen bonding. At higher pH, the deprotonated fatty acids aggregate into smaller micelles, a geometry that allows for greater charge repulsion between neighboring anionic lipids. At acidic or neutral pH, the protonated acids lose their amphiphilicity and condense into oil droplets.

---

<sup>19</sup> These are not just considerations of convenience; laboratory manipulations at elevated temperature are often not possible, and high lipid concentrations preclude spectroscopic analyses.

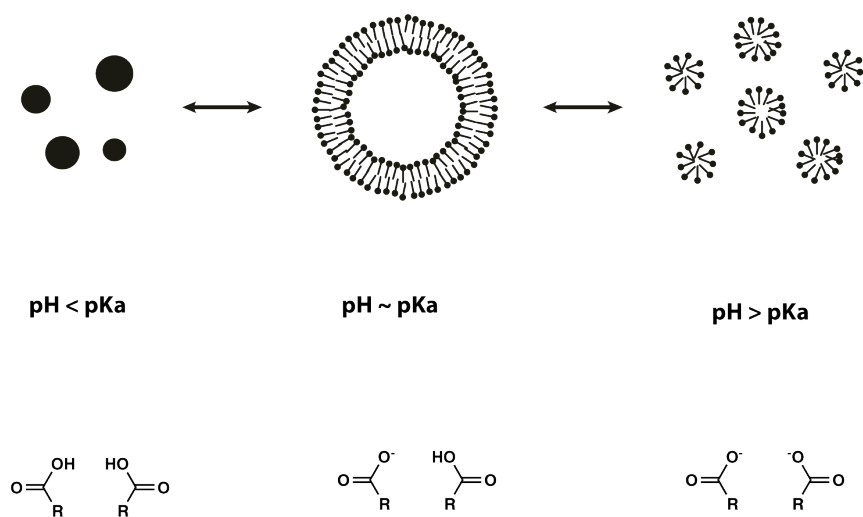


**Figure 5:** pH dependence of fatty acid aggregation. Acidic or neutral solutions (left) lead to fatty acids aggregating as protonated species, which results in oil droplets. Alkaline solutions (right) result in micellar aggregation of the fully deprotonated acids. However, solutions near the aggregate pKa (center) of the fatty acids allow for vesicle assembly due to a mixture of both protonated and deprotonated acids.

The dependence of fatty acid aggregation on head group protonation allows for changes in solution pH to drive vesicle assembly. When a solution of alkaline micelles ( $\text{pH} > 10$ ) is introduced into a buffered solution at  $\text{pH} 8.5$ , the micelle phase is destabilized and de novo vesicle assembly occurs. This process is catalyzed by pre-formed [80] or mineral surfaces [81, 82], both of which may act as a surface on which newly formed bilayers can organize. Although pH-driven membrane assembly is not prebiotically necessary, it proves useful as a model for investigating the mechanisms by which assembly occurs. In chapter 2 (Appendix A), I use the fluorescent probe Laurdan, which is sensitive to its local microenvironment, to structurally track the micelle to vesicle transition.

Fatty acid aggregation is also concentration dependent, as detailed in chapters 2-4. All molecular assembly processes must overcome the statistical cost of aggregation, a phenomenon well characterized for surfactant micelles, including alkaline fatty acids. Langmuir first observed that micelle aggregation occurs only above a critical concentration, termed a critical micelle concentration, above which the concentration of monomers in equilibrium with the aggregates remains constant. Fatty acid membrane assembly has been observed to have an analogous critical aggregation concentration ( $cac$ ), only above which aggregates begin to form. In chapter 4, I confirm this critical concentration for a series of unsaturated fatty acids, and show that monomer concentrations stay largely constant above each  $cac$ . Critical concentrations are described in terms of a pseudophase transition [83], in which the critical concentration is derived as:

$$\Delta G = RT \ln cac \quad (4)$$

$$cac = e^{\Delta G / RT} \quad (5)$$

where  $\Delta G$  is the molar free energy difference between the lipid in the aggregate versus free in solution,  $R$  is the gas constant,  $T$  is temperature in kelvin, and  $cac$  is the critical aggregation concentration expressed in units of mole fraction in the system<sup>20</sup>. This free energy term is the energetic gain associated with solubilizing the lipid in the membrane and is dominated by the hydrophobic effect. The hydrophobic effect is proportional to the molecular surface area of non-polar groups, and is therefore additive; each methylene in the chain contributes approximately -3.5 kJ/mol to this value<sup>21</sup>. Therefore,

---

<sup>20</sup> These can be calculated simply as the molar concentration divided by the solvent concentration (55 M for water).

<sup>21</sup> There is also a head group contribution, which is dependent on a number of factors, and small adjustments depending on the unsaturation of the lipid.

$$cac \propto e^{n \left( \frac{-3.5 \text{ kJ}}{RT \text{ mol}} \right)} \quad (6)$$

where  $n$  is the chain length. This relationship explains why critical concentrations increase exponentially with decreasing chain length. For example, in laboratory conditions<sup>22</sup> oleic acid (C18) has a cac of  $\sim 20 \mu\text{M}$ , myristoleic acid (C14) 2 mM, and decanoic acid (C10) 40 mM.

The high critical concentrations of short-chain fatty acids pose a seemingly significant challenge for prebiotic membrane assembly, as these species are the dominant products of abiotic fatty acid synthesis. This is an example of a general ‘concentration problem’ in the origin of life, in which proposed chemical and physical assembly processes require high concentrations of substrates and building blocks, respectively [84]. If prebiotic chemistry occurred in a diluting body of water<sup>23</sup>, how could cellular self-assembly occur? Physical concentrations, such as evaporation or eutectic freezing, have long been proposed to have been essential in order to concentrate otherwise dilute solutions. In chapter 2 we experimentally validate a novel concentrating mechanism that was proposed by Braun and colleagues based on mass transfer simulations [85]. Vertically oriented channels in hydrothermal vents could have acted as natural thermal diffusion columns, which concentrate solutes through the coupling of thermophoresis and a unicellular convective flow. Thermal diffusion columns have a long history of use in industrial separation processes and can highly concentrate molecules based on their Soret coefficient, which is a

---

<sup>22</sup> In this work: 0.2 M sodium bicine buffer at pH 8.5 at 293 K.

<sup>23</sup> This is a strong argument against life beginning simply at the surface of oceans; large bodies of water would have diluted any ‘prebiotic soup’ into a much too thin broth.



measure of their thermal diffusivity<sup>24</sup>. We validated their proposal using a glass microcapillary model and showed that modest temperature gradients (20° K) could drive the extreme accumulation (> 10<sup>5</sup> fold enrichment) of nucleotides, oligonucleotides and lipids at the bottom of the capillary. This accumulation was able to drive the assembly of large fatty acid vesicles from an initially dilute solution below the cac [87].

An alternative solution to the concentration problem for membrane assembly potentially lies in the thermodynamics of fatty acid mixtures (chapter 4). While short-chain fatty acids were the predominant prebiotic lipid, abiotic synthesis would have resulted in a polydisperse mixture of different length fatty acids, generally decreasing in abundance exponentially or logarithmically with chain length. This abundance pattern has been confirmed in Fischer-Tropsch experiments (e.g., Figure 1 in reference [9]) and in meteorite extracts (e.g., Figure 2 in reference [72]). How would vesicle aggregation proceed in these complex mixtures? Analogous theoretical and experimental work on mixed detergent micelles, including alkaline fatty acids [88], derived the critical concentration,  $c$ , for a mixture of  $n$  components as:

$$\frac{1}{c} = \sum_{i=1-n} \frac{X_i}{c_i} \quad (7)$$

where  $X_i$  is the fraction of the mixture of the  $i$ th component. The derivation of this equation is in chapter 3. For mixture of two components, this simplifies to:

$$c = \frac{c_1 c_2}{X_1 c_2 + (1 - X_1) c_1} \quad (8)$$

---

<sup>24</sup> This is not a well-understood phenomenon, but describes the weak tendency of molecules to drift along a thermal gradient in a manner reminiscent of electrophoresis (86).

where  $c_1$  and  $c_2$  are the critical concentrations for the individual components alone. Thus, the critical concentration of the mixture is heavily skewed by the component with the lower individual concentration, even as a minor component. I found that vesicle assembly largely follows this relationship for binary mixtures of both short, saturated and long, unsaturated fatty acids. For example, 10% oleic acid (C18) lowers the cac of myristoleic acid (C14) from 2 mM to 100  $\mu$ M. Thus, the cac of prebiotic mixtures of fatty acids would be heavily skewed by minor amounts of long chain fatty acids. This would have allowed membrane assembly to occur at much lower concentrations than would be expected based on the cac of the predominant components. Theoretical work on mixed micelles also predicts that the composition of the resulting aggregates at low concentrations would then be relatively enriched in the long-chain species [89], which has implications for prebiotic membrane composition.

In addition to dictating aggregate assembly, we found that concentration is an important variable in fatty acid vesicle-micelle equilibrium (chapter 4). Fatty acid solutions at pH 8.5, in which vesicles are the preferred aggregate phase, also feature significant amounts of coexisting micelles. The vesicle to micelle partition increases with fatty acid concentration and relatively dilute solutions can be largely micellar. This is likely a result of the much smaller micelle size ( $\sim$  50 fatty acids versus  $>$  100,000 for vesicles), which would be entropically favored at low concentrations. The ability of fatty acids to coexist as vesicles, micelles and monomers in solutions is indicative of the dynamic properties of these aggregates.

## Fatty acid membrane dynamics

While fatty acid membranes are stable over indefinite timescales, their monomers exchange rapidly between neighboring vesicles in the solution. Jim Hamilton and colleagues extensively studied fatty acid exchange between phospholipid vesicles by utilizing the ability of fatty acids to act as ionophores, which acidify the interior of the vesicles to which they are added [90]. These experiments demonstrated that exchange is sufficiently rapid to make fatty acid transporters unnecessary in cells. Fatty acid desorption from the bilayer is the rate-limiting step in exchange and occurs on millisecond to second timescales. The desorption of a lipid from a bilayer can be modeled as an Arrhenius process:

$$k_{off} = Ae^{\Delta G/RT} \quad (9)$$

where  $k_{off}$  is the intrinsic desorption rate of a fatty acid from a bilayer (off rate),  $\Delta G$  is the free energy change of a fatty acid going from the membrane to the solution,  $A$  is a proportionality constant,  $R$  is the gas constant, and  $T$  is temperature in kelvin. Since the free energy resulting from the hydrophobic effect is additive with each additional methylene in the chain, equation 9 can be rederived to:

$$k_{off} \propto e^{n \left( \frac{-3.5 \text{ kJ}}{RT \text{ mol}} \right)} \quad (10)$$

where  $n$  is the number of carbons in the lipid (e.g., 18 for oleic acid). Thus, off rates, like  $k_{on}$ , scale exponentially with chain length, which has been confirmed for fatty acids in both phospholipid membranes [91] and fatty acid membranes (chapter 5). This relationship also

explains the disparate inter-vesicle dynamics of fatty acids and phospholipids. Since phospholipids have two acyl chains,  $n$  is effectively doubled, which dramatically reduces the off rate. Thus, while fatty acids feature residence times of well under a second in the membrane, their corresponding phospholipids are kinetically trapped in their respective membranes for days to months [59].

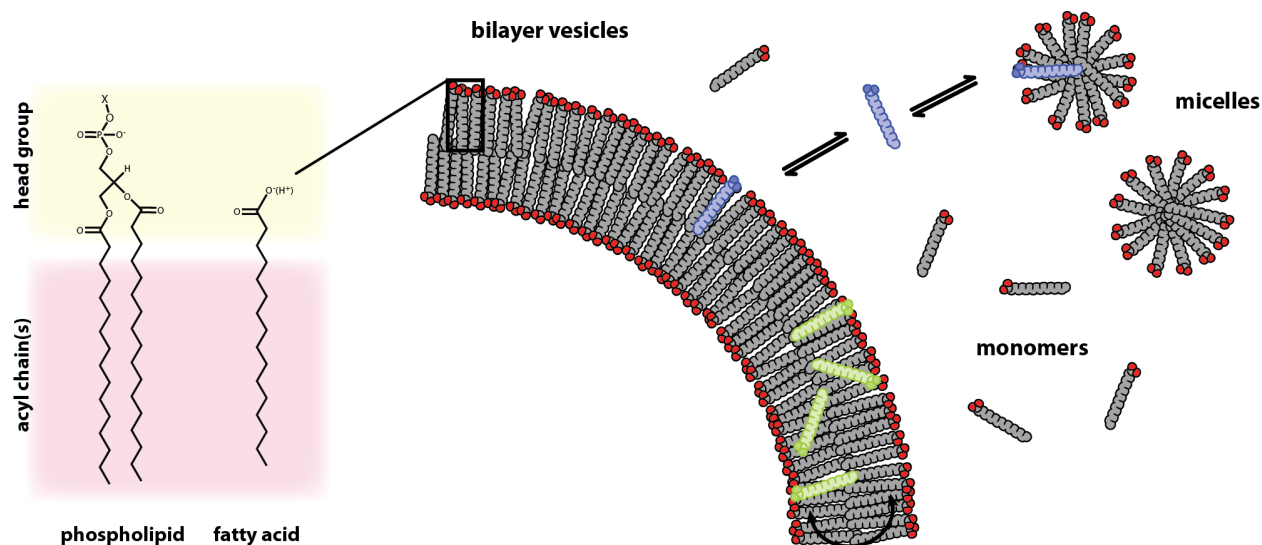


**Figure 6:** Fatty acid membrane dynamics. The solubility of fatty acid monomers allows them to rapidly exchange between vesicles, coexisting micelles, and a monomer pool (purple). Fatty acid flip-flop across the bilayer (yellow) is also fast due to the easily neutralized carboxylate head group (yellow). These dynamic processes occur only on very slow timescales for phospholipids, which are insoluble and feature large, polar head groups. Figure adapted from reference 84.

Inter-vesicle exchange is not limited by fatty acid equilibration within the bilayer, as flip-flop between the leaflets is very fast, in contrast to phospholipids. The rapidity of flip flop occurs because the small carboxyl head groups of fatty acids are rapidly neutralized by protonation or

soap formation. The flip-flop of the uncharged protonated acid is very fast (under a millisecond) [92], while the zwitterionic soap is somewhat slower (seconds) [93]. These rates are unaffected by the length of the fatty acid, as would be expected from the partition of the head group into the membrane being rate limiting. As we will see, these simple dynamic properties of fatty acid membranes have surprising consequences for the potential functions of primitive cell membranes.

### **Models for the function of early cell membranes**

For a protocell to reproduce, its membrane has to grow, divide, and mediate the transport of chemical building blocks, all without the assistance of any complex protein machinery. Primitive cell membranes thus had to be functionally more complex than modern cell membranes, as they could only utilize intrinsic and environmental processes to accomplish these tasks.

In modern cells, phospholipids are constructed by membrane-localized enzymes, and are incorporated into the membrane at their site of synthesis<sup>25</sup>. However, in the absence of internal, metabolic lipid synthesis, what thermodynamic forces could drive the process of membrane growth? The phase transitions inherent to fatty acid aggregates potentially offer a general route. Luisi and colleagues first demonstrated that the pH-controlled phase transition of fatty acids can be used to drive vesicle growth by adding alkaline fatty acid micelles to a buffered suspension of pre-formed vesicles [80]. In these experiments, micelles are destabilized upon pH drop and thus either incorporate into pre-existing vesicles or nucleate de novo vesicles. In chapter 4 we show

---

<sup>25</sup> In eukaryotes, transfer of lipids between organelles requires vesicle-mediate endomembrane trafficking or specific protein carriers.

that the concentration-dependent equilibrium between micelles and vesicles can similarly drive growth. Upon solution concentration, the micelle to vesicle partition decreases, causing excess micelles to incorporate into pre-existing vesicles. This mechanism has potential prebiotic relevance in light of proposed physical concentrating methods (see above).

Vesicle growth was first studied using electron microscopy [80] and dynamic light scattering [94]. More recent work in our lab has used Förster resonance energy transfer (FRET) to quantitatively track changes in membrane area [81, 95]. Membrane growth can be followed through the strong dependence of FRET efficiency on the statistical distance between donor and acceptor fluorophores anchored to the membrane. These studies have highlighted the kinetic competition between vesicle growth and de novo vesicle nucleation. In the case of pH-driven growth, efficiency is inversely dependent on the rate of micelle addition, with efficiency approaching 100% if the micelle feedstock is introduced very slowly [95].

An alternative growth mechanism lies in the ability of fatty acid vesicles to undergo competition for monomers that exchange between them, a process that also provides a potential route for Darwinian selection in primitive cells [96, 97]. Osmotically-swollen vesicles exhibit membrane tension, which is relieved through their growth at the expense of isotonic vesicles in the solution that shrink as a result [96]. High concentrations of RNA and its associated cations can also drive this phenomenon, which could have provided a selective growth advantage for efficient genetic replication. However, it is unclear if such high concentrations of RNA are plausible given the likely inefficiency of early replication. More fundamentally, the rapid rate of strand reannealing in even moderate oligonucleotide concentrations would have inhibited template copying before

the evolution of single-strand binding machinery<sup>26</sup>. Osmotically-driven growth also inherently results in a tensed, spherical vesicle morphology, which makes division challenging and geometrically necessitates content loss. Recent work, explained in detail in chapter 5 and summarized below, has shown that the incorporation of small amounts of phospholipids can efficiently drive competition, a process that has implications for early membrane evolution [97].

Membrane division appears to be a more challenging task for a primitive cell, both because of the complexity of extant division machinery and the lack of an easily identifiable driving force. Early work on fatty acid vesicle division utilized pressure-driven extrusion through small pores as a model for primitive cellular division [81]. However, extrusion is prebiotically implausible and the process results in significant loss of encapsulated contents. A more plausible and robust pathway results from the growth of multilamellar vesicles (MLV), which form spontaneously in lipid suspensions [98]. Vesicle growth by fatty acid addition results in a rapid increase of membrane surface area as new monomers are incorporated in the bilayer. However, the rate of the corresponding increase in volume is osmotically limited by the permeability of solutes in the media; if the solution contains highly charged molecules, for example, volume growth is slower (hours to days). Since the volume between adjacent bilayers in MLVs is minimal, the outermost bilayer emerges as a thin tubule that gradually elongates. The result is the transformation of the initially spherical vesicles into long, filamentous vesicles, which are highly unstable and readily divide into daughter vesicles upon exposure to mild shear forces, with negligible loss of encapsulated content. Given an environment rich in slowly permeating solutes and the presence

---

<sup>26</sup> This effect is responsible for the plateau in polymerase chain reaction (PCR) yields regardless of number of cycles and substrate availability.

of mild shear forces, growth and division become inherently coupled. In chapter 5 I show that this process, first demonstrated for pH-driven growth, also occurs during phospholipid-driven vesicle competition.

Although the physical mechanism of shear-induced division remains unclear, the process may be related to the previously reported ‘pearling instability’ in tubular membrane vesicles [99, 100]. When a surface tension is induced on a membrane, it drives vesicle shape fluctuations that minimize the membrane surface area. This energy minimization causes initially tubular vesicles to pinch off into attached spherical structures that appear as beads on a string. In previous experiments surface tension was induced directly via optical trap pulling; shear force induction of membrane surface tension has not been thoroughly explored. An unexpected addendum to these physical models of vesicle division is the recent report of a similar process occurring in vivo [101-103]. Mutant L-form (cell-wall less) bacterial strains have been shown to divide without the standard fission machinery but rather by a physical process that appears, at least visually, to involve the pearling instability.

Membrane growth and division would have been essential for a primitive cell cycle, but would also have had to couple with copying of the encapsulated genetic polymer. Because abiotic nucleotide chemistry is rather complex [11], activated substrates would have had to cross the cell membrane from the environment to participate in copying chemistry. As discussed above, phospholipid membranes are generally impermeable to all but small, non-polar molecules in the absence of specific protein transporters, an essential feature for cells that synthesize their building blocks internally. Large, polar molecules, such as nucleotides, are all but impermeable.



However, studies of fatty acid-based membranes have shown much higher intrinsic membrane permeability, especially when the fatty acids were mixed with their associated glycerol monoesters and fatty alcohols [104]. These components also structurally stabilize fatty acid membranes, inhibiting aggregation from divalent cations [105] and increasing thermostability [106]. Using such mixtures, the permeation of activated nucleotides is fast enough to allow for chemical copying of encapsulated oligonucleotides, which do not leak out, in model systems [104].

How can we reconcile the surprising leakiness of primitive cell membranes with models for membrane permeation? Somewhat unexpectedly, fatty acid membranes are intrinsically less ordered and more fluid (by a factor of 2 to 5) than membranes composed of their corresponding phospholipids. This is surprising since acyl composition entirely determines membrane fluidity in phospholipid membranes. The glycerol backbone of diacyl lipids likely reduces the mobility of phospholipid chains, thereby increasing membrane order relative to unconstrained fatty acids. Overton's rule models solute permeation as proportional to its diffusion coefficient through the membrane, which can be approximated using the Stokes-Einstein equation for translational diffusion of a sphere:

$$D_T = \frac{k_B T}{6\pi\mu R} \quad (11)$$

where  $D_T$  is the translation diffusion coefficient,  $k_B$  is Boltzmann's constant,  $T$  is temperature in Kelvin,  $\mu$  is the viscosity of the medium, and  $R$  is the radius of the object. Substituting this in for  $D_M$  in equation 2 yields:

$$P_M = \frac{K_p k_B T}{6\pi\mu_M R h} = \frac{1}{\mu_M} \left( \frac{K_p k_B T}{6\pi R h} \right) \quad (12)$$

Therefore, membrane permeability of any solute is inversely proportional to the viscosity of the membrane, or proportional to fluidity. This conclusion is quantitatively sufficient to explain observed differences in permeability between membranes of pure fatty acids and phospholipids with similar acyl composition, such as the permeability of ribose in oleic acid and POPC membranes [107].

The dramatic increase in permeability due to the incorporation of fatty alcohols and monoesters is not, however, explained by changes in membrane fluidity. In fact, these components seem to increase the order of fatty acid membranes. A possible explanation lies in the large head group of glycerol monoesters, which provide the lipid with a high intrinsic curvature and could stabilize transient pores in the membrane. Consistent with this hypothesis is the observation that the fatty acid monoester of sorbitol, a larger, 6-carbon sugar, further increases membrane permeability compared to its corresponding glycerol monoester [104]. These sugars also feature hydrogen-bonding groups that could assist permeation through solute interactions during flip-flop. Flip-flop mediated permeation is well characterized for the case of cation permeation through fatty acid membranes, which occurs on the timescale of seconds depending on the ionic radius of the cation [93]. This is explained by the flip-flop of fatty acid soaps, in which the associated cation rapidly exchanges with those in the solution. Proton permeation occurs even more readily by this same mechanism but is rate limited by the slower cation permeation due to the build up of a membrane potential [93].

The permeability properties of single chain membranes argue strongly for a heterotrophic model for the first cells, in which building blocks are synthesized externally and then diffuse in. This model is minimally complex, and thus could have allowed for cellular self-assembly provided a rich chemical environment [106]. However, these same properties would have also necessitated the evolution of modern cell membranes before much of the characteristic features of biology had arisen. The evolution of internalized metabolism requires that cells retain chemical products in order to gain a selective advantage. Furthermore, proton gradients, which decay rapidly in fatty acid membranes, are essential for non-glycolysis ATP production<sup>27</sup>. Therefore the evolution of modern, phospholipid-based membranes was a critical step during early evolution of cells and was required in advance of other aspects of cellular complexity.

### **Models for the early evolution of cell membranes**

An appealing aspect of fatty acids as models for primitive membrane lipids is their extant role as components of phospholipids, which provides an obvious chemical route for the evolution of membrane lipids<sup>28</sup>. Phospholipid synthesis occurs via successive acyltransfers of activated fatty acids onto a glycerol-phosphate backbone yielding phosphatidic acid, the simplest phospholipid.

---

<sup>27</sup> It has been proposed that minimizing proton permeation has driven extremophiles to evolve extremely viscous cell membranes (55)

<sup>28</sup> This could similarly be true for isoprenoid pyrophosphates, the substrates of archaeal phospholipids. However, single-chain isoprenoid membranes have been demonstrated and there are no abiotic mechanisms to their synthesis; isoprenoids are clearly enzymatic inventions.

Fatty acids are activated either as thioesters (to coenzyme A<sup>29</sup> or acyl carrier proteins) or as acyl phosphates [108]<sup>30</sup>. All these reactions are carried out by protein enzymes in cells, but could have been carried out by primitive catalysts, whether RNA, peptides, or small molecules, in early biology.

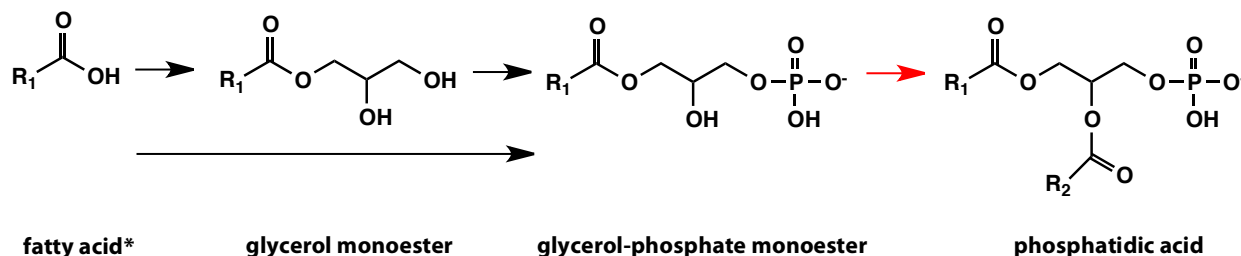


**Figure 7:** Chemical pathway from fatty acids to phospholipids. Glycerol or glycerol-phosphate undergoes two acylations with fatty acids, which first must be activated (\*) e.g. as thioesters. The second acyltransfer (red) leads to the first diacyl lipid product in the pathway, phosphatidic acid, whose head group can then be further elaborated upon to yield other phospholipids.

The adoption of phospholipids had to occur gradually to allow for the evolution of more efficient catalysts and so early membrane evolution likely featured mixtures of lipid containing fatty acids, glycerol monoesters, and increasing amounts of phospholipid. In such an evolutionary process, there had to be selective advantages driving the emergence and refinement of the necessary catalysts. What selective pressures could have been associated with early phospholipid synthesis? In chapter 5 I describe how even small amounts of phospholipid can drive the growth

<sup>29</sup> CoA and other nucleotide-derived cofactors are likely molecular remnants of ribozyme-mediated chemistry and thus serve as a principle piece of direct evidence for the RNA world hypothesis.

<sup>30</sup> This mode of activation was only recently discovered, yet is the primary mechanism in most bacteria.

of fatty acid-based vesicles at the expense of neighboring vesicles containing no or less phospholipid. Competitive growth would have provided a strong selective advantage for the incorporation of increasing amounts of phospholipid in the membrane. In large MLV, growth occurs via the filamentous shape transformation (described above) and therefore causes vesicle division. Phospholipid assembly from environmentally synthesized fatty acids could have thus been an early mechanism for cell growth and division.

Phospholipids cause competition for fatty acid monomers through two mechanisms: 1) Phospholipid insolubility entropically favors their dilution by the exchanging fatty acids; and 2) Changes in membrane fluidity, described above, reduce the intrinsic fatty acid off-rate with increasing phospholipid content. Both mechanisms depend on the double-chain nature of phospholipids and therefore can be driven by a single chemical reaction, the second acyltransfer during phospholipid synthesis. This reaction is of particular interest because it is the first in phospholipid synthesis for which a selectable catalyst, such as RNA, could have arisen. Previous steps, such as fatty acid activation or the first glycerol-phosphate acylation, produce single-chain products, which rapidly exchange between membranes and thus could not accumulate in the cell of their synthesis. Only once fatty acids were incorporated into an insoluble diacyl lipid could a selectable catalyst for these intermediates arise. Initial environmental synthesis of these intermediates is chemically reasonable: Abiotic synthesis of sugar phosphates [109, 110] and glycerol monoesters [111] has been reported, while carboxylic acid activation could have been performed by a variety of condensing agents.

The potential for RNA-catalyzed lipid acyltransferase is supported by previously reported aminoacyltransferase ribozymes that were isolated from a random library by in vitro selection [112]. In ongoing work, we have developed an in vitro selection process for a lipid acyltransferase ribozyme that could drive vesicle competition and serve as a model for early phospholipid catalysts. The primary challenge of such a ribozyme is the solubility inherent to RNA<sup>31</sup>, which can be incompatible with the membrane localization of its substrates. The ability of single-chain lipids, especially short chain versions, to form coexisting monomer or micellar phases could therefore be critical to overcoming this problem. An acyltransferase ribozyme would also need to feature significant turnover to significantly alter the lipid composition of a vesicle; previous in vitro selections have been lacking in this regard, but this is likely a selection artifact<sup>32</sup>.

An alternative laboratory model for phospholipid assembly is presented in chapter 7. We utilized a copper(I)-catalyzed cycloaddition to link an oleoyl azide, a fatty acid analogue, and an alkyl lysophospholipid. These type of reactions are colloquially termed ‘click’ reactions because of their specificity and robustness in water, which rival enzymatic reactions [113]. The resulting product mimics a phospholipid, with a 1,2,3-triazole substituting for an ester linkage. The substrates of this reaction, however, do not form membranes: azides are not amphiphilic, condensing into oil droplets, and lysophospholipids feature too high of an intrinsic curvature,

---

<sup>31</sup> This is a major advantage for protein enzymes and transporters, which can use chemical diversity of amino acids to localize to the membrane. The likely inability RNA to be a membrane component is an argument against mode for complex cells utilizing RNA exclusively during early evolution.

<sup>32</sup> In vitro selections for catalyst are generally performed in *cis* to allow for the pull-down of active library members and thus high turnover is not selected for.

forming micelles. When carried out in water, this reaction therefore leads to the de novo assembly of membranes, which bud off as vesicles from the surface of the azide droplets [114]. In ongoing work, we are modifying this reaction to take place inside pre-existing membranes using hydrophobic copper-binding ligands. We plan on using this reaction to study repeated cycles of phospholipid-driven growth and division in fatty acid vesicles.

### **Implications for early cellular evolution**

Results presented here describe early membrane evolution as a deterministic outcome of the intrinsic properties of single-chain lipid membranes<sup>33</sup>. Provided environmental sources for the necessary substrates, phospholipid synthesis would have almost certainly arisen early during the evolution of life due the strong selective advantage it provides protocells with single-chain lipid membranes. The transition to fully phospholipid membranes would have then proceeded driven by continued competitive growth. In chapter 5 I describe how such a transition in membrane composition would have corresponded to a decrease in membrane fluidity and thus solute permeability. I demonstrate an exponential reduction in the permeability of ribose with increasing phospholipid content in fatty acid membranes, as well as similar results for the leakage of an activated nucleotide.

A gradual decline in membrane permeability would have had significant consequences if early cells were heterotrophic in nature, as is argued above. This could have provided a selective

---

<sup>33</sup> Asking whether evolutionary outcomes are deterministic or stochastic is a fundamental question of evolutionary biology, and has been most notably contemplated for the role of phosphates in nucleic acids and metabolites (115).

pressure for the further evolution of biological machinery needed to counter the reduction in intrinsic membrane permeability. Early transporters could have included short peptides [116] or membrane-bound aptamers [117]. Alternatively, reductions in membrane permeability could have helped drive the adoption of internalized building block synthesis (metabolism). Early metabolic activities could have been quite simple, such as nucleotide assembly by ribozymes [118], allowing for the synthesis of building blocks from more permeable precursors.

In summary, the physical properties of primitive cell membranes would have predisposed their ensuing evolution to phospholipid membranes. In turn, early membrane evolution could have been an important driver for the evolution of cellular complexity, such as metabolism and mediated transport. Membranes have continued to evolve over the succeeding 4 billion years, and modern cells synthesize a tremendous variety of lipid products<sup>34</sup>, with significant diversity between divergent cellular lineages. While the origin of life necessitated lipid membranes as boundary structures, this subsequent evolution has primarily been driven by their role as a physical environment in which biological machinery functions. Further study of their physical properties is thus of critical importance to understanding their evolution.

## Overview

The following chapters of this dissertation present experimental work related to the origin and early evolution of cell membranes. Chapters 2 and 3 demonstrate how physical processes

---

<sup>34</sup> For example, *Saccharomyces cerevisiae*, as a model eukaryote, contains over 250 distinct lipid species (119). These comprise several major classes, with subsequent chain and head-group diversity yielding combinatorial diversity. Bacterial membranes tend to be much simpler, but feature great diversity between different lineages.



(chapter 2) or intrinsic molecular properties (chapter 3) could have allowed fatty acid membranes to assemble under reasonable prebiotic conditions of concentration. Chapter 4 characterizes the phase properties of fatty acid aggregates, especially in relation to concentration, and demonstrates their applicability for driving growth. Chapter 5 describes the selective growth advantage provided by phospholipids to fatty acid membrane compartments and characterizes the reduction in membrane permeability that would have occurred during the transition from single-chain to phospholipid membranes. Chapter 6 describes a synthetic reaction that mimics a key step in phospholipid synthesis and uses it to drive vesicle assembly.

## References

1. Sleep, N.H., et al., *Annihilation of ecosystems by large asteroid impacts on the early Earth*. Nature, 1989. **342**(6246): p. 139-42.
2. Schopf, J.W., et al., *Laser--Raman imagery of Earth's earliest fossils*. Nature, 2002. **416**(6876): p. 73-6.
3. Mojzsis, S.J., et al., *Evidence for life on Earth before 3,800 million years ago*. Nature, 1996. **384**(6604): p. 55-9.
4. Koonin, E.V., *Comparative genomics, minimal gene-sets and the last universal common ancestor*. Nat Rev Micro, 2003. **1**(2): p. 127-136.
5. Miller, S.L., *A production of amino acids under possible primitive earth conditions*. Science, 1953. **117**(3046): p. 528-9.
6. Gabel, N.W. and C. Ponnampuruma, *Model for origin of monosaccharides*. Nature, 1967. **216**(5114): p. 453-5.
7. Ring, D., et al., *Prebiotic synthesis of hydrophobic and protein amino acids*. Proc Natl Acad Sci U S A, 1972. **69**(3): p. 765-8.
8. Rushdi, A.I. and B.R. Simoneit, *Lipid formation by aqueous Fischer-Tropsch-type synthesis over a temperature range of 100 to 400 degrees C*. Orig Life Evol Biosph, 2001. **31**(1-2): p. 103-18.

9. Simoneit, B.R.T., *Prebiotic organic synthesis under hydrothermal conditions: an overview*. Advances in Space Research, 2004. **33**(1): p. 88-94.
10. Yuen, G.U., J.G. Lawless, and E.H. Edelson, *Quantification of monocarboxylic acids from a spark discharge synthesis*. Journal of molecular evolution, 1981. **17**(1): p. 43-47.
11. Powner, M.W., B. Gerland, and J.D. Sutherland, *Synthesis of activated pyrimidine ribonucleotides in prebiotically plausible conditions*. Nature, 2009. **459**(7244): p. 239-42.
12. Pizzarello, S., *The Chemistry of Life's Origin: A Carbonaceous Meteorite Perspective*. Accounts of Chemical Research, 2006. **39**(4): p. 231-237.
13. Ziurys, L.M., *The chemistry in circumstellar envelopes of evolved stars: following the origin of the elements to the origin of life*. Proc Natl Acad Sci U S A, 2006. **103**(33): p. 12274-9.
14. Ziurys, L.M., et al., *Chemical complexity in the winds of the oxygen-rich supergiant star VY Canis Majoris*. Nature, 2007. **447**(7148): p. 1094-1097.
15. Snyder, L.E., *Interferometric observations of large biologically interesting interstellar and cometary molecules*. Proc Natl Acad Sci U S A, 2006. **103**(33): p. 12243-8.
16. Forster, A.C. and G.M. Church, *Towards synthesis of a minimal cell*. Mol Syst Biol, 2006. **2**: p. 45.
17. Glass, J.I., et al., *Essential genes of a minimal bacterium*. Proc Natl Acad Sci U S A, 2006. **103**(2): p. 425-30.
18. Szostak, J.W., D.P. Bartel, and P.L. Luisi, *Synthesizing life*. Nature, 2001. **409**(6818): p. 387-90.
19. Woese, C.R., *The genetic code : the molecular basis for genetic expression*. Modern perspectives in biology 1967, New York: Harper & Row. viii, 200p.
20. Kruger, K., et al., *Self-splicing RNA: autoexcision and autocyclization of the ribosomal RNA intervening sequence of Tetrahymena*. Cell, 1982. **31**(1): p. 147-57.
21. Guerrier-Takada, C., et al., *The RNA moiety of ribonuclease P is the catalytic subunit of the enzyme*. Cell, 1983. **35**(3 Pt 2): p. 849-57.
22. Steitz, T.A. and P.B. Moore, *RNA, the first macromolecular catalyst: the ribosome is a ribozyme*. Trends Biochem Sci, 2003. **28**(8): p. 411-8.
23. Wilson, D.S. and J.W. Szostak, *In vitro selection of functional nucleic acids*. Annu Rev Biochem, 1999. **68**: p. 611-47.

24. Bartel, D.P. and J.W. Szostak, *Isolation of new ribozymes from a large pool of random sequences [see comment]*. Science, 1993. **261**(5127): p. 1411-8.
25. Johnston, W.K., et al., *RNA-catalyzed RNA polymerization: accurate and general RNA-templated primer extension*. Science, 2001. **292**(5520): p. 1319-25.
26. Lincoln, T.A. and G.F. Joyce, *Self-sustained replication of an RNA enzyme*. Science, 2009. **323**(5918): p. 1229-32.
27. Wochner, A., et al., *Ribozyme-catalyzed transcription of an active ribozyme*. Science, 2011. **332**(6026): p. 209-12.
28. Inoue, T. and L.E. Orgel, *A nonenzymatic RNA polymerase model*. Science, 1983. **219**(4586): p. 859-62.
29. Schrum, J.P., et al., *Efficient and Rapid Template-Directed Nucleic Acid Copying Using 2'-Amino-2',3'-dideoxyribonucleoside-5'-Phosphorimidazolid Monomers*. Journal of the American Chemical Society, 2009. **131**(40): p. 14560-14570.
30. Deck, C., M. Jauker, and C. Richert, *Efficient enzyme-free copying of all four nucleobases templated by immobilized RNA*. Nat Chem, 2011. **3**(8): p. 603-608.
31. Orgel, L.E., *Prebiotic chemistry and the origin of the RNA world*. Crit Rev Biochem Mol Biol, 2004. **39**(2): p. 99-123.
32. Oro, J., S.L. Miller, and A. Lazcano, *The origin and early evolution of life on Earth*. Annu Rev Earth Planet Sci, 1990. **18**: p. 317-56.
33. Oparin, A.I. and S. Morgulis, *The origin of life* 1938, New York,: The Macmillan Company. viii p., 2 l., 270 p.
34. Robertson, J.D., *The ultrastructure of cell membranes and their derivatives*. Biochemical Society symposium, 1959. **16**: p. 3-43.
35. Fernandez-Moran, H. and J.B. Finean, *Electron microscope and low-angle x-ray diffraction studies of the nerve myelin sheath*. The Journal of biophysical and biochemical cytology, 1957. **3**(5): p. 725-48.
36. Stoeckenius, W. and D.M. Engelman, *Current models for the structure of biological membranes*. The Journal of cell biology, 1969. **42**(3): p. 613-46.
37. Gorter, E. and F. Grendel, *On bimolecular layers of lipoids on the chromocytes of the blood*. The Journal of Experimental Medicine, 1925. **41**(4): p. 439-443.

38. Davson, H. and J.F. Danielli, *The permeability of natural membranes* 1943, Cambridge Eng. New York,: The University press; The Macmillan company. x, 361 p.
39. Langmuir, I., *The constitution and fundamental properties of solids and liquids: II. Liquids*. Journal of the American Chemical Society, 1917. **39**(9): p. 1848-1906.
40. Tanford, C., *The hydrophobic effect and the organization of living matter*. Science, 1978. **200**(4345): p. 1012-8.
41. Israelachvili, J.N., D.J. Mitchell, and B.W. Ninham, *Theory of self-assembly of hydrocarbon amphiphiles into micelles and bilayers*. Journal of the Chemical Society, Faraday Transactions 2: Molecular and Chemical Physics, 1976. **72**: p. 1525-1568.
42. Overton, C.E., *Ueber die osmotischen eigenschaften der lebenden pflanzen- und tierzelle*, in *Vierteljahrsschrift der naturforschenden gesellschaft*, D.F. Rudio, Editor 1895: Zurich.
43. Meyer, H., *Zur Theorie der Alkoholnarkose*. Naunyn-Schmiedeberg's Archives of Pharmacology, 1899. **42**(2): p. 109-118.
44. Missner, A. and P. Pohl, *110 years of the Meyer-Overton rule: predicting membrane permeability of gases and other small compounds*. Chemphyschem : a European journal of chemical physics and physical chemistry, 2009. **10**(9-10): p. 1405-14.
45. Leo, A., C. Hansch, and D. Elkins, *Partition coefficients and their uses*. Chemical Reviews, 1971. **71**(6): p. 525-616.
46. YUNGER, L.M. and R.D. CRAMER, *Measurement and Correlation of Partition Coefficients of Polar Amino Acids*. Molecular Pharmacology, 1981. **20**(3): p. 602-608.
47. Van Mooy, B.A.S., et al., *Sulfolipids dramatically decrease phosphorus demand by picocyanobacteria in oligotrophic marine environments*. Proceedings of the National Academy of Sciences, 2006. **103**(23): p. 8607-8612.
48. Dupuy, A.D. and D.M. Engelman, *Protein area occupancy at the center of the red blood cell membrane*. Proceedings of the National Academy of Sciences of the United States of America, 2008. **105**(8): p. 2848-52.
49. Bergenstaahl, B.A. and P. Stenius, *Phase diagrams of dioleoylphosphatidylcholine with formamide, methylformamide and dimethylformamide*. The Journal of Physical Chemistry, 1987. **91**(23): p. 5944-5948.
50. Southall, N.T., K.A. Dill, and A.D.J. Haymet, *A View of the Hydrophobic Effect*. The Journal of Physical Chemistry B, 2002. **106**(3): p. 521-533.
51. Lee, B., *Solvent reorganization contribution to the transfer thermodynamics of small nonpolar molecules*. Biopolymers, 1991. **31**(8): p. 993-1008.

52. Singer, S.J. and G.L. Nicolson, *The fluid mosaic model of the structure of cell membranes*. Science, 1972. **175**(4023): p. 720-31.
53. Kornberg, R.D. and H.M. McConnell, *Lateral diffusion of phospholipids in a vesicle membrane*. Proceedings of the National Academy of Sciences of the United States of America, 1971. **68**(10): p. 2564-8.
54. Saffman, P.G. and M. Delbruck, *Brownian motion in biological membranes*. Proceedings of the National Academy of Sciences of the United States of America, 1975. **72**(8): p. 3111-3.
55. Valentine, D.L., *Adaptations to energy stress dictate the ecology and evolution of the Archaea*. Nat Rev Microbiol, 2007. **5**(4): p. 316-23.
56. Stubbs, G.W., B.J. Litman, and Y. Barenholz, *Microviscosity of the hydrocarbon region of the bovine retinal rod outer segment disk membrane determined by fluorescent probe measurements*. Biochemistry, 1976. **15**(13): p. 2766-2772.
57. Sinensky, M., *Homeoviscous Adaptation, A Homeostatic Process that Regulates the Viscosity of Membrane Lipids in Escherichia coli*. Proceedings of the National Academy of Sciences, 1974. **71**(2): p. 522-525.
58. Kornberg, R.D. and H.M. McConnell, *Inside-outside transitions of phospholipids in vesicle membranes*. Biochemistry, 1971. **10**(7): p. 1111-20.
59. Abreu, M.S., M.J. Moreno, and W.L. Vaz, *Kinetics and thermodynamics of association of a phospholipid derivative with lipid bilayers in liquid-disordered and liquid-ordered phases*. Biophysical journal, 2004. **87**(1): p. 353-65.
60. Liu, J. and J.C. Conboy, *1,2-Diacyl-Phosphatidylcholine Flip-Flop Measured Directly by Sum-Frequency Vibrational Spectroscopy*. Biophysical journal, 2005. **89**(4): p. 2522-2532.
61. Barsukov, L.I., et al., *Investigation of the inside-outside distribution, intermembrane exchange and transbilayer movement of phospholipids in sonicated vesicles by shift reagent NMR*. Biochimica et Biophysica Acta (BBA) - Biomembranes, 1980. **598**(1): p. 153-168.
62. Bangham, A.D. and R.W. Horne, *Negative Staining of Phospholipids and Their Structural Modification by Surface-Active Agents as Observed in the Electron Microscope*. Journal of molecular biology, 1964. **8**: p. 660-8.
63. Deamer, D.W., *From "banghasomes" to liposomes: a memoir of Alec Bangham, 1921-2010*. FASEB journal : official publication of the Federation of American Societies for Experimental Biology, 2010. **24**(5): p. 1308-10.

64. Hargreaves, W.R., S.J. Mulvihill, and D.W. Deamer, *Synthesis of phospholipids and membranes in prebiotic conditions*. Nature, 1977. **266**(5597): p. 78-80.
65. Rao, M., M.R. Eichberg, and J. Oro, *Synthesis of phosphatidylcholine under possible primitive earth conditions*. Journal of molecular evolution, 1982. **18**(3): p. 196-202.
66. Allen, W.V. and C. Ponnampereuma, *A possible prebiotic synthesis of monocarboxylic acids*. Currents in modern biology, 1967. **1**(1): p. 24-8.
67. Goto, K., et al., *Synthesis of hydrocarbons under presumed prebiotic conditions using high-frequency discharge*. Journal of molecular evolution, 1986. **23**(2): p. 113-118.
68. McCollom, T.M., G. Ritter, and B.R. Simoneit, *Lipid synthesis under hydrothermal conditions by Fischer-Tropsch-type reactions*. Orig Life Evol Biosph, 1999. **29**(2): p. 153-66.
69. Larralde, R., M.P. Robertson, and S.L. Miller, *Rates of decomposition of ribose and other sugars: implications for chemical evolution*. Proceedings of the National Academy of Sciences of the United States of America, 1995. **92**(18): p. 8158-60.
70. Levy, M. and S.L. Miller, *The stability of the RNA bases: implications for the origin of life*. Proceedings of the National Academy of Sciences of the United States of America, 1998. **95**(14): p. 7933-8.
71. Yuen, G.U. and K.A. Kvenvolden, *Monocarboxylic Acids in Murray and Murchison Carbonaceous Meteorites*. Nature, 1973. **246**(5431): p. 301-303.
72. Naraoka, H., A. Shimoyama, and K. Harada, *Molecular distribution of monocarboxylic acids in Asuka carbonaceous chondrites from Antarctica*. Orig Life Evol Biosph, 1999. **29**(2): p. 187-201.
73. Gebicki, J.M. and M. Hicks, *Ufasomes are stable particles surrounded by unsaturated fatty acid membranes*. Nature, 1973. **243**(5404): p. 232-4.
74. Gebicki, J.M. and M. Hicks, *Preparation and properties of vesicles enclosed by fatty acid membranes*. Chemistry and physics of lipids, 1976. **16**(2): p. 142-60.
75. Hargreaves, W.R. and D.W. Deamer, *Liposomes from ionic, single-chain amphiphiles*. Biochemistry, 1978. **17**(18): p. 3759-3768.
76. Deamer, D.W., *Boundary structures are formed by organic components of the Murchison carbonaceous chondrite*. Nature, 1985. **317**(6040): p. 792-794.
77. Cistola, D.P., et al., *Ionization and phase behavior of fatty acids in water: application of the Gibbs phase rule*. Biochemistry, 1988. **27**(6): p. 1881-8.

78. Haines, T.H., *Anionic lipid headgroups as a proton-conducting pathway along the surface of membranes: a hypothesis*. Proc Natl Acad Sci U S A, 1983. **80**(1): p. 160-4.
79. Maurer, S.E., et al., *Chemical evolution of amphiphiles: glycerol monoacyl derivatives stabilize plausible prebiotic membranes*. Astrobiology, 2009. **9**(10): p. 979-87.
80. Berclaz, N., et al., *Growth and Transformation of Vesicles Studied by Ferritin Labeling and Cryotransmission Electron Microscopy*. The Journal of Physical Chemistry B, 2001. **105**(5): p. 1056-1064.
81. Hanczyc, M.M., S.M. Fujikawa, and J.W. Szostak, *Experimental models of primitive cellular compartments: encapsulation, growth, and division*. Science, 2003. **302**(5645): p. 618-22.
82. Hanczyc, M.M., S.S. Mansy, and J.W. Szostak, *Mineral surface directed membrane assembly*. Orig Life Evol Biosph, 2007. **37**(1): p. 67-82.
83. Clint, J.H., *Surfactant Aggregation* 1992, Glasgow and London: Blackie.
84. Budin, I. and J.W. Szostak, *Expanding roles for diverse physical phenomena during the origin of life*. Annual review of biophysics, 2010. **39**: p. 245-63.
85. Baaske, P., et al., *Extreme accumulation of nucleotides in simulated hydrothermal pore systems*. Proceedings of the National Academy of Sciences of the United States of America, 2007. **104**(22): p. 9346-51.
86. Duhr, S. and D. Braun, *Why molecules move along a temperature gradient*. Proceedings of the National Academy of Sciences of the United States of America, 2006. **103**(52): p. 19678-82.
87. Budin, I., R.J. Bruckner, and J.W. Szostak, *Formation of protocell-like vesicles in a thermal diffusion column*. Journal of the American Chemical Society, 2009. **131**(28): p. 9628-9.
88. Shinoda, K., *The Critical Micelle Concentration of Soap Mixtures (Two-Component Mixture)*. The Journal of Physical Chemistry, 1954. **58**(7): p. 541-544.
89. Clint, J.H., *Micellization of mixed nonionic surface active agents*. Journal of the Chemical Society, Faraday Transactions 1: Physical Chemistry in Condensed Phases, 1975. **71**: p. 1327-1334.
90. Kamp, F. and J.A. Hamilton, *pH gradients across phospholipid membranes caused by fast flip-flop of un-ionized fatty acids*. Proceedings of the National Academy of Sciences of the United States of America, 1992. **89**(23): p. 11367-70.

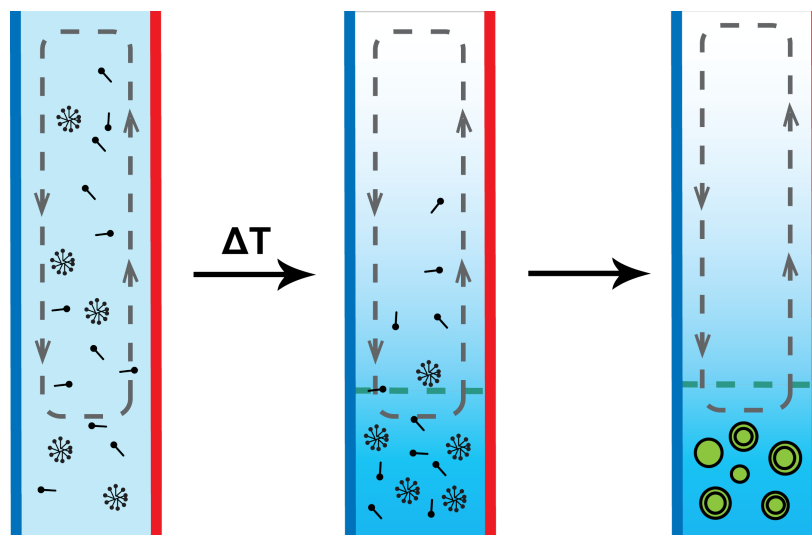
91. Zhang, F., F. Kamp, and J.A. Hamilton, *Dissociation of long and very long chain fatty acids from phospholipid bilayers*. *Biochemistry*, 1996. **35**(50): p. 16055-60.
92. Kamp, F., et al., *Fatty acid flip-flop in phospholipid bilayers is extremely fast*. *Biochemistry*, 1995. **34**(37): p. 11928-37.
93. Chen, I.A. and J.W. Szostak, *Membrane growth can generate a transmembrane pH gradient in fatty acid vesicles*. *Proc Natl Acad Sci U S A*, 2004. **101**(21): p. 7965-70.
94. Rasi, S., F. Mavelli, and P.L. Luisi, *Matrix effect in oleate micelles-vesicles transformation*. *Orig Life Evol Biosph*, 2004. **34**(1-2): p. 215-24.
95. Chen, I.A. and J.W. Szostak, *A kinetic study of the growth of fatty acid vesicles*. *Biophys J*, 2004. **87**(2): p. 988-98.
96. Chen, I.A., R.W. Roberts, and J.W. Szostak, *The emergence of competition between model protocells*. *Science*, 2004. **305**(5689): p. 1474-6.
97. Budin, I. and J.W. Szostak, *Physical effects underlying the transition from primitive to modern cell membranes*. *Proceedings of the National Academy of Sciences of the United States of America*, 2011. **108**(13): p. 5249-54.
98. Zhu, T.F. and J.W. Szostak, *Coupled Growth and Division of Model Protocell Membranes*. *J Am Chem Soc*, 2009. **131**(15): p. 5705-5713.
99. Bar-Ziv, R. and E. Moses, *Instability and "pearling" states produced in tubular membranes by competition of curvature and tension*. *Phys Rev Lett*, 1994. **73**(10): p. 1392-1395.
100. Bar-Ziv, R., T. Tlusty, and E. Moses, *Critical Dynamics in the Pearling Instability of Membranes*. *Physical Review Letters*, 1997. **79**(6): p. 1158.
101. Leaver, M., et al., *Life without a wall or division machine in Bacillus subtilis*. *Nature*, 2009. **457**(7231): p. 849-53.
102. Kandler, G. and O. Kandler, *Untersuchungen über die Morphologie und die Vermehrung der pleuropneumonie-ähnlichen Organismen und der L-Phase der Bakterien*. *Archives of Microbiology*, 1954. **21**(2): p. 178-201.
103. Kandler, G., O. Kandler, and O. Huber, *Untersuchungen über die Morphologie und die Vermehrung der pleuropneumonieähnlichen Organismen und der L-Phase der Bakterien*. *Archives of Microbiology*, 1954. **21**(2): p. 202-216.
104. Mansy, S.S., et al., *Template-directed synthesis of a genetic polymer in a model protocell*. *Nature*, 2008. **454**(7200): p. 122-5.



105. Chen, I.A., K. Salehi-Ashtiani, and J.W. Szostak, *RNA catalysis in model protocell vesicles*. Journal of the American Chemical Society, 2005. **127**(38): p. 13213-9.
106. Mansy, S.S. and J.W. Szostak, *Thermostability of model protocell membranes*. Proc Natl Acad Sci U S A, 2008. **105**(36): p. 13351-5.
107. Sacerdote, M.G. and J.W. Szostak, *Semipermeable lipid bilayers exhibit diastereoselectivity favoring ribose*. Proc Natl Acad Sci U S A, 2005. **102**(17): p. 6004-8.
108. Lu, Y.J., et al., *Acyl-phosphates initiate membrane phospholipid synthesis in Gram-positive pathogens*. Molecular cell, 2006. **23**(5): p. 765-72.
109. Bryant, D.E., et al., *On the prebiotic potential of reduced oxidation state phosphorus: the H-phosphinate-pyruvate system*. Chemical Communications, 2010. **46**(21): p. 3726-3728.
110. Pasek, M.A., 2012.
111. Apel, C. and D. Deamer, *The Formation Of Glycerol Monodecanoate By A Dehydration Condensation Reaction: Increasing The Chemical Complexity Of Amphiphiles On The Early Earth*. Origins of Life and Evolution of Biospheres, 2005. **35**(4): p. 323-332.
112. Li, N. and F. Huang, *Ribozyme-Catalyzed Aminoacylation from CoA Thioesters*, *Ā*. Biochemistry, 2005. **44**(11): p. 4582-4590.
113. Kolb, H.C., M.G. Finn, and K.B. Sharpless, *Click Chemistry: Diverse Chemical Function from a Few Good Reactions*. Angewandte Chemie International Edition, 2001. **40**(11): p. 2004-2021.
114. Budin, I. and N.K. Devaraj, *Membrane assembly driven by a biomimetic coupling reaction*. Journal of the American Chemical Society, 2012. **134**(2): p. 751-3.
115. Westheimer, F., *Why nature chose phosphates*. Science, 1987. **235**(4793): p. 1173-1178.
116. Pohorille, A. and D. Deamer, *Self-assembly and function of primitive cell membranes*. Research in Microbiology, 2009. **160**(7): p. 449-456.
117. Janas, T., T. Janas, and M. Yarus, *A membrane transporter for tryptophan composed of RNA*. RNA, 2004. **10**(10): p. 1541-1549.
118. Unrau, P.J. and D.P. Bartel, *RNA-catalyzed nucleotide synthesis*. Nature, 1998. **395**(6699): p. 260-3.
119. Ejsing, C.S., et al., *Global analysis of the yeast lipidome by quantitative shotgun mass spectrometry*. Proceedings of the National Academy of Sciences, 2009. **106**(7): p. 2136-2141.

## Chapter 2: Formation of protocell-like vesicles in a thermal diffusion column

Itay Budin, Raphael J. Bruckner, and Jack W. Szostak



*Note: a version of the following was published in the Journal of the American Chemical Society.*

**Abstract:** Many of the properties of bilayer membranes composed of simple single-chain amphiphiles seem to be well-suited for a potential role as primitive cell membranes. However, the spontaneous formation of membranes from such amphiphiles is a concentration-dependent process in which a significant critical aggregate concentration ( $c_{ac}$ ) must be reached. Since most scenarios for the prebiotic synthesis of fatty acids and related amphiphiles would result in dilute solutions well below the  $c_{ac}$ , the identification of mechanisms that would lead to increased local amphiphile concentrations is an important aspect of defining reasonable conditions for the origin of cellular life. Narrow, vertically oriented channels within the mineral precipitates of hydrothermal vent towers have previously been proposed to act as natural Clusius–Dickel thermal diffusion columns, in which a strong transverse thermal gradient concentrates dilute

molecules through the coupling of thermophoresis and convection. Here we experimentally demonstrate that a microcapillary acting as a thermal diffusion column can concentrate a solution of oleic acid. Upon concentration, self-assembly of large vesicles occurs in regions where the cac is exceeded. We detected vesicle formation by fluorescence microscopy of encapsulated dye cargoes, which simultaneously concentrated in our channels. Our findings suggest a novel means by which simple physical processes could have led to the spontaneous formation of cell-like structures from a dilute prebiotic reservoir.

## **Introduction**

Lipid membrane encapsulation is ubiquitous in biology and is thought to have been an essential aspect of the earliest cell-like structures (1). Bilayer membranes composed of simple single-chain amphiphiles, such as fatty acids, seem to be well-suited for a potential role as primitive cell membranes (2,3). However, the spontaneous formation of such membranes can only occur above a critical aggregate concentration (cac) (Table S1 in the Supporting Information). Since most scenarios for the prebiotic synthesis of fatty acids and related amphiphiles would result in dilute solutions well below the cac (4) the identification of mechanisms that would lead to increased local amphiphile concentrations is an important aspect of defining reasonable conditions for the origin of cellular life.

Recently, Baaske et al. (5) proposed that temperature gradients generated in deep-sea alkaline vents could have greatly concentrated diverse molecular species in a prebiotic setting. Vertically oriented microchannels within the carbonate rock precipitates are proximal to both hot vent

water and cold ocean water (6). A lateral thermal gradient across a vertical channel results in convective flow (as heated fluid rises and cooled fluid sinks) and concurrent thermal diffusion (thermophoresis) of molecules along the temperature gradient (Figure 1A). It has been known since the 1930s that coupling of thermophoresis and convective flows can lead to differential concentration effects in both gases and liquid solvents (7, 8). Thermal diffusion columns (or Clusius–Dickel separations) were used for industrial purifications during the middle of the 20th century (9). Using experimentally measured thermal diffusion coefficients, Baaske et al. performed simulations suggesting that nucleotides and nucleic acid oligomers could be locally concentrated in the prebiotic vent context outlined above. Here we experimentally demonstrate that a microcapillary thermal diffusion column can concentrate dilute solutions of nucleotides, oligonucleotides, and fatty acids. Upon concentration, the self-assembly of large vesicles containing encapsulated DNA occurs in regions where the cac of the fatty acid is exceeded. Our findings suggest a novel means by which simple physical processes could have led to the spontaneous formation of cell-like structures from a dilute prebiotic reservoir.

## **Results**

To mimic the narrow channels found in vent formations, we used square borosilicate microcapillaries. Each capillary was loaded with an initial solution and attached to a reservoir with a volume ~150 times greater than the capillary volume. We then applied a temperature gradient by clamping the capillary between a heat source and a heat sink kept at constant temperatures. Convective, unicellular flow was confirmed by visualization of the flow pattern of

2  $\mu\text{m}$  polystyrene beads in capillaries under a temperature gradient (Movie S1 in the Supporting Information).

Within 24 h at a thermal gradient ( $\Delta T$ ) of 30 K, linear capillaries exhibited a significant concentrating effect, with a bottom-to-top concentration gradient of  $\sim 800$ -fold as measured for the nonquenching fluorescent dye 8-hydroxypyrene-1,3,6-trisulfonic acid salt (HPTS) (Figure 1B). On our experimental time scale, concentration was primarily due to depletion of solute from the upper region of the capillary (Text S1 in the Supporting Information). We expect that over longer time periods, concentration would continue via the accumulation of molecules from the reservoir.

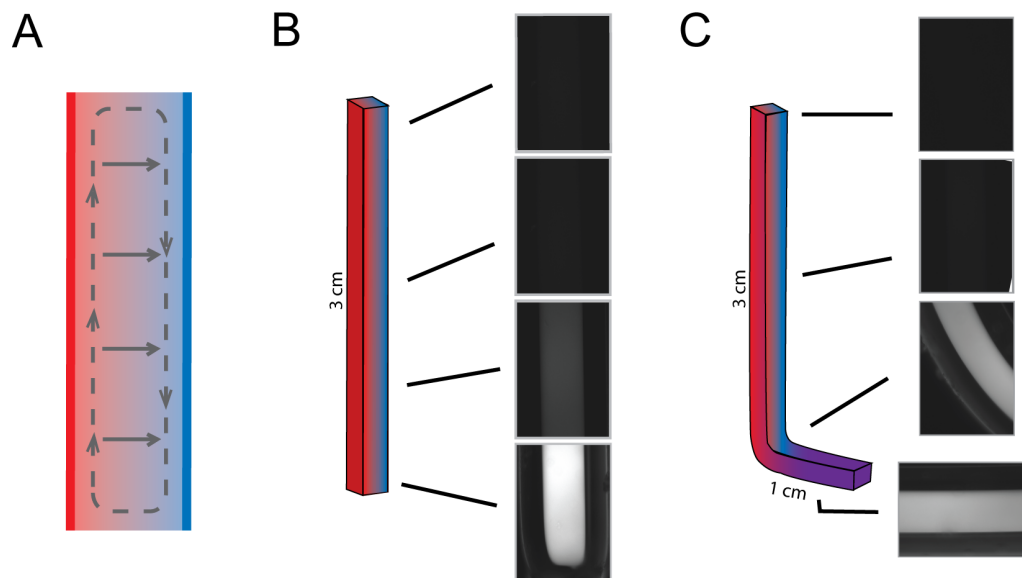


**Figure 1:** Microcapillary thermal diffusion columns concentrate small molecules. (A) Schematic diagram of a thermal diffusion column showing coupling of convective flow (dashed path) and thermophoresis (solid arrows). (B) Fluorescence microscopy images of a linear capillary ( $\sim 3$  cm length,  $200 \mu\text{m}$  i.d., initially loaded with  $30 \mu\text{M}$  HPTS) after 24 h at  $\Delta T = 30$  K, revealing a strong concentration gradient of HPTS from top to bottom in the capillary. (C) Image of a bent capillary run under identical conditions. The protruding portion (purple) was kept at  $4^\circ\text{C}$  and acted as a reservoir for the accumulation of the concentrated molecules.

We observed a similar concentration effect with fluorescently labeled nucleic acids. This effect was enhanced with increasing molecular size (Table 1). The difference in the accumulations of mono- and oligonucleotides is due to the dependence of the Soret coefficient [the ratio of thermal diffusivity (DT) to molecular diffusivity (D)] on polymer length and was qualitatively predicted by simulation (5) In addition, there was a large inhibitory effect of salt on the concentration effect, as predicted by measured Soret coefficients (10) (Table 1 and Figure S1 in the Supporting Information). Oceanic salt concentrations are very high (~0.5 M) and could have been even higher ( $\geq 0.7$  M) during the late Hadean era (11, 12). Salt concentrations in this range would have limited the effectiveness of thermophoresis as a concentration mechanism in marine environments. Analogous fresh-water hydrothermal systems might therefore have provided a much more robust concentrating effect.

**Table 1:** Bottom-to-Top Accumulation of Solutes in a Linear Microcapillary<sup>a</sup>

	HPTS	dCTP <sup>b</sup>	dA 20mer <sup>c</sup>
low salt <sup>d</sup>	$8 \times 10^2$	$10^3$	$10^4$
high salt <sup>e</sup>	25	65	110

<sup>a</sup> Indicated solutes ran at 20-40  $\mu$ M and  $\Delta T = 30$  K for 24 hours. Concentration visualized along the capillary by quantitative fluorescence microscopy. <sup>b</sup> Fluorescently labeled with Cy3. <sup>c</sup> Fluorescently labeled with fluorescein. <sup>d</sup> 10 mM Tris pH 7.5. <sup>e</sup> 10 mM Tris pH 7.5, 100 mM NaCl.

As it is unlikely that microchannels with such large aspect ratios would be oriented to maintain a uniform thermal gradient throughout, we explored the properties of an alternative capillary geometry. We prepared capillaries bent at 90° near the bottom, with a short (~1 cm) length extending away from the temperature gradient. This design led to solute accumulation in the

protruding portion of the capillary, over which there was no temperature gradient (Figure 1C and Figure S1), as dye first concentrated near the bottom of the vertical segment and then diffused into the adjacent horizontal segment. Such a geometry could therefore result in a low-temperature, high-concentration reservoir of molecules initially concentrated in a thermal diffusion column (e.g., see Figure 4 in ref (5)).

In order to investigate concentration-dependent vesicle self-assembly, we first showed that fatty acids can become highly concentrated within thermal diffusion columns. Linear capillaries were loaded with 60  $\mu\text{M}$   $^3\text{H}$ -labeled oleate at pH 11 to prevent vesicle assembly. The capillaries were incubated at  $\Delta T = 30$  K for 24 h and then fractionated, after which the oleate concentrations were determined by liquid scintillation. Fractions (0.75 cm or 300 nL) from the bottom of the capillary showed a 5-fold accumulation over those taken from the top (Figure S2). The concentration of fatty acids in a thermal diffusion column leads to the possibility of vesicle formation from a dilute solution. However, the convective flow running along the concentration gradient poses a problem, in that newly formed vesicles would be carried up the capillary, where they would dissolve as a result of the low local fatty acid concentration.

To circumvent the destructive effects of convective flow, we utilized the bent capillary geometry described above. We were able to visualize the formation of multilamellar vesicles after incubation for 48 h at  $\Delta T = 30$  and pH  $\sim 8.5$  (Figure 2). These vesicles adhered to the glass wall and were unusually large and monodisperse (Text S2). We confirmed that these structures were indeed vesicles by the encapsulation of fluorescent dye, which was included in the starting solution. After incubation, the capillaries were gently purged with dye-free buffer, leaving only

the vesicle-encapsulated cargo to be visualized (Figure 2B). We used a similar protocol to demonstrate that such vesicles can encapsulate fluorescently tagged DNA oligomers (Figure S3).

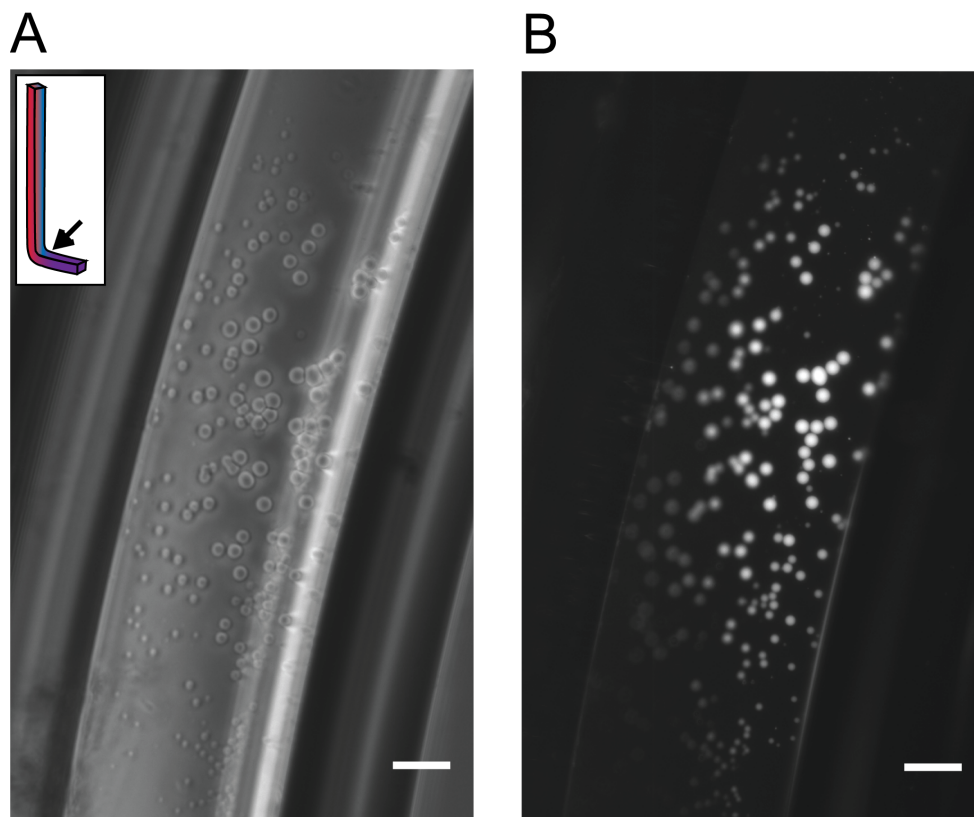


**Figure 2:** Locally concentrated oleate forms vesicles in bent capillaries incubated at  $\Delta T = 30$  for 48 h. (A) Phase-contrast image of a bent capillary loaded with  $70 \mu\text{M}$  buffered oleate and  $40 \mu\text{M}$  HPTS. The oleate concentrated in the capillary and formed large vesicles. (B) Fluorescence image of the same frame. HPTS in the solution was washed away with dye-free buffer, leaving only encapsulated cargo to be visualized. Scale bars =  $50 \mu\text{m}$ .

## Discussion

Recent protocell models are based on fatty acid vesicles containing encapsulated nucleic acid polymers capable of self-replication (13). Our experiments demonstrate that thermal gradients across narrow channels can provide the energy necessary to concentrate dilute molecular



solutions and thus allow the self-assembly of cell-like structures from an initially homogeneous dilute solution. They also highlight the potential hazards (and advantages) of self-assembly in environments where building blocks are concentrated only locally. While the dynamic properties of fatty acids are necessary for protocell growth, division, and solute permeability (3, 13) the same dynamic properties dictate that fatty acid bilayer membranes are not kinetically trapped structures. Any prolonged disruption of the temperature gradient (and thus the concentration gradient) would cause the system to equilibrate to an isotropic state with consequent dissolution of the vesicles. In such a variable environment, early cellular life might have been discontinuous, with the genetic information alternately residing within protocells and free in solution. Occasional disruption of the cellular state followed by re-encapsulation of genetic molecules could have allowed genetic exchange (recombination) or provided a means for genetic molecules to migrate to new niches. Such a variable environment would also impose a strong selective pressure for the evolution of a more stable cellular state, perhaps based on the evolution of the catalytic machinery for the synthesis of more complex chemical components, such as diacyl lipids. In view of the chasm between the complexity of fundamental cellular processes and the simple systems from which they must have once arisen, further study of relevant physical processes will lead to important clues as to how life first began.

## **Acknowledgments**

R.J.B. was supported by a fellowship from the Harvard Origins Initiative. This work was supported in part by Grant EXB02-0031-0018 from the NASA Exobiology Program. J.W.S. is an Investigator of the Howard Hughes Medical Institute. The authors thank Dr. H. Stone, Dr. J.

Higgins, and S. Tobé for helpful discussions and Dr. A. Ricardo, M. Elenko, T. Zhu, and Q. Dufton for comments on the manuscript.

## References

1. Szostak, J.W.; Bartel, D.P.; Luisi, P.L. *Nature* **2001**, 409, 387-90.
2. Hanczyc, M.M.; Fujikawa, S.M.; Szostak, J.W. *Science* **2003**, 302, 618-22.
3. Zhu, T.; Szostak, J.W. *J. Am. Chem. Soc.* **2009**, Article ASAP, DOI: 10.1021/ja900919c.
4. Rushdi, A.I.; Simoneit B.R.T. *Orig. Life. Evol. Biosph.* **2001**, 31, 103-18.
5. Baaske, P.; Weinert, F.M.; Duhr, S.; Lemke, K.H.; Russell, M.J.; Braun, D. *Proc. Natl. Acad. Sci. USA.* **2007**, 104, 9346-51.
6. Kelley, D.S.; *et. al.* *Nature* **2001**, 412, 145-9.
7. Clusius, K.; Dickel, G. *Naturewissenschaften* **1938**, 26, 546.
8. Furry, W.H.; Onsager, L. *Phys. Rev. Lett.* **1939**, 55, 1083-95.
9. Jones, A.C.; Milberger, E.C. *Ind. & Eng. Chem.* **1953**, 45, 2689-96.
10. Duhr, S.; Braun, D. *Proc. Natl. Acad. Sci. USA.* **2006**, 103, 19678-82.
11. Holland, H.D. *The Chemical Evolution of the Atmosphere and Oceans*; Princeton University Press: Princeton, 1984, 110-1.
12. Knauth, L.P. *Paleo* **2005**, 219, 53-69.
13. Mansy, S.S.; Schrum, J.P.; Krishnamurthy, M.; Tobé, S.; Treco, D.A.; Szostak, J.W. *Nature* **2008**, 454, 122-5.

## Supporting Information

Includes Materials and Methods, Text S1-S2 with references, Table S1 with references, Figures S1-S5, and Movie S1.

### Materials and Methods

**Thermal diffusion columns:** Borosilicate microcapillaries (VitroCom, Mountain Lakes, NJ) with a square cross section (ID 200  $\mu\text{m}$ , OD 400  $\mu\text{m}$ ) were cut to  $\sim 3$  cm and sealed via microforge (Narishige, Japan). Bent capillaries were cut to  $\sim 4$  cm, shaped over an open flame, with a 90° corner 3 cm from the top, and sealed with epoxy. All capillaries were attached to 100-200  $\mu\text{L}$  reservoirs with epoxy. Linear capillaries were loaded with the starting solution via centrifugation (2000 rpm for 15 minutes in a custom built holder). Bent capillaries were loaded by pipette before being sealed.

**Thermal gradient:** Capillaries with attached reservoirs were loaded with an initial solution and clamped between a heat source and sink in a custom built apparatus. The heat source block was attached to a high performance hot plate (IKA, Wilmington, NC) to maintain a constant temperature, which was monitored by a temperature probe attached to the block. The sink was cooled by coolant circulation from a ultra-low temperature cold bath (Thermo Scientific, Waltham, MA). Since the insulating glass walls of the capillary were relatively thick, the temperature gradient across the solution was significantly lower than that between the hot and cold blocks. Therefore temperature gradients across the solution ( $\Delta T$ ) were calculated by

modeling steady state heat conduction across a composite slab (1). Taking the heat flux across the solution as equal to the total heat flux:

$$\frac{\Delta T}{\left(\frac{ID}{k_w}\right)} = \frac{T_H - T_C}{\left(\frac{OD - ID}{k_g} + \frac{ID}{k_w}\right)}$$

Where  $T_H$  and  $T_C$  are the heat sink temperatures and  $k_w$  and  $k_g$  are the thermal conductivities for water (0.6 W/mK) and borosilicate glass (1.13 W/mK). Solving for the temperature difference across the solution:

$$\Delta T = \frac{ID(T_H - T_C)}{\frac{k_w}{k_g}(OD - ID) + ID}$$

Since  $ID = (OD - ID) = 200 \mu\text{m}$

$$\Delta T = \frac{T_H - T_C}{\frac{k_w}{k_g} + 1}$$

Therefore, for a  $\Delta T$  of 30 K, we set  $T_H - T_C = 45$ ; the heat source was kept at 50° C and the sink at 5° C.

**Solutions:** Oleate (Nu-chek Prep, Eugene, OR) solutions were prepared either by evaporation and rehydration of a stock solution in methanol, or by dilution of an 80  $\mu\text{M}$  stock solution in buffer. Unless otherwise noted, all oleate solutions were buffered by 0.2 M Bicine (Sigma-Aldrich, St. Luis, MO), titrated with NaOH to pH 8.5. Bulk vesicle preparations were made by dissolving oleate in buffer followed by gentle shaking overnight. For fluorescence accumulation experiments, the following solutes were used: HPTS (Sigma-Aldrich), 20 bp poly-A DNA with a

5' carboxyfluorescein modification (Integrated DNA Technologies, Coralville, IA), and Cy3-dCTP (GE Biosciences, Britain). For bilayer staining experiments, Rhodamine 6G (Sigma-Aldrich) was included in the vesicle solution at 2 nM.

**Capillary imaging:** Capillaries were viewed with a Nikon TE2000S inverted epifluorescence microscope with extra long working distance (ELWD) objective lenses. The illumination source was either a bright field lamp through a phase contrast filter (Nikon) or a metal halide lamp (EXFO, Canada) with a  $480\pm 20$  nm (for HPTS and labeled oligomers) or a  $546\pm 5$  nm (for Cy3-dCTP and Rhodamine staining) optical filter. Fluorescence emission was filtered either at  $535\pm 25$  nm (for HPTS and labeled oligomers) or 590 nm long pass (for Cy3-dCTP and Rhodamine staining). Images were taken with a CCD camera (Hamamatsu Photonics, Japan) and processed with commercial software (Phylum Live, Lexington, MA and ImageJ, NIH). Fluorescence was quantified using the image analysis software ImageJ and normalized to the corresponding value for the initial starting solution. Standard curves for fluorescent solutes were used to ensure that fluorescence was linearly dependent on concentration in the ranges used.

**Capillary streamline visualization:** Dye-labeled (Dragon Green)  $1.90\ \mu\text{m}$  microspheres (Bangs Laboratories, Fishers, IN) were diluted 100-fold in a 1:1 solution of water and deuterium oxide (final density = 1.05 g/mL). The capillary was loaded with this solution and imaged with a CMOS camera (Vision Research, Wayne, NJ) connected to an ELWD 10x objective (Nikon) through an InfiniTube (Infinity, Boulder, CO). The microspheres were illuminated with a hand-held UV lamp that was directed orthogonally to the camera path.

**Oleate accumulation:**  $^3\text{H}$ -Oleate (Moravek Biochemicals, Brea, CA) in methanol was evaporated and resuspended in water with one mole equivalent of NaOH. The resulting solution of labeled micelles was loaded into a linear capillary and subjected to a temperature gradient for 24 hours. The capillary was then fractionated into 0.75 cm lengths using forceps and a wire cutter. Fractions were crushed in 100  $\mu\text{L}$  water to disperse the solution and centrifuged to remove the glass (12,000 RPM for 10 minutes). The supernatant was then added to 2 mL of scintillation cocktail (MP Biomedicals, Costa Mesa, CA). Counts were read using a Beckman Coulter LS6500 scintillation counter and normalized to values taken from an equivalent volume of 60  $\mu\text{M}$   $^3\text{H}$ -oleate.

**Vesicle imaging:** Vesicle cargo encapsulation was visualized by gently replacing the buffer in the capillary with dye-free buffer. The sealed bottom of the capillary was first snapped off and the reservoir was loaded with a buffered solution of 80  $\mu\text{M}$  oleate (equal to the cac; to prevent vesicle dissolution). The dye-free buffer was then allowed to flow through the capillary by gravity until  $> 2$  mL of buffer ( $\sim 1000$  times the capillary volume) had flowed through. Alternatively, cargo-free vesicles and bulk vesicle preparations were visualized with Rhodamine 6G membrane staining.

### **Text S1: Analysis of solute transport into a microcapillary**

On our experimental time scale (24-48 hours), concentration was achieved primarily by local redistribution of the initial solute in the capillary, not by accumulation of solute from the reservoir. Therefore, regions of the capillary near the top were almost completely depleted of

solute. This significantly limited the absolute concentration that could be achieved in our capillaries: while we were able to achieve concentration gradients (bottom/top final concentrations) of over 1000 fold, the absolute concentration at the bottom of the capillary was only ~10 fold higher than the initial concentration. However, over much longer times, we would expect continued diffusion of solute from the reservoir into the capillary to result in much higher solute concentrations at the bottom of the capillary, assuming a dilute starting solution. Therefore, although vesicle formation in our experiments was limited to initial oleate concentrations > 30  $\mu\text{M}$ , over long time scales we expect that sub- $\mu\text{M}$  initial concentrations would still allow oleate to accumulate to concentrations above the cac.

This technical limitation of our experimental system was due to the slow diffusion of molecules from the reservoir into the top of the capillary, at which point they could enter the convective flow. There was a gap of ~0.5 cm between the reservoir and the onset of the thermal gradient in the capillary across which the solute (DNA nucleotide and oligomer, oleate micelle) from the reservoir had to diffuse. We can model this transport as a one-dimensional diffusive flux at steady state:

$$J_{A,x} = D \cdot A \cdot \frac{dC}{dx} = D \cdot A \cdot \frac{C_{\text{reservoir}} - C_{\text{capillary,top}}}{d_{\text{res,cap}}}$$

where A is the cross sectional area of the capillary and  $d_{\text{res,cap}}$  is the distance from the reservoir to the capillary (~0.5 cm). D is the molecular diffusion coefficient:  $4 \times 10^{-6} \text{ cm}^2/\text{s}$  for a single nucleotide (S2),  $10^{-6} \text{ cm}^2/\text{s}$  for an ~20mer oligonucleotide (S2), and  $2.8 \times 10^{-6} \text{ cm}^2/\text{s}$  for an oleate micelle (S3). Taking the top concentration as ~0 (totally depleted) and the reservoir concentration at 40  $\mu\text{M}$ , the flux from the reservoir into the capillary was 11 picomoles/day of the single nucleotides, 7 picomoles/day of the 20mer, and 20 picomoles/day of oleate. That

represents 23%, 6%, and 12%, respectively, of the initial solute in the capillaries. Therefore, over the time course of our experiments (~24 hours), the amount of a new solute diffusing from the reservoir into the capillary was small compared to the amount of solute that was initially loaded into the capillary.

### **Text S2: Description and analysis of vesicle formation**

Unexpectedly, the vesicles that formed in the bent capillaries were quite large: up to ~6  $\mu\text{m}$ , with their size dependent on the starting oleate concentration (Figure S4). They assembled in discrete, adherent populations, with a surprising degree of size uniformity. As expected, the number of vesicles was significantly increased by using a low salt buffer, likely due to increased oleate accumulation (Figure S5). Because of the diffusion limitation discussed above, the concentration of oleate was largely limited by the redistribution of the oleate within the capillary itself. Therefore, if we assume all of the oleate in the capillary was concentrated into the extruded portion, the maximum oleate concentration was ~280  $\mu\text{M}$  for a starting concentration of 70  $\mu\text{M}$ . Concentrations in this range form far smaller vesicles in bulk preparations (Figure S4C). Higher concentration solutions, which can form large vesicles, produce highly polydisperse populations (Figure S4D).

We attribute these unusual features to the mechanism by which the vesicles formed in our experiments. The fatty acid accumulation in the capillary extended into the protruding segment, where the convective flow is blocked by the geometry and absence of the temperature gradient. Here, nascent vesicles were able to nucleate in the absence of convective flow. As fatty acids



continued to concentrate, they preferentially incorporated into the pre-formed vesicles instead of nucleating newer vesicles, a kinetically slower process (S4). Our group has previously noticed that when adding micelles to a buffered vesicle solution, the efficiency of vesicle growth (as opposed to new vesicle nucleation) increases with lower micelle addition rates (S4). Here, the thermal diffusion column accumulates low concentrations of fatty acids extremely slowly (over the course of hours), which would strongly favor growth of existing vesicles over the nucleation of new vesicles. Thus, an initial population of small nascent vesicles all underwent similar growth by the incorporation of continuously accumulating fatty acids. This led to a relatively small number of large monodisperse vesicles. The adherence of the vesicles could have further assisted vesicle survival by preventing diffusion back into the convective flow. However, the surface adsorption of the vesicles was not permanent; a small portion of the large vesicles could be seen to exhibit Brownian motion (and were thus detached from the glass) in our experiments. Extended incubation at room temperature led to additional vesicles detaching into the solution.

It is also important to note that vesicle formation is not specific to the geometry we used, but rather would be promoted by any method of disrupting the convective flow from running along the concentration gradient. For example, we observed vesicles in linear capillaries in which there were unintended blockages of the convective flow due to a large particle or an air bubble. Another possible approach is altering the diameter of the capillaries to allow for the thermophoretic trapping of newly formed vesicles, thereby preventing them from flowing back into the low concentration region. Capillaries with narrower diameters are predicted to more efficiently concentrate large, aggregate structures, such as vesicles (S2). However, a narrower capillary would also be less efficient at concentrating fatty acids below the  $cac$ , which are present

as more diffusive monomers and micelles. Thus, lipid polymorphism represents a unique problem for thermal accumulation, which we were able to circumvent by geometrically disrupting the convective flow. An alternative approach might be to use capillaries with variable diameters, so that dilute fatty acids are efficiently concentrated and newly formed vesicles remain thermophoretically trapped in the high concentration region.

### Table S1

**Table 1:** Approximate critical aggregation concentrations (cac) for prebiotically relevant lipids.

Decanoic acid (C10)	Myristoleic acid (C14:1)	Myristoleic acid with monomyristolein (2:1)	Palmitoleic acid (C16:1)	Oleic acid (C18:1)	Phospholipids
100 mM <sup>5</sup>	4 mM <sup>6</sup>	1 mM <sup>7</sup>	250 μM <sup>8</sup>	80 μM <sup>9</sup>	< 10 nM <sup>10</sup>

Figures S1-S5

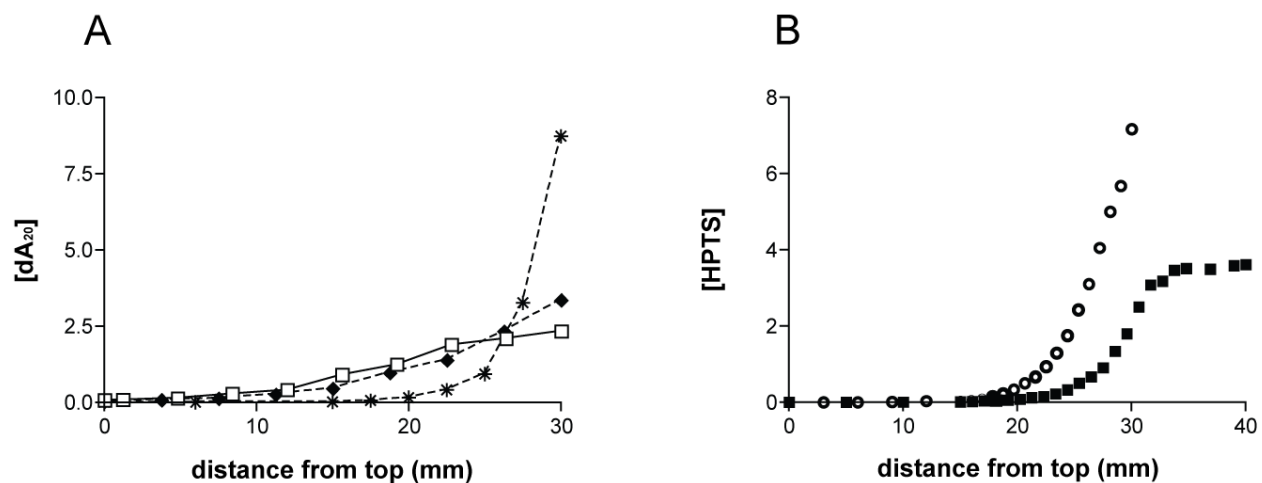


**Figure S1.** Effect of salt concentration and capillary geometry on concentration in thermal diffusion columns. (A) Redistribution of fluorescently labeled DNA 20mer in 3 cm linear capillaries incubated at  $\Delta T = 30$  K for 24 hours. Individual experiments were performed at 10 mM Tris 7.5 with (\*) no added salt ( $\blacklozenge$ ) 100 mM NaCl and ( $\square$ ) 250 mM NaCl (connecting lines added for clarity). (B) Effect of capillary geometry on concentration of HPTS at  $\Delta T = 30$  K for 24 hours in 10 mM Tris 7.5. (o) Linear capillary (3 cm length) ( $\blacksquare$ ) Bent capillary with a 3 cm vertical length and a 1 cm isothermal orthogonal protrusion. Accumulation extends into and is kept constant in the protruding portion (30-40 mm). All concentrations normalized to the initial solute concentration in the capillary before incubation.

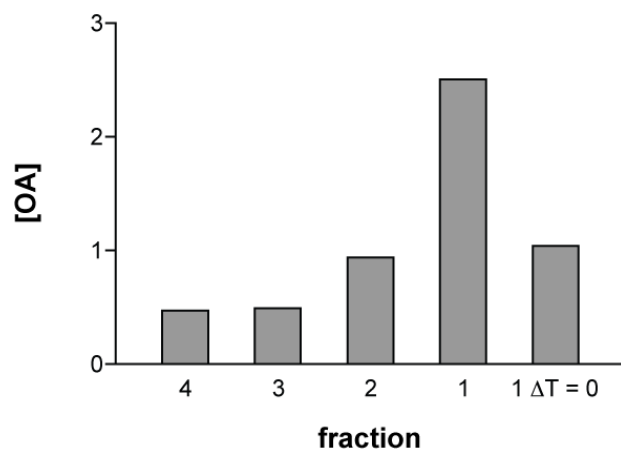


**Figure S2.** Microcapillary thermal diffusion column concentrates oleic acid.  $60 \mu\text{M}$   $^3\text{H}$  oleate at pH 11 after 24 hours was run in a linear microcapillary at  $\Delta T = 30 \text{ K}$ . The capillary was fractionated (300 nL each) and oleate concentration was measured by liquid scintillation counting. The top fraction (1) contained a  $> 5$  fold increase in concentration over the bottom fraction (4), a 2.5 fold increase over the initial concentration. Fractions in capillaries incubated isothermally ( $\Delta T = 0$ ) showed no accumulation. Oleate concentrations normalized to the initial concentration in the capillary before incubation.

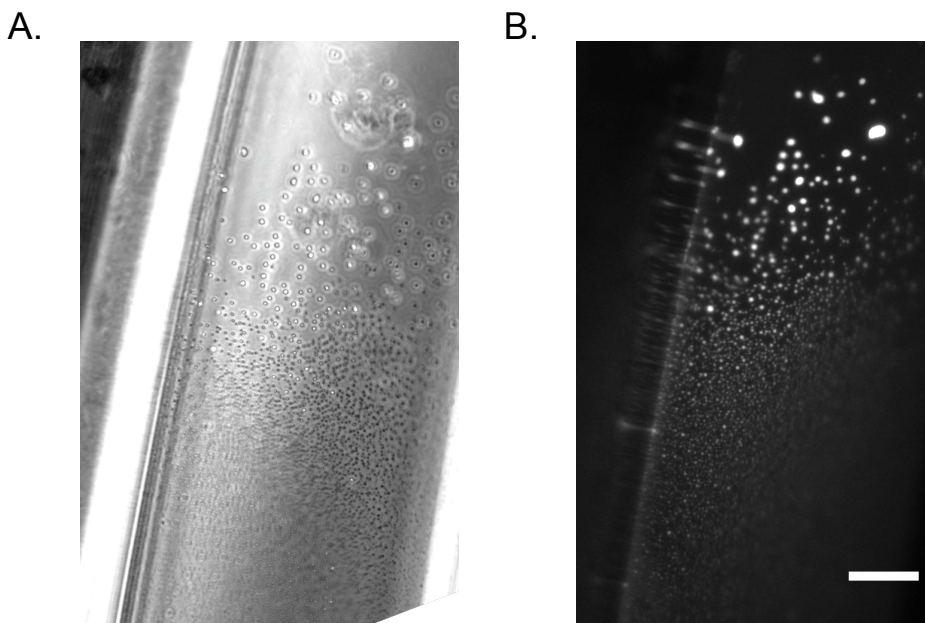


**Figure S3.** Vesicles formed in thermal diffusion column can encapsulate nucleic acids. (A) Phase contrast and (B) epifluorescence image of 50  $\mu\text{M}$  oleic acid incubated at  $\Delta T = 30$  K for 48 hours. 1 mM of fluorescein-tagged DNA oligonucleotides (poly-A 20mer) was also included in the starting solution and was co-concentrated with the oleic acid. Non-encapsulated DNA was washed away after incubation, leaving only encapsulated cargo to be visualized. Scale bar = 60  $\mu\text{m}$ .

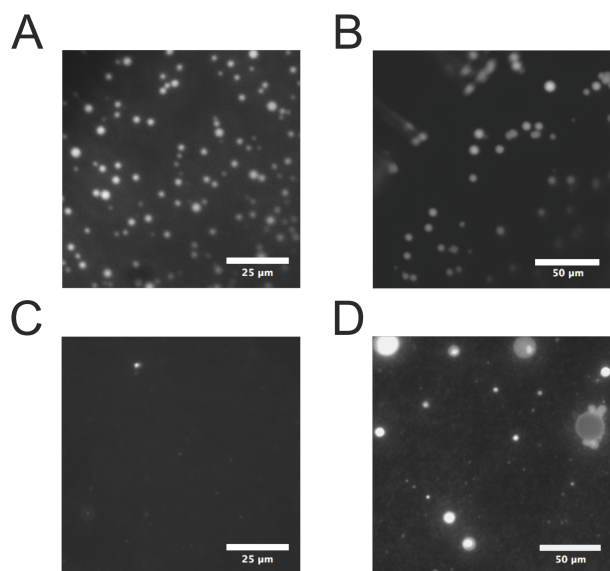


**Figure S4.** Vesicles formed in bent capillaries are large and monodisperse relative to those formed in bulk solution. (A) Oleic acid vesicles formed in a capillary with a starting fatty acid concentration of 40  $\mu\text{M}$  and (B) 70  $\mu\text{M}$ . In comparison, vesicles formed in bulk at (C) 250  $\mu\text{M}$  are mostly too small to see and at (D) 25 mM are polydisperse (diluted 1:10 after vesicle formation for visual clarity). All vesicles stained with the membrane dye Rhodamine 6G.

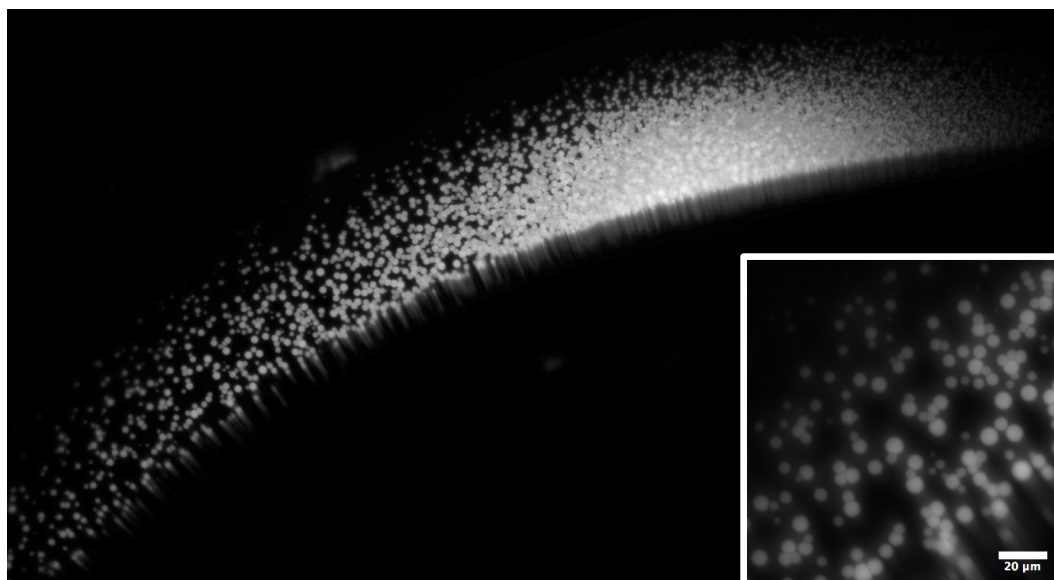


**Figure S5.** Vesicle formation in a bent capillary under a low salt concentration. Oleic acid (60  $\mu\text{M}$ ) was incubated at  $\Delta T = 30\text{K}$  for 48 hours in 20 mM  $\text{Na}^+\text{Bicine}$  pH 8.5. Compared to similar experiments performed at 0.2 M  $\text{Na}^+$  (Figure 2), a significant enhancement in the number of assembled vesicles is demonstrated. Insert: close-up of vesicles from same image. Vesicles stained with the membrane dye Rhodamine 6G.

### Movie S1

Example of the convective flow in a microcapillary (200  $\mu\text{m}$  ID) under a lateral thermal gradient of 30 K (left wall is cooled, right wall is heated). Flow is visualized with dye-labeled polystyrene beads and is shown at 30x speed.

Available at:

[http://molbio.mgh.harvard.edu/szostakweb/publications/Szostak\\_pdfs/Budin\\_et\\_al\\_JACS\\_2009\\_SI\\_MOV.avi](http://molbio.mgh.harvard.edu/szostakweb/publications/Szostak_pdfs/Budin_et_al_JACS_2009_SI_MOV.avi)

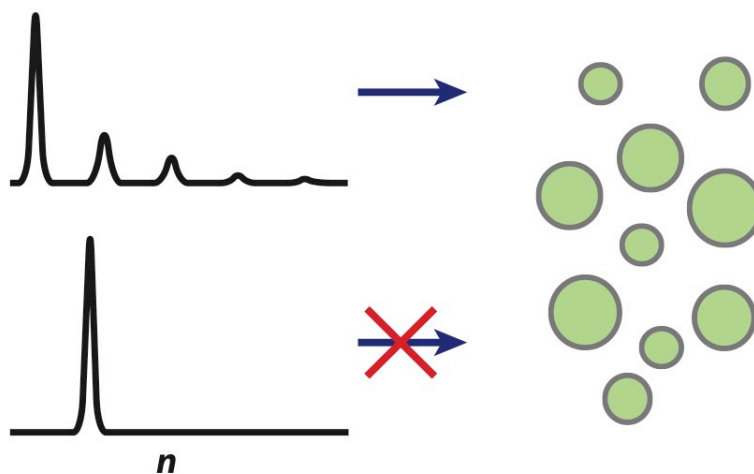
## References

1. Datta, A.K. *Biological and Bioenvironmental Heat and Mass Transfer*. Marcel Dekker: New York, 2002, 240-2.
2. Baaske, P.; Weinert, F.M.; Duhr, S.; Lemke, K.H.; Russell, M.J.; Braun, D. *Proc. Natl. Acad. Sci. USA*. **2007**, 104, 9346-51.
3. Stewart, J.M.; Driedzic, W.R.; Berkelaar, J.A. *Biochem. J.* **1991**, 275, 569-73.
4. Chen, I.A.; Szostak, J.W. *Biophys. J.* **2004**, 87, 988-98.
5. Mansy, S.S.; Schrum, J.P.; Krishnamurthy, M.; Tobé, S.; Treco, D.A.; Szostak, J.W. *Nature* **2008**, 454, 122-5.
6. Hanczyc, M.M.; Fujikawa, S.M.; Szostak, J.W. *Science* **2003**, 302, 618-22.
7. Chen, I.A.; Szostak, J.W. *Science* **2004**, 305, 1474-6.
8. Measured by Dynamic Light Scattering as described in S9.
9. Chen, I.A.; Szostak, J.W. *Proc. Natl. Acad. Sci. USA*. **2004**, 101, 7965-70.
10. Abreu, M.S.; Moreno, M.J.; Vaz, W.L. *Biophys. J.* **2004**, 87, 353-65.



### Chapter 3: Heterogeneity in fatty acid chain-length drives membrane assembly

Itay Budin and Jack W. Szostak



**Abstract:** The assembly of membranes composed of fatty acids and related single-chain amphiphiles has been proposed as a potential early step in the origin of life. Models for prebiotic fatty acid synthesis yield a majority of short chain products, which form membrane vesicles but only at very high concentrations. These critical aggregation concentrations would have posed a formidable challenge for prebiotic self-assembly. Here we asked whether mixtures of fatty acids with varying chain-lengths, as are produced from abiotic chemistry, form vesicles at significantly lower concentrations than would be expected from their primary, short chain-length components. We found that the critical aggregation concentration of fatty acid vesicles is lowered dramatically by minor amounts of long-chain species, which is quantitatively consistent with models previously derived for the assembly of mixed micelles. Our results demonstrate how the chemical heterogeneity intrinsic to prebiotic systems could have lowered the thermodynamic barriers to their self-assembly.

## Introduction

Because of their prebiotic plausibility, fatty acids have long been proposed to serve a role as early cell membrane lipids [1, 2]. Abiotic syntheses of fatty acids by Fischer Tropsch-type chemistry [3] or by spark-discharge reaction reactions [4] yield mixtures of fatty acids, fatty alcohols, and alkanes. The distribution of these products with respect to their chain length is as expected from a non-enzymatic condensation process, with abundance decreasing logarithmically with carbon number. The most abundant species in these mixtures are therefore short ( $<C_{12}$ ), saturated fatty acids, which are also the primary species found in carbonaceous chondrite extracts [5]. However, small amounts of longer-chain fatty acids, with decreasing abundance, would also be expected in abiotic mixtures.

Single component fatty acid membranes have been studied extensively as models for primitive cell membranes and have shown properties that would have made them well-suited to such a role [6]. Short and medium chain ( $\leq C_{14}$ ) fatty acid membranes feature remarkably high intrinsic solute permeability, which is a requirement for a heterotrophic primitive cell model [7]. Membrane growth and division has also been demonstrated via several pathways, all of which utilize the aqueous solubility of single-chain lipids such as fatty acids [2, 8, 9]. However, this intrinsic solubility also provides a thermodynamic barrier to membrane assembly. Fatty acids are characterized by significant critical aggregation concentrations, only above which they aggregate into membrane vesicles. Critical concentrations are a result of the entropic cost of aggregation, and generally increase exponentially with decreasing chain length. Thus, while long chain fatty acids assemble at reasonable concentrations (e.g., oleic acid 20  $\mu\text{M}$ ), short chain species require

very high concentrations (e.g., decanoic acid 40 mM, octanoic acid 250 mM). Since the latter is the abiotically more abundant component, these concentration requirements pose a potential hurdle for the assembly of primitive cells. Because acyl unsaturation is an enzymatic (and oxygen dependent) feature of lipid synthesis, long chain fatty acids also suffer from high melting temperature (e.g., stearic acid 70° C) and thus form waxes in mild conditions.

Solvent phase transitions, such as evaporation and eutectic freezing, have been proposed as prebiotic concentration mechanism, but act on solutes indiscriminately. This is particularly problematic for fatty acids, which precipitate in moderate (> 5 mM) divalent or high (> 300 mM) monovalent cation concentrations. Processes that concentrate solutes more specifically, such as thermal diffusion columns [10], necessitate very particular and rare microenvironments and are thus of debatable prebiotic relevance. We hypothesized that the heterogeneity intrinsic to abiotic fatty acid chemistry could provide a more general solution to the concentration problem for membrane assembly. If small fractions of long-chain species nucleate vesicle assembly or otherwise lower its entropic barrier, fatty acid mixtures could assemble at lower concentrations than would be expected due to their mean chain length. Mixtures of single chain lipids with variable head groups have previously been utilized for increased thermostability [11], permeability [7], and mild effects on aggregation concentrations [12]. However, the properties of fatty acid membranes with acyl chain polydispersity have not been explored. We have shown (chapter 4) that fatty acid membrane assembly largely follows the pseudophase transition characteristic of micellar assembly, which is characterized constant concentration of monomers above the cac. We therefore asked if aggregation models previously developed for mixed surfactant micelles, which are of significant commercial value, apply to the assembly of fatty

acid vesicles. These models predict that the cac is heavily weighted by the long-chain species in the mixture and that the resulting aggregate is enriched in them.

## Theory

Phase behavior of multicomponent surfactant systems has been studied extensively in the context of critical micellar concentrations of surfactant mixtures [13-17]. We take the approach of Holland [14] to derive the critical aggregation concentration (cac) for an ideal mixture of fatty acids. The chemical potential of species  $i$  as a monomer can be expressed as:

$$(1) \quad \mu_i = \mu_i^\circ + RT \ln C_i^m$$

where  $\mu_i$  is the monomeric chemical potential of species  $i$ ,  $\mu_i^\circ$  is its standard chemical potential, and  $C_i^m$  is the concentration of the monomer  $i$  in units of mole fraction in solvent (i.e. molar concentration divided by  $\sim 55$ ). This assumes the activity coefficient of the free monomer is 1 (acts ideally), approximating free dispersal of monomers with no interactions. In a mixed aggregate,

$$(2) \quad \mu_i^a = \mu_i^{a,o} + RT \ln f_i x_i$$

where  $\mu_i^a$  is the chemical potential of  $i$  in the mixed aggregate,  $\mu_i^{a,o}$  is the chemical potential of  $i$  in a pure aggregate of species  $i$ ,  $f_i$  is the activity coefficient for  $i$  in the aggregate (a measure of its interactions with other molecules), and  $x_i$  is the mole fraction of  $i$  in the mixed aggregate. For the pure aggregate of  $i$ , we can apply a pseudophase model, and thus:

$$(3) \quad \mu_i^{a,o} = \mu_i^\circ + RT \ln cac_i$$

where  $cac_i$  is the critical aggregation concentration (cac) for species  $i$  in a single-component system. At the concentration of the cac, monomers and aggregates are isoenergetic and the free energy of the monomer species is equal to that of the aggregate. Therefore,

$$(4) \quad \mu_i^a = \mu_i$$

Substituting in equations (1) and (2):

$$(5) \quad \mu_i^{a,o} + RT \ln f_i x_i = \mu_i^\circ + RT \ln C_i^m$$

and (3):

$$(6) \quad \mu_i^\circ + RT \ln cac_i + RT \ln f_i x_i = \mu_i^\circ + RT \ln C_i^m$$

which simplifies to:

$$(7) \quad C_i^m = f_i x_i cac_i$$

If we take the case of a solution at the mixed cac (right at the formation of the first aggregates), the concentration of monomer  $i$  ( $C_i^m$ ) is simply a product of its mole fraction of total lipids,  $X_i$ , and the total lipid concentration, which at that point is equal to the mixed cac ( $cac$ ). Therefore,

$$(8) \quad C_i^m = X_i cac$$

Combining with (7) and rearranging:

$$(9) \quad \frac{X_i cac}{f_i cac_i} = x_i$$

Since the mole fractions of components  $i$  in the mixed micelle must sum to 1,

$$\sum_{i=1}^n x_i = 1$$

Therefore,

$$(10) \quad \sum_{i=1}^n \frac{X_i cac}{f_i cac_i} = 1 = cac \sum_{i=1}^n \frac{X_i}{f_i cac_i}$$

$$\frac{1}{cac} = \sum_{i=1}^n \frac{X_i}{f_i cac_i}$$

This is a general expression for the cac of a system with n components, each with mole fractions  $X_i$ ,  $cac_i$  for their behavior in single-component systems, and activity coefficient  $f_i$ . For micelles, fatty acids have shown ideal behavior [13], i.e. an activity coefficient of 1, thus simplifying this further. For an ideal, binary system, equation 10 equates to:

$$\frac{1}{cac} = \frac{X_1}{cac_1} + \frac{X_2}{cac_2} = \frac{X_1}{cac_1} + \frac{(1 - X_1)}{cac_2}$$

Or:

$$(12) \quad cac = \frac{cac_1 cac_2}{X_1 cac_2 + (1 - X_1) cac_1}$$

Since concentrations are  $\ll 1$ , this term is dominated by the lower of the two cacs, which corresponds to the longer chain lipid.

## Methods

We utilize three complementary methods to experimentally monitor aggregation in this study:

1) Light scattering, or turbidity, can detect vesicle assembly as a result of a sudden increase in the slope of light scattering (or absorbance) plotted against concentration. This is because vesicles are much larger (50 nm to several  $\mu\text{m}$ ) than micelles or monomers and Rayleigh scattering scales with diameter to the sixth power. This method works well in single-component systems or in very dilute systems with low critical concentrations. However, mixed systems do

not feature a constant monomer concentration above the critical concentration, so a discontinuity in scattering is not necessarily clear.

2) Spectroscopic methods can detect aggregation as a result of changes in the colorimetric or fluorescent behavior of a dye molecule in the presence of aggregates. In this study we use pinacyanol chloride, a cyanine dye, which undergoes a dramatic colorimetric change in the presence of hydrophobic aggregates [18]. Solutions containing low concentrations (25  $\mu\text{M}$ ) of pinacyanol turn from a clear purple to a strong blue in the presence of aggregates, which can be seen visually (quite vividly) or by measuring absorbance ratios. This change is a result of the dependence of the hydrophobic dye's self-aggregation on the polarity of its solvent environment [19]. The major advantage of this method is its sensitivity; since the dye partitions to any hydrophobic environment, the read out is binary (presence of aggregates vs. none) instead of a weighted average between two states. No concentration extrapolations are therefore needed. The major disadvantage is that the assay does not distinguish between the type of aggregate, e.g. micelle or vesicle. However, in chapter 4 we show that fatty acid vesicle solutions feature only a single cac for both vesicle and micelle assembly. This method is also not necessarily accurate for very dilute solutions (e.g. long chain fatty acids), as the stoichiometry of the dye vs. aggregates becomes limiting.

3) The large size of vesicle aggregates allows for their detection by monitoring the line broadening effect of NMR peaks associated with slow-tumbling aggregates. NMR can also be used to track changes in aggregates by small changes chemical shifts [20], but this is unlikely to be useful for mixtures with varying composition. A variety of fatty acids labeled with  $^{13}\text{C}$  at the

carbonyl group are commercially available and provide distinct, single peaks at ~180 ppm. This method is not nearly as convenient as light scattering, requiring very long acquisition times, and is not as sensitive as pinacyanol, as line widths are weighted averages of the individual states. However, NMR has the capability of discerning the aggregation state of individual, labeled components in a mixture of otherwise unlabeled species, while the other methods cannot discern the composition of aggregates. Example data for the cac of decanoic acid (40 mM) by each method is shown in Figure 1.



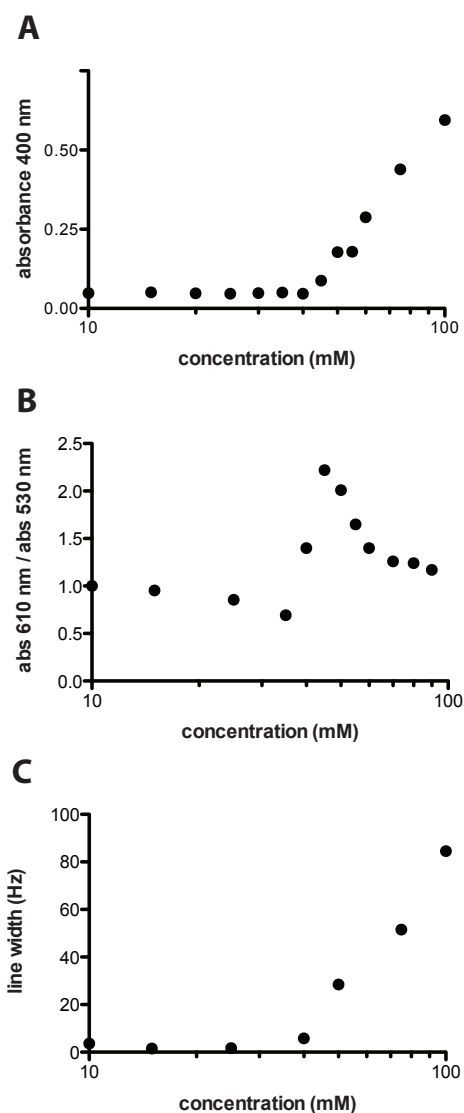


**Figure 1:** Methods for detecting fatty acid vesicle assembly. (A) Aggregation detected by light scattering. Absorbance readings measure solution turbidity, which increases with vesicle abundance. The cac can thus be measured via the sudden increase of slope in the plot. (B) Aggregation detected by pinacyanol chloride. The sudden increase in the red to green absorption ratio indicates the presence of pinacyanol monomers, which are only solubilized in the presence of hydrophobic microenvironments. This change corresponds to the vivid pink/purple to blue color change in the solution. The absorbance ratio falls back close to 1 at high concentrations due to the turbidity of the vesicle solution, which drowns out the dye absorbance. (C) Aggregation detected by changes in  $^{13}\text{C}$  1D NMR line width. The slow tumbling times of vesicle aggregates causes the broadening of peaks associated with this motion. The given line width represents a weighted average of monomer/micelles (sharp peaks) and vesicles (broad peaks) and starts increasing at the cac.

**Materials and sample preparations:** All fatty acids were obtained from Nu-check, except for  $1\text{-}^{13}\text{C}$  decanoic acid (Cambridge Isotopes Laboratories). All other reagents were from Sigma-Aldrich. Solutions were prepared in buffer, either 0.1 M POPSO 8.2 for decanoic acid experiments or 0.2 M bicine 8.5 for oleate/myristoleate solutions, and allowed to equilibrate over

night at 30° C. For spectroscopic cac determination, pinacyanol chloride was added in heated buffer to a final concentration of 25  $\mu$ M and allowed to incubate for > 15 minutes before analysis.

**Measurements:** Light scattering intensities were recorded on a Precision Detectors PD2000 dynamic light scatterer. Absorbance readings were taken on a Molecular Devices spectramax 384 plate reader. 1D  $^{13}$ C13 spectra were recorded on a Varian 400 MHz NMR, with line width being measured at half-peak height. Micrographs were taken on a Nikon TE2000S inverted microscope with 100X oil objective; samples were stained with Rhodamine 6G to visualize membranes.

## Results

We first measured the cac for binary mixture of monounsaturated fatty acids: myristoleic acid (MA, C14:1, cac 2 mM) and oleic acid (OA, C18:1, cac 20  $\mu$ M) by light scattering intensities (Figure 2). Measured cac values matched those predicted by theory well, with 10% oleic acid lowering the cac of myristoleate to 125  $\mu$ M, an almost 20-fold reduction. Encouraged by these results, we then tested a more prebiotically-relevant mixture of decanoic acid (DA, C10:0, cac 40 mM) with either myristoleic acid or myristic acid (C14:0) (Figure 3). These measurements were taken using pinacyanol chloride, for reasons mentioned above. Measured cacs for decanoic acid and myristoleic acid matched predicted values very closely, with 10% of the longer lipid lowering the cac 4-fold. Myristic acid cannot form vesicles independently at 30° C because of its high melting temperature ( $\sim$ 55 ° C), yet had a quantitatively similar affect on decanoic acid as its

unsaturated analogue. The ability of short chain, low-melting temperature fatty acids to solubilize long chain fatty acids below their melting temperature is thus a viable mechanism for lowering aggregation concentrations.

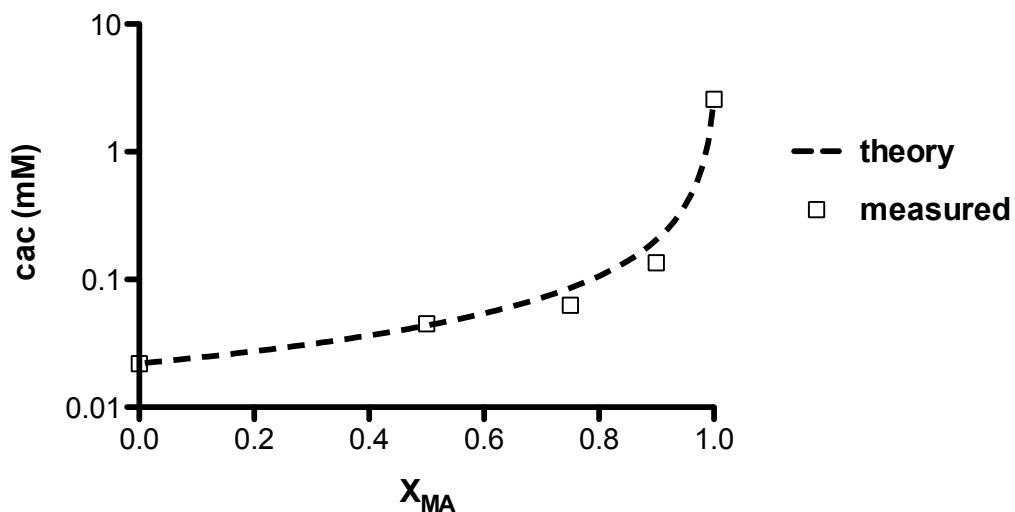


**Figure 2:** Critical aggregation concentrations for binary mixtures of myristoleic acid (MA) and oleic acid as a function of MA fraction.  $cac$  was determined by light scattering intensities of serial dilutions. Predicted values were calculated from ideal theory using equation 12.

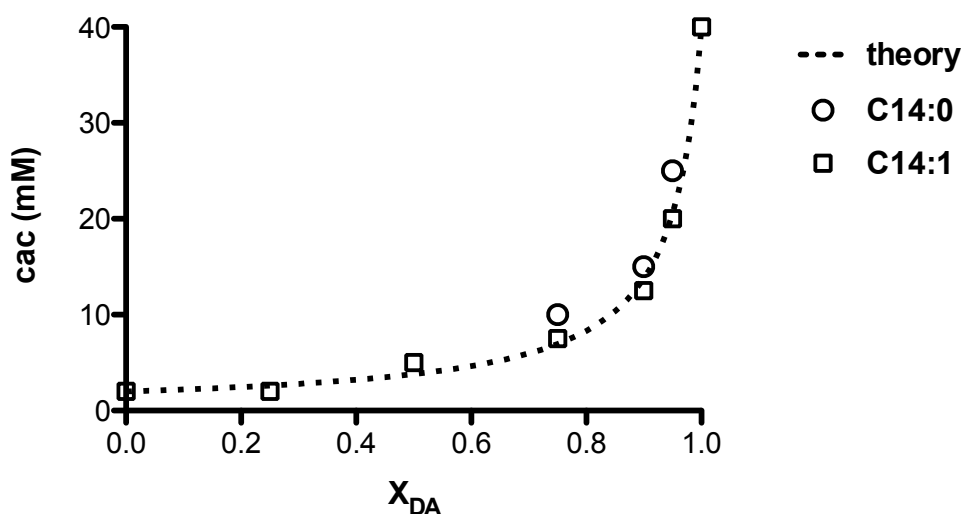


**Figure 3:** Critical aggregation concentrations for binary mixtures of decanoic acid (DA) and either myristoleic acid (C14:1) or myristic acid (C14:0). Predicted values were calculated for the former using equation 12. Myristic acid notably lowers cac despite its inability to form vesicles at this temperature (30 °C).

We next tested whether our model predicts the cac of multi-component fatty acid mixtures. We measured cac for a series of ternary mixtures containing decanoic acid, myristoleic acid, and octanoic acid (C8:0, cac 250 mM) using pinacyanol chloride. We kept the ratio of the myristoleic acid to octanoic acid at 1:2 while varying the decanoic acid content in the mixture (Figure 4). Therefore the mean chain-length in this series remained constant ( $n = 10$ ), while the chain-length polydispersity of the mixture increased with decreasing decanoic acid content. Our data largely followed the ideal mixing model, with slightly lower values than expected. This deviation represents a non-ideality to the model, with activity coefficient of  $< 1$ . Nonetheless, this experiment demonstrates how fatty acid polydispersity can cause large decreases in cac (~8-fold) without altering the average chain-length in the mixture.

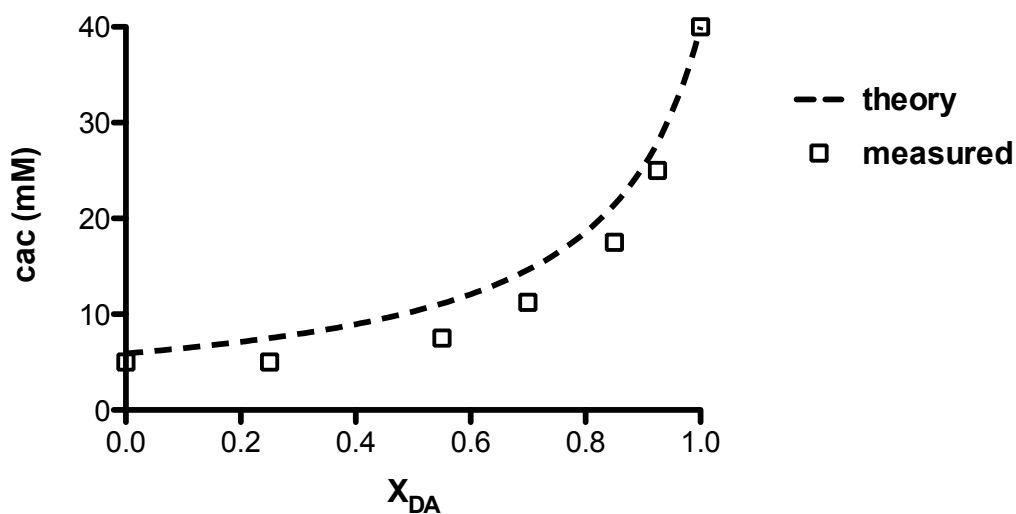


**Figure 4:** Critical aggregation concentrations for a ternary mixture of decanoic acid (DA), octanoic acid and myristoleic acid. The ratio of octanoic to myristoleic acid was kept at 2:1, with their sum equal to  $1 - X_{DA}$ . The mean chain length of the mixtures is thus constant at  $n = 10$  throughout this range. Polydispersity thereby increases with decreasing  $X_{DA}$  and lowers the cac. Predicted values were calculated from theory using equation 10 with an activity coefficient of 1.

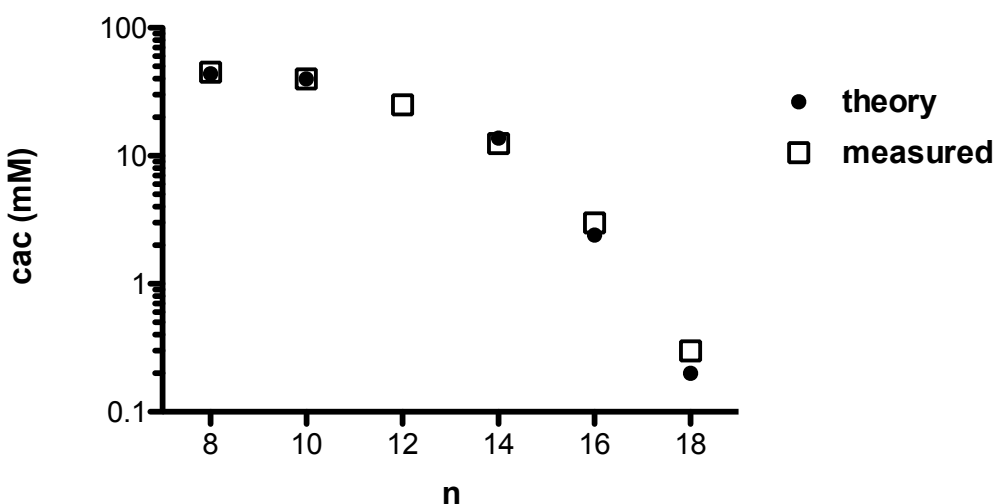


**Figure 5:** Effect of minor component chain length on critical aggregation concentration. Decanoic acid was mixed with 10 mol % of the given chain length fatty acid. The minor

component was saturated for  $n = 8, 10,$  and  $12$  and unsaturated for  $n = 14, 16,$  and  $18$ . Predicted values were calculated from theory using equation 12 in the cases where the minor component assembled vesicles independently at this temperature ( $30\text{ }^{\circ}\text{C}$ ).

Our data suggests that minor components of long-chain fatty acids can dramatically lower the concentration barrier for assembly of primarily short-chain membranes. To test this further we measured the cac of decanoic acid in binary mixtures with 10% fatty acid with varying chain length (Figure 5). Where possible, our ideal model fit the measured values extremely well, and the effect of long-chain fatty acids was substantial, e.g. 10% C16:1, 15-fold reduction, 10% C18:1, 100-fold reduction. We followed these findings microscopically and were able to observe dense fields of large vesicles in 15 mM decanoic acid with 5% oleic acid (Figure 6), for which we measured a cac of 0.5 mM. Equivalent concentrations of pure decanoic acid featured no visible structures. To confirm that these vesicles featured substantial amounts of decanoic acid, as opposed to oleic acid vesicles, we measured line broadening of  $^{13}\text{C}$  decanoic acid in the sample. We confirmed a substantial increase in line width as compared to a pure decanoic acid solution at the same concentration. By using a standard curve of line width vs. concentration (e.g. Figure 1) and assuming a weighted average contribution to line width, we estimated that 10% of the total decanoic acid was partitioning into the vesicles. Assuming a very high oleic acid partition, the vesicles in this solution featured a mean composition of 70% decanoic acid and 30% oleic acid. Thus, the longer chain species is enriched 6-fold compared to the total lipid concentrations.

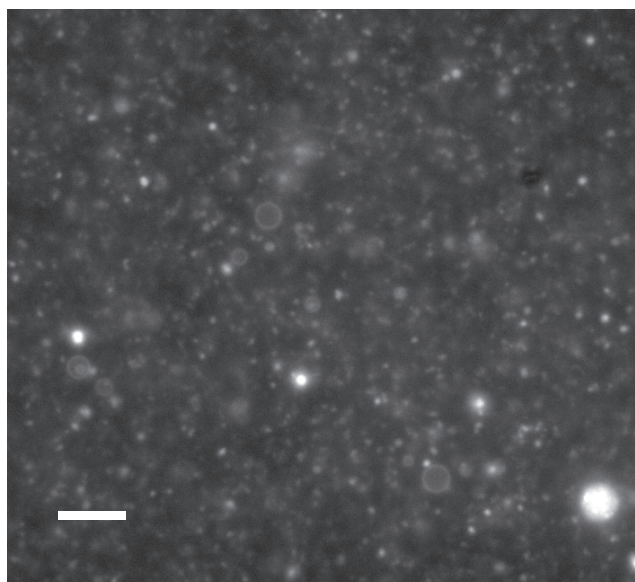


**Figure 6:** Visible vesicles are abundant in a solution of 14.25 mM decanoic acid, 0.75 mM oleic acid. The oleic acid component (5 mol %) lowers the cac of the system from 40 mM to 500  $\mu$ M. Sample labeled with the non-polar staining dye Rhodamine 6G. Scale bar, 6  $\mu$ m.

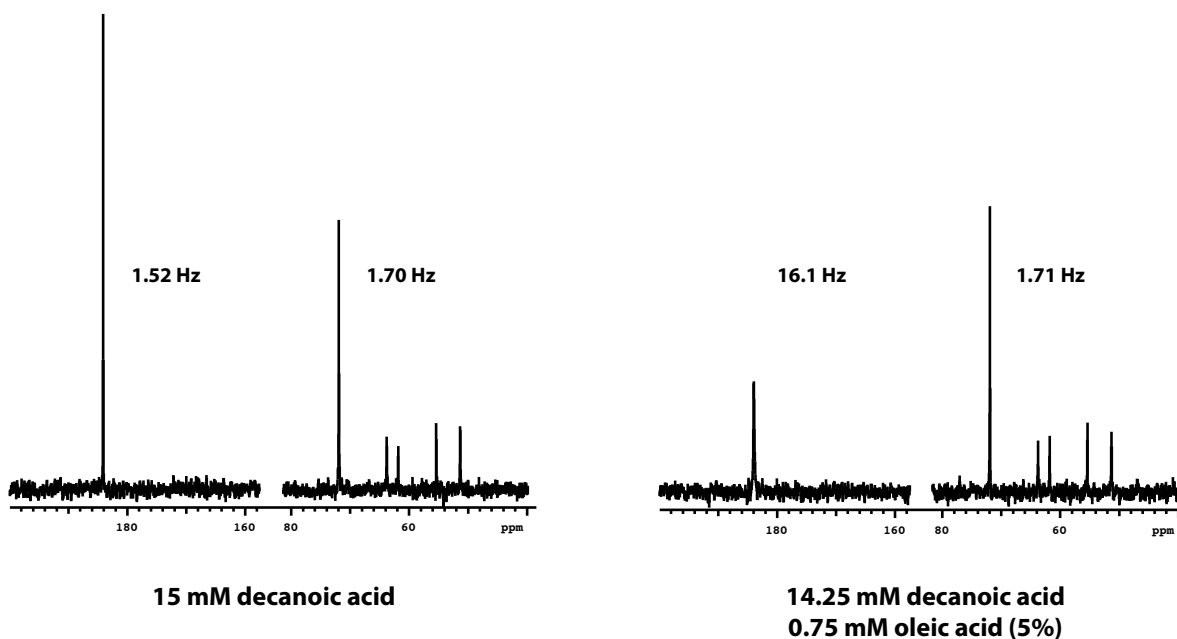


**Figure 7:** Vesicle incorporation of decanoic acid at concentrations substantially below its individual cac. Left: 1D spectrum of 1-<sup>13</sup>C decanoic acid (183 ppm) shows a narrow peak (1.52 Hz), consistent with a purely monomer phase. 10 mM 2-<sup>13</sup>C glycerol (72 ppm) was added to the sample as a reference peak (1.70 Hz). Right: Addition of 5 mol % unlabeled oleic acid drives the aggregation of the 1-<sup>13</sup>C decanoic acid, resulting in peak broadening to 16.1 Hz. We estimate that

this corresponds to vesicles composed of 70% decanoic acid and 30 % oleic acid. Line widths were taken at half-peak height; experiment was performed at 30 °C.

## **Discussion**

The chemical heterogeneity intrinsic to abiotic chemistry has long been a challenge for thinking about the origin of life. However, more recent models propose that heterogeneity could assist self-assembly or self-replication processes in certain cases [21]. Here we show that mixtures of varying length fatty acids self-assemble into membranes at significantly lower concentrations than would be expected based on their major components. This idea was inspired by analogous work on mixed surfactant micelles and we find that the ideal mixing models developed for those systems apply to mixed fatty acid vesicles. Because abiotic fatty acid synthesis inherently results in such mixtures, these models provide a useful quantitative framework for thinking about the conditions needed for primitive membrane assembly.

The thermodynamics of vesicle assembly from fatty acid mixtures also carry implications for the acyl composition of primitive membrane models, which is the key determinant in membrane permeability and thermostability. In mixed systems, aggregate composition might deviate significantly from relative solution concentrations. The ideal mixed micelle model used here has been extended to predict the composition of mixed aggregates, which are enriched in the long chain species in dilute concentrations [15]. These models match experimental data in the few cases where such measurements have been possible, such as by extrapolating conductivities of anionic surfactant mixtures [22]. Quantifying the composition of aggregates is a challenge



because of the rapid dynamics inherent to these systems, but the NMR approach we introduce here is a potential strategy for circumventing that.

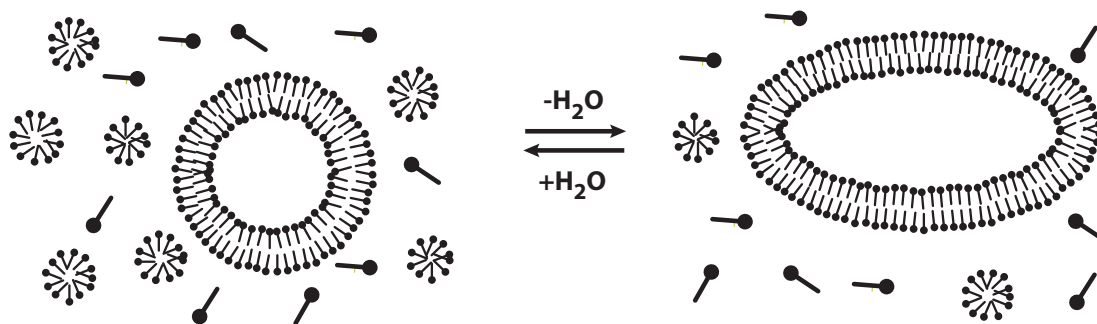
## References:

1. Hargreaves, W.R. and D.W. Deamer, *Liposomes from ionic, single-chain amphiphiles*. *Biochemistry*, 1978. **17**(18): p. 3759-3768.
2. Hanczyc, M.M., S.M. Fujikawa, and J.W. Szostak, *Experimental models of primitive cellular compartments: encapsulation, growth, and division*. *Science*, 2003. **302**(5645): p. 618-22.
3. Simoneit, B.R.T., *Prebiotic organic synthesis under hydrothermal conditions: an overview*. *Advances in Space Research*, 2004. **33**(1): p. 88-94.
4. Yuen, G.U., J.G. Lawless, and E.H. Edelson, *Quantification of monocarboxylic acids from a spark discharge synthesis*. *Journal of molecular evolution*, 1981. **17**(1): p. 43-47.
5. Yuen, G.U. and K.A. Kvenvolden, *Monocarboxylic Acids in Murray and Murchison Carbonaceous Meteorites*. *Nature*, 1973. **246**(5431): p. 301-303.
6. Budin, I. and J.W. Szostak, *Expanding roles for diverse physical phenomena during the origin of life*. *Annual review of biophysics*, 2010. **39**: p. 245-63.
7. Mansy, S.S., et al., *Template-directed synthesis of a genetic polymer in a model protocell*. *Nature*, 2008. **454**(7200): p. 122-5.
8. Zhu, T.F. and J.W. Szostak, *Coupled Growth and Division of Model Protocell Membranes*. *J Am Chem Soc*, 2009. **131**(15): p. 5705-5713.
9. Budin, I. and J.W. Szostak, *Physical effects underlying the transition from primitive to modern cell membranes*. *Proceedings of the National Academy of Sciences of the United States of America*, 2011. **108**(13): p. 5249-54.
10. Duhr, S. and D. Braun, *Why molecules move along a temperature gradient*. *Proceedings of the National Academy of Sciences of the United States of America*, 2006. **103**(52): p. 19678-82.
11. Mansy, S.S. and J.W. Szostak, *Thermostability of model protocell membranes*. *Proceedings of the National Academy of Sciences of the United States of America*, 2008. **105**(36): p. 13351-5.
12. Lu, Y.J., et al., *Acyl-phosphates initiate membrane phospholipid synthesis in Gram-positive pathogens*. *Molecular cell*, 2006. **23**(5): p. 765-72.
13. Shinoda, K., *The Critical Micelle Concentration of Soap Mixtures (Two-Component Mixture)*. *The Journal of Physical Chemistry*, 1954. **58**(7): p. 541-544.

14. Holland, P.M. and D.N. Rubingh, *Nonideal multicomponent mixed micelle model*. The Journal of Physical Chemistry, 1983. **87**(11): p. 1984-1990.
15. Clint, J.H., *Micellization of mixed nonionic surface active agents*. Journal of the Chemical Society, Faraday Transactions 1: Physical Chemistry in Condensed Phases, 1975. **71**: p. 1327-1334.
16. Motomura, K., M. Yamanaka, and M. Aratono, *Thermodynamic consideration of the mixed micelle of surfactants*. Colloid & Polymer Science, 1984. **262**(12): p. 948-955.
17. Clint, J.H., *Surfactant Aggregation* 1992, Glasgow and London: Blackie.
18. Corrin, M.L. and W.D. Harkins, *Determination of the Critical Concentration for Micelle Formation in Solutions of Colloidal Electrolytes by the Spectral Change of a Dye*. Journal of the American Chemical Society, 1947. **69**(3): p. 679-683.
19. West, W. and S. Pearce, *The Dimeric State of Cyanine Dyes*. The Journal of Physical Chemistry, 1965. **69**(6): p. 1894-1903.
20. Cistola, D.P., et al., *Ionization and phase behavior of fatty acids in water: application of the Gibbs phase rule*. Biochemistry, 1988. **27**(6): p. 1881-8.
21. Szostak, J.W., *An optimal degree of physical and chemical heterogeneity for the origin of life?* Philosophical transactions of the Royal Society of London. Series B, Biological sciences, 2011. **366**(1580): p. 2894-901.
22. Mysels, K.J. and R.J. Otter, *Conductivity of mixed sodium decyl and dodecyl sulfates, and the composition of mixed micelles*. Journal of Colloid Science, 1961. **16**(5): p. 462-473.

## Chapter 4: Multi-phase coexistence allows for the concentration-driven growth of protocell membranes

Itay Budin, Anik Debnath, and Jack W. Szostak



**Abstract.** The first protocell membranes likely assembled from fatty acids and related single chain lipids available in the prebiotic environment. The intrinsic physicochemical properties of these molecules had to therefore facilitate the spontaneous membrane growth and division. Depending on their chemical and physical environment, fatty acids can transition between several different phases, including soluble monomers, micelles, and lamellar vesicles. Here we address the concentration dependence of fatty acid aggregation, which is dominated by entropic considerations. We quantitatively distinguish between fatty acid phases using a combination of physical and spectroscopic techniques, including the fluorescent analogue Laurdan, whose emission is sensitive to structural differences between micellar and lamellar aggregates. We find that the monomer-aggregate transition largely follows a characteristic pseudophase model of molecular aggregation, but that the composition of the resulting aggregate phase is also concentration dependent. Low concentration vesicle solutions feature significant amounts of coexisting micelles, likely as an entropic result of their smaller size, while concentrated solutions

favor vesicles. We subsequently show that this micelle-vesicle equilibrium can be used to drive the growth of pre-existing vesicles upon an increase in amphiphile concentration either through solution evaporation or addition of excess lipids. Prebiotic concentrating mechanisms could have thus provided a simple physical mechanism for the growth of early cell membranes.

## **Introduction**

Membranes composed of fatty acids and their single-chain derivatives have been proposed to serve a role as early cell membranes, analogous to phospholipid-based membranes in all modern cells. Initial support for this hypothesis arose from the prebiotic likelihood of these molecules and their ability to spontaneously assemble into bilayer vesicles [1, 2]. Fatty acids and other oxygenated alkanes can be robustly synthesized via Fischer-Tropsch-type chemistry [3, 4] and membrane-forming samples of these molecules have been discovered in abiotic environments such as meteorites [5, 6]. More recently, the functional properties of fatty acid membranes have been studied [7-10] and are consistent with a putative role for fatty acids as early membrane lipids. Particularly striking is the ability of fatty acid vesicles to undergo inter-vesicle competition through exchange of monomers [11, 12]. These processes depend on a coexisting solution state to allow for exchange and thus motivated us to investigate the structural composition of fatty acid vesicle solutions.

Fatty acid membranes generally assemble only at narrow, alkaline pH ranges (~7-9, depending on chain length), near the apparent pKa of the aggregate acid. This condition allows approximately equal proportions of protonated and anionic carboxylates, which likely form a

bilayer-stabilizing hydrogen bonding network [13, 14]. At higher pH, fatty acids aggregate into soap micelles, which allow for greater charge repulsion of the anionic head groups. In neutral or acidic conditions, they lose their amphiphilicity and condense into oil droplets. This pH-dependent phase behavior has been extensively characterized by NMR, X-ray diffraction, and electron spin resonance (ESR) [13, 15, 16]. Subsequent work has utilized the pH-dependence of fatty acid aggregation to drive the de novo assembly of vesicles [7, 17] or growth of pre-existing vesicles by introducing alkaline solutions to buffer [7, 18].

Molecular assembly is also intrinsically concentration dependent because of the statistical entropic cost of aggregation. Detergent solutions, for example, feature a critical micellar concentration (cmc), only above which aggregation occurs. These processes can be described as phase equilibria, with critical concentrations analogous to solubilities. Critical aggregation concentrations (cac) have been observed for fatty acid vesicle solutions [2, 19], suggesting that monomers coexist with vesicles at those concentrations. Asymmetries in ESR data have provided evidence for micelle-vesicle coexistence in two fatty acid systems [15, 16]. Because of their large size ( $n > 10^5$ ), membrane vesicles have a higher entropic cost than smaller ( $n \sim 50$ ) micellar aggregates. We therefore asked if aggregate composition could be concentration dependent, with lower concentration solutions favoring micelle assembly. Notably, low concentration solutions near the cac are the likely prebiotic scenario for fatty acid membranes and are thus of particular interest [20].

To explore this putative multi-phase coexistence, we first sought methods to quantitatively characterize the equilibrium between fatty acid monomers, micelles, and vesicles at low

concentrations. Because of the techniques used, previous studies could only examine fatty acid aggregation behavior at concentrations an order of magnitude or more above the apparent  $cac$ . We distinguished between aggregates using the fluorescent fatty acid analogue Laurdan (6-dodecanoyl-2-dimethylaminonaphthalene), whose emission red shifts with increasing solvent polarity [21]. Laurdan has been used extensively to study structural features of membranes, e.g. lipid packing [22], membrane bending [23], and phase segregation [24]. Since micelles feature greater head group solvation than more tightly packed bilayers, we predicted that Laurdan would be a sensitive means of distinguishing these two aggregate states. We used this assay alongside surface tension measurements, which can quantify monomer concentrations, to characterize the equilibrium between these states. Our data describes a micelle-vesicle equilibrium above the  $cac$  in which dilute solutions are relatively enriched in micelles. Changes in fatty acid concentration therefore drive the incorporation of micelles into coexisting vesicles (upon concentration) or the dissolution of vesicles into micelles (upon dilution). We use this phase property to drive the growth of fatty acid vesicles upon solution evaporation, a process with potential prebiotic relevance to the growth of early cell membranes.

## **Results**

We first sought to characterize the fatty acid monomer phase by measuring solution surface tension, which is lowered as a function of added fatty acid monomer. We measured surface tensions of serial dilutions for a series of unsaturated fatty acids ranging from 14 to 18 carbons. From these surface tensions (Figure S1), we calculated monomer concentrations (Materials and Methods). Pseudophase equilibria feature abrupt transition points in concentration, above

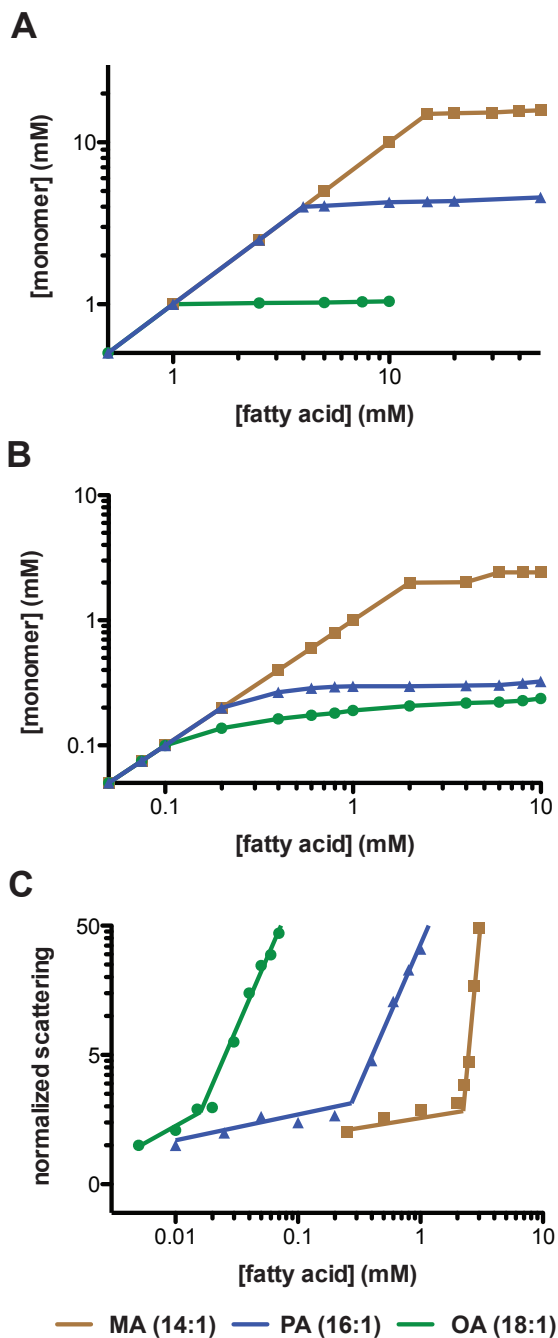


**Figure 1:** The monomer-aggregate transition in fatty acid systems. Fatty acid monomer concentrations were measured as a function of total concentration for a series of monounsaturated fatty acids at pH 10.5 (A) and 8.5 (B). Monomer concentrations were derived from surface tension plots since aggregates are not surface active. The plateau points in (A) correspond to critical micellar concentrations, while in (B) to critical aggregation concentrations, above which both vesicle and micelle assembly occur. (C) Vesicle assembly monitored independently by light scattering of serial dilutions at pH 8.5. Abrupt increases in light scattering indicates the assembly of vesicles, which are much larger than monomers and micelles or micelles in solution. Critical aggregation concentrations in (B) match vesicle assembly concentrations in (C): 0.02 mM for oleate (C18:1), 0.25 mM for palmitoleate (C16:1), and 2 mM for myristoleate (C14:1).



which the monomer concentration stays constant and all additional lipids are incorporated into aggregates [25]. As expected, this was the case for a series of unsaturated fatty acids forming micelles at high pH (Figure 1A). The critical micellar concentrations (cmcs) of these components scale exponentially with chain length as a result of the additive nature of the hydrophobic effect.

Monomer concentrations in fatty acid solutions at pH 8.5 (Figure 1B) also plateaued at critical concentrations, though not as abruptly as at pH 10.5. This is somewhat surprising because vesicles contain very large aggregate numbers, and should therefore more closely resemble a pure phase transition. We reasoned that this effect could be due to fatty acids aggregating into multiple states, e.g. vesicles and micelles, above the critical concentration. We considered the possibility that micelle aggregation occurs at a lower concentration than vesicle assembly at pH 8.5, i.e. the system has two critical concentrations – a behavior that has been observed in cationic/anionic surfactant mixtures [26]. However, vesicle cmcs measured independently using light scattering (Figure 1C) were at the same concentration, or even slightly lower, than the critical concentrations in the surface tension plots. We therefore concluded that there is no aggregation (e.g. micelles) at concentrations below which vesicle assembly occurs and that the system features a single cmc.

These initial experiments motivated us to find experimental techniques to distinguish between micellar and lamellar aggregates. This is a challenge because of the large size difference between micelles and vesicles (precluding microscopy or light scattering), the rapid exchange between them (precluding any sort of physical separation), and their similar chemical environments (precluding dyes sensitive to non-polar environments). Laurdan is a C12 fatty acid analogue with

a fluorescent naphthalene derivative that features an emission spectrum that is sensitive to the polarity of its environment. Previous work in our laboratory had used Laurdan to monitor structural changes during fatty acid membrane bending [23] and so we reasoned it would be sensitive to larger changes in aggregate structure (Figure 2A).

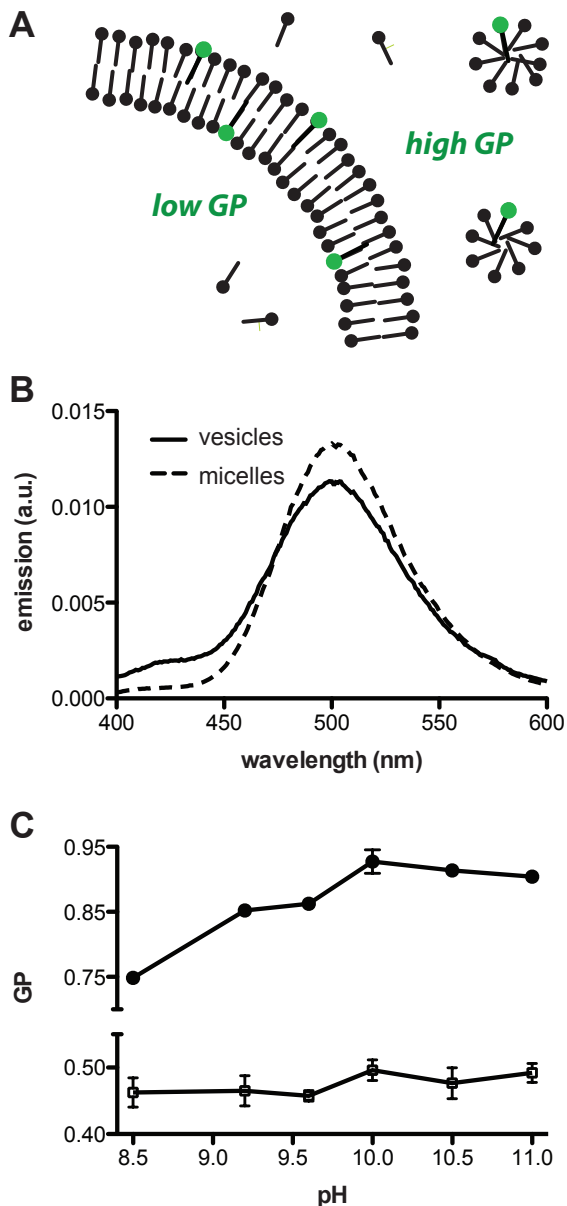


**Figure 2:** Laurdan as a probe of fatty acid aggregate composition. (A) High curvatures intrinsic to micellar geometries are expected to result in a higher GP for Laurdan molecules within them as compared to planar bilayers. (B) Emission spectrum for 25  $\mu$ M Laurdan (excitation 364 nm) in 10 mM oleate either at pH 8.5 (vesicles) or 10.5 (micelles). (C) Dependence of Laurdan GP on pH in 10 mM oleate with (open squares) or without (closed circles) 1% v/v Triton X100, which solubilizes all aggregates. Error bars indicate S.D. ( $n = 3$ ).

We observed a red shift in the Laurdan emission when incubated as a minor component (1:400) in fatty acid micelles as compared to vesicles (Figure 2B). This is explained by the high curvature of the micelle geometry, which results in increased water penetration compared to bilayers. We quantified this spectral shift using a standard unit-less ratio of emission intensities, termed a Generalized Polarization (GP) parameter (Materials and Methods). In oleate solutions, GP increased monotonically with pH until plateauing above pH 10 (Figure 2C). This was consistent with the pH-dependent change from a lamellar to micellar phase, with intermediate values (e.g. at pH 9) reflecting a coexisting state of vesicles and micelles [19]. These pH-dependent changes in GP were not observed when detergent (Triton X100) was present and thus were not caused by the pH change per se, but rather the structure of the resulting aggregate. GP was also notably insensitive to vesicle radius, and thus mean curvature, in extruded samples (Figure S4). This was consistent with our previous results on bending relaxation in fatty acid vesicles [23].

We next asked if the Laurdan GP is dependent on the concentration of the fatty acid solution. At concentrations below the aggregation concentrations, Laurdan emission and GP were low, likely reflecting the insolubility of the dye in the absence of hydrophobic aggregates (Figure S3). Upon aggregation, GP remained constant with regard to concentration for the three fatty acids tested at pH 10.5 (Figure 3A). Therefore, the micelle aggregate is structurally consistent over this concentration range, though it is likely heterogeneous in nature. In contrast, solutions at pH 8.5 showed a dramatic dependence of GP on concentration (Figure 3B). Concentrations just above  $c_{ac}$  had GP close to that for micelles, which decreased as the concentration increased. We interpreted this data to indicate a concentration-dependence on fatty acid aggregation, with

micelles favored in low concentration solutions. We also observed this effect in oleate solutions at pH 9.2, with GP plateauing to an intermediate value reflecting a roughly equal mixture of micelles and vesicles (Figure 3C). Assuming that Laurdan partitions representatively between micelles and vesicles, its emission in a solution can be modeled as a weighted average between characteristic micelle and vesicle emissions (Materials and Methods). Using this approach, we approximated the micelle to vesicle partition coefficient as a function of concentration in the systems tested (Figure 3D). These are relative partition coefficients in regards to the reference vesicle solutions at 30 or 50 mM, and are thus expressed as apparent  $X_m/X_v$ .

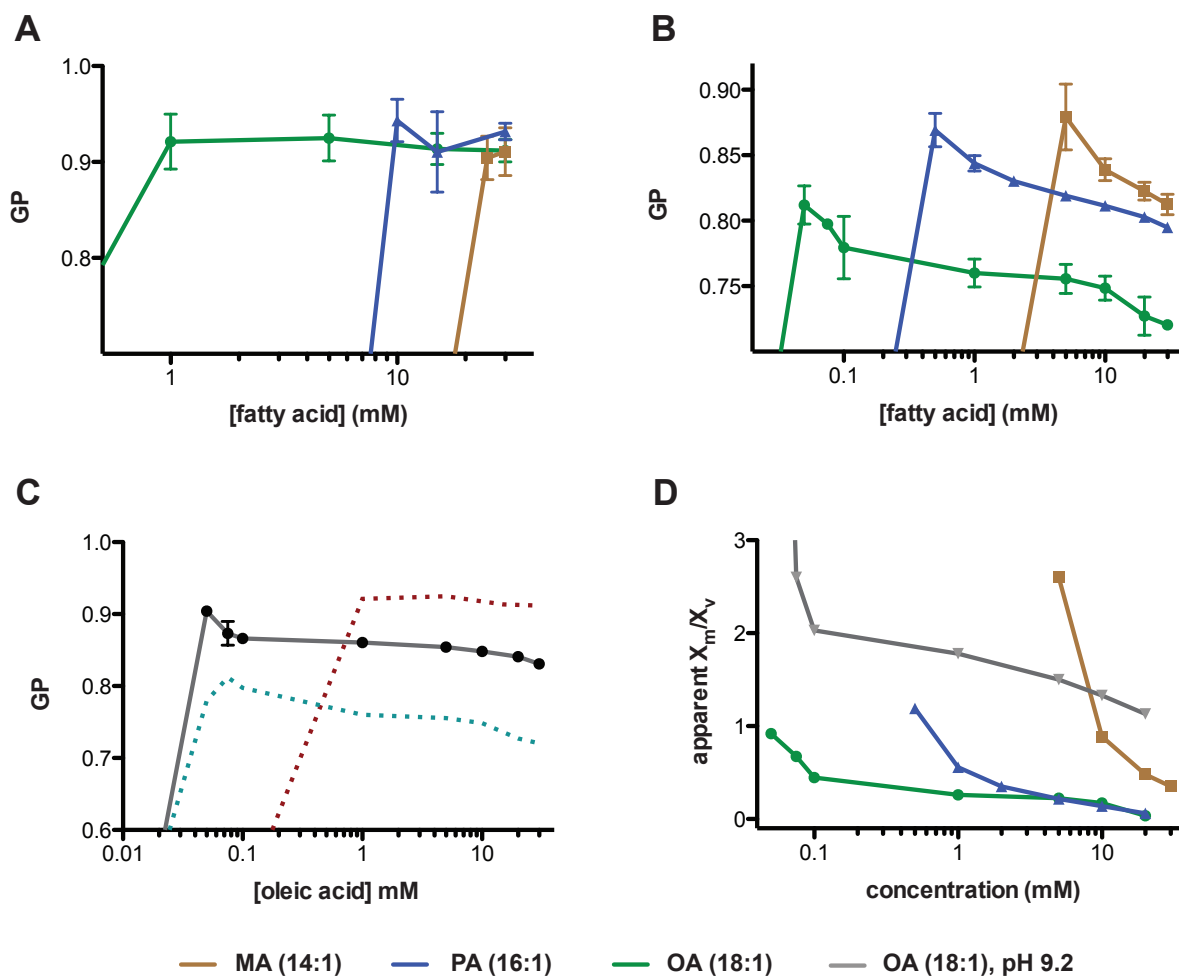


**Figure 3:** Concentration dependence of Laurdan GP. (A) GP as a function of concentration for monounsaturated fatty acids at pH 10.5. GP is constant for concentrations above the cmc. (B) GP as a function of concentration for monounsaturated fatty acids at pH 8.5. GP drops monotonically once above the cac, reflecting a change in the aggregate composition. (C) GP as a function of concentration in oleate at pH 9.2. Dotted lines representing equivalent curves for pH 10.5 (red) and 8.5 (blue) are provided for clarity. (D) Apparent micelle to vesicle partition coefficients as a function of concentration in vesicle solutions at pH 8.5 or 9.2. Low concentration solutions are enriched in micellar aggregates. Error bars indicate S.D. (n = 3).

We tested the concentration dependence of the vesicle fraction independently by turbidity of vesicle of solutions, which were extruded to 50 nm to control for effects of vesicle size. Phospholipid (dimyristoleoyl phosphocholine) solutions, which only form vesicles, featured a linear increase in turbidity with concentration, corresponding to the expected linear increase in vesicle abundance (Figure S4). In contrast, the absorbance of myristoleate solutions increased non-linearly above the cac, with more dilute solutions depleted in vesicle abundance (Figure 4A). From these absorbance values, we calculated apparent micelle to vesicle partition coefficients, assuming the excess fatty acid incorporates as micelles (Materials and Methods). These values corresponded well with the partition coefficients derived from Laurdan measurements (Figure 4B).

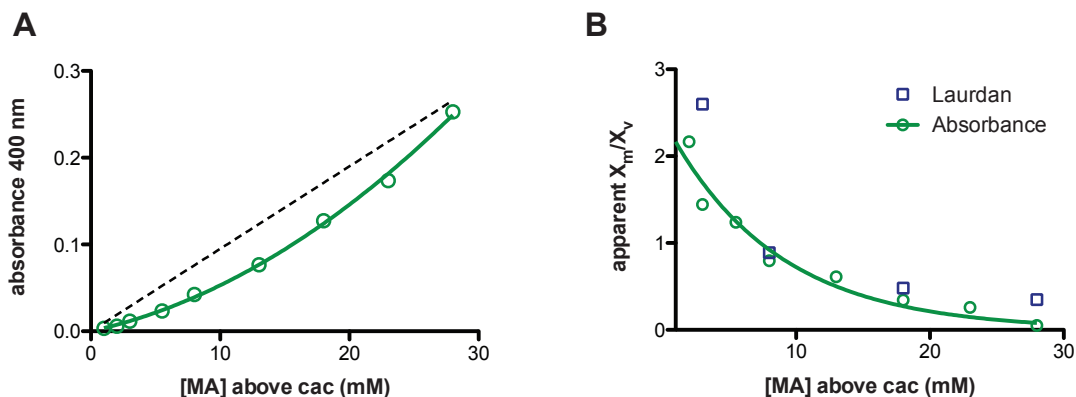


**Figure 4:** Concentration-dependence of vesicle abundance in myristoleate solutions. (A) Turbidity of myristoleate solutions at pH 8.5 extruded to 50 nm. Dashed line is the expected absorbance if the vesicle abundance scaled linearly with concentration, relative to the absorbance at 50 mM. Concentrations given are solution concentrations above the myristoleate cac, 2mM. (B) Apparent micelle to vesicle partition coefficients for myristoleate at pH 8.5 as derived from absorbance readings. Partition coefficients align with those taken from Laurdan GP (blue squares).

The shift from micelles to vesicles upon pH drop has long been used as a model system for vesicle growth. We therefore hypothesized that the concentration-dependence of the micelle-vesicle equilibrium could provide an additional mechanism for the growth of pre-existing fatty acid vesicles. In this scenario, a rise in amphiphile concentration causes the incorporation of excess micellar fatty acids into vesicles, and dilution would analogously drive their shrinkage or dissolution. We tested this possibility by monitoring changes in the membrane area of 100 nm vesicles using a Forster resonance energy transfer (FRET) growth assay [7, 18]. This assay quantitatively relates changes in FRET between membrane anchored FRET pairs to changes in dye concentrations and therefore membrane surface area (Materials and Methods). We first

diluted 10 mM myristoleate vesicles to 5 mM with buffer and observed a rapid reduction in surface area (Figure 5). The dilution buffer contained 2 mM myristoleate, at the cac, so shrinkage was not due to general aggregate dissolution. This shrinkage was subsequently relaxed by the addition of preformed 20 mM myristoleate vesicles, which effectively returned the solution lipid concentration back to 10 mM. We were likewise able to demonstrate multiple cycles of growth and shrinkage by modulating the fatty acid concentration in the solution (Figure 5).

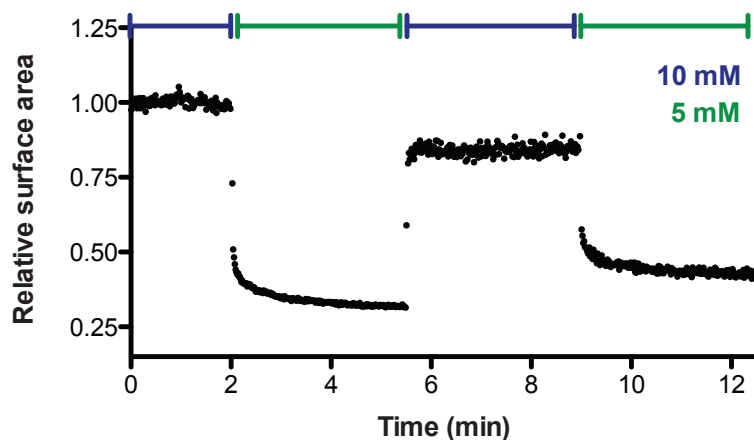


**Figure 5:** Reversible vesicle growth driven by amphiphile concentration changes.

Myristoleate vesicles, initially at 10 mM, shrink in surface area upon dilution to 5 mM. Surface area grows back to near the initial value upon concentration via the addition of preformed vesicles and subsequently shrinks upon further dilution. Changes in membrane area are tracked by the FRET between donor and acceptor phospholipids, which remain in the vesicles due to their insolubility.

We next asked whether concentration-driven growth is robust enough to drive the previously observed filamentous shape transition in large, multilamellar vesicles. Growth of such vesicles by addition of multi-fold excess of micelles has been shown drive the transformation of initially spherical vesicles into extended filamentous vesicles [10, 12]. This pathway provides a

straightforward route for protocell division due to the intrinsic fragility of this morphology, which breaks up into daughter vesicles in the presence of mild shear forces [10]. To test this possibility, we prepared large myristoleate vesicles by large pore dialysis at a concentration of 5 mM. The initially spherical vesicles were brought to a concentration of 10 mM via the addition of pre-formed myristoleate vesicles and within 20 minutes had grown into long, thin filamentous vesicles (Figure 6). The shape transition occurs because volume growth is osmotically limited by solute (buffer) permeation, thus geometrically necessitating high surface area morphologies.

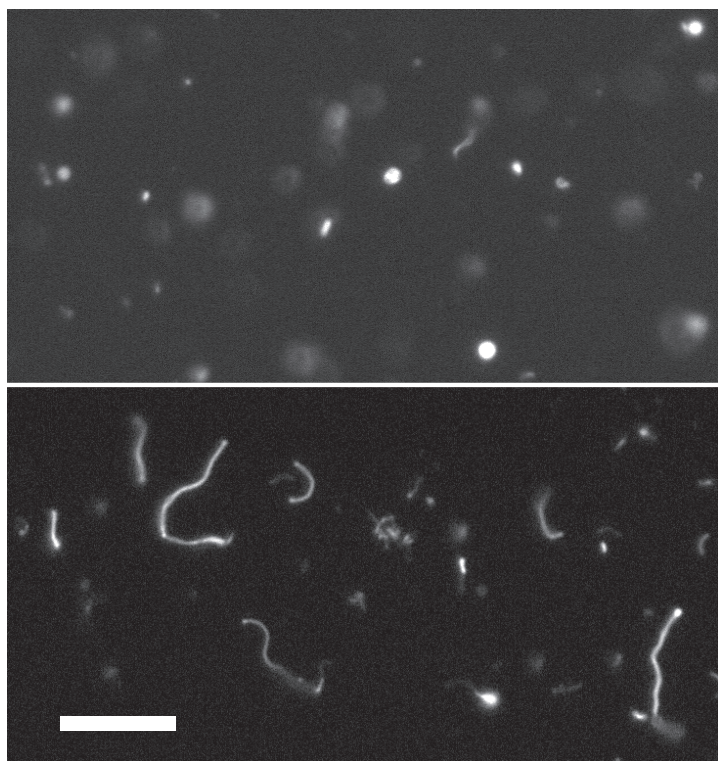


**Figure 6:** Growth of large vesicles by increase in amphiphile concentration. Multilamellar ( $\sim 4 \mu$ ) myristoleate vesicles, initially spherical (top), grow into long, filamentous vesicles upon addition of a concentration pre-formed vesicle solution (bottom). Growth occurs via this pathway because of the osmotically-limited increase in vesicle volume, and is similar to processes seen upon addition of alkaline micelles. Vesicles were labeled with a soluble fluorescent dye, which stayed entrapped during the experiment. Top image taken immediately after mixing, bottom taken

20 minutes later. Scale bar,  $30 \mu$ .



The simplest prebiotic mechanism for increasing lipid concentration would be by general solution evaporation. We therefore set up experiments to test whether gentle evaporation of fatty acid vesicle solutions could drive membrane growth through the incorporation of coexisting micelles (Figure 7). Solutions of myristoleate vesicles, initially at a lipid concentration of 5 mM, were allowed to evaporate under warm (35° C) agitation. Membrane area, monitored by FRET at discrete time points, approximately doubled over 24 hours as the lipid concentration rose to ~10 mM. This growth was similar in magnitude with that predicted from apparent micelle-vesicle partitions in Figure 4B (dashed line, Materials and Methods), and thus was consistent with our model for concentration-driven growth. Growth was not observed for phospholipid vesicles, which do not feature a coexisting solution state of micelles or monomers and thus were not predicted to change in membrane area upon concentration.

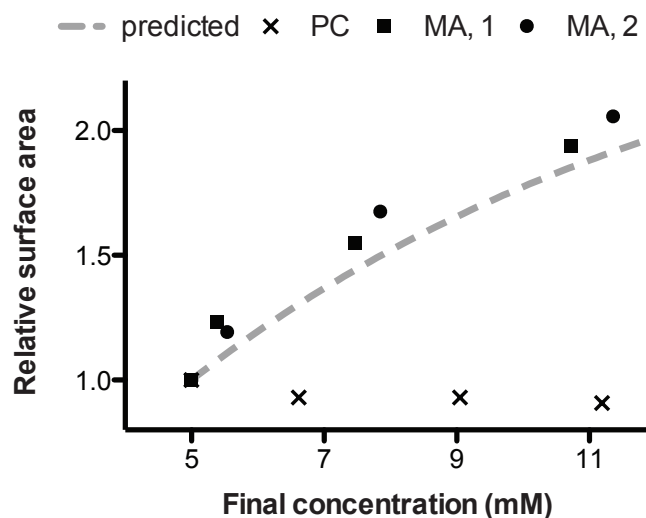


**Figure 7:** Solution evaporation drives the growth of fatty acid vesicles. Myristoleate (MA) vesicles, initially at 5 mM lipid concentration, were incubated in a solution undergoing gentle evaporation (Materials and Methods) and changes in surface area were monitored by FRET at time points of 3, 10, and 24 hours. Data is shown for two independent

experiments and is in agreement with that predicted from measured apparent micelle-vesicle partition coefficients (dashed line). An identical experiment with dimyristoleoyl phosphocholine (PC) vesicles did not show growth.

## Discussion

We have used a combination of physical and spectroscopic assays to characterize the phase behavior of fatty acid solutions in order to better understand models for prebiotic membrane assembly and function. Notably, we introduced the application of Laurdan to structurally differentiate between different fatty acid aggregates. This assay was complementary to standard approaches for measuring fatty acid monomer concentration (via surface tension) and vesicle abundance (via light scattering). At a given temperature and pressure, there are two determinants of fatty acid phase behavior in our system: pH, which controls head group ionization, and concentration, which entropically regulates aggregate size. Laurdan GP increases monotonically from pH 8.5 to pH 10, which reflects the previously identified transition from vesicle to micelle aggregates as the fatty acids become fully ionized and thus favor a higher curvature geometry. More surprisingly, we also found that GP at pH 8.5 decreases with concentration above the cac. We interpret this to reflect a concentration-dependent micelle-vesicle equilibrium, with lower concentrations favoring the smaller micellar aggregate and higher concentrations favoring the enthalpically favored vesicle aggregate. This behavior is independent of the concentration-dependent transition from monomers to aggregates (vesicles or micelles), which largely follows a pseudophase equilibrium that is characteristic of surfactant aggregation. The abundance of micelles at lower concentrations can be reasoned entropically, since these aggregates are much smaller than vesicles. The increasing magnitude of this effect with shorter chain length lipids (e.g. myristoleate vs. oleate) supports this hypothesis, as micelle aggregation number (and thus size) has a strong inverse dependence on chain length [27]. Our model for fatty acid aggregation is summarized in Figure S5.

Our results present a potentially simple mechanism for the growth of primitive cell membranes. Changes in concentration were almost certainly a feature of microenvironments on the prebiotic earth, and has previously been proposed to assist in building block chemistry [28], nucleic acid purification [29, 30], genetic copying [31], and vesicle assembly [19]. Subjected to a concentrating environment, dilute solutions of pre-assembled protocells could have undergone growth as coexisting micelles incorporated into their bilayers. There are several prebiotically relevant concentrating methods, but slow evaporation, as would be expected in a warm pond, is the simplest and is demonstrated to drive growth here (Figure 7). Growth could also occur as a result of the deposition of new fatty acids into the environment, which would effectively raise the solution concentration and is mimicked in experiments here via the addition of pre-formed vesicles (Figures 5 and 6).

The apparent reversibility of concentration-driven growth (e.g. Figure 5) provides a potential limitation to continuous growth by this mechanism. If solution concentration were followed by dilution, such as in drying and precipitation cycles, vesicle growth would be subsequently relaxed. However, there could be several kinetic barriers to vesicle shrinkage upon dilution. For example, the build up of osmotic gradients across the membrane upon membrane loss could temporarily stabilize vesicles relative to the solution state, as has been previously shown in these systems [11]. Alternatively, spontaneous vesicle division [32] following growth into filamentous morphologies (e.g. Figure 6) could retard shrinkage, as membrane loss would be favored from undivided vesicles characterized by excess membrane area. If shrinkage can be arrested in a

subset of the vesicle population, cycles of concentration and dilution would provide a continuing  
– and selective - growth mechanism.

## Supporting Figures

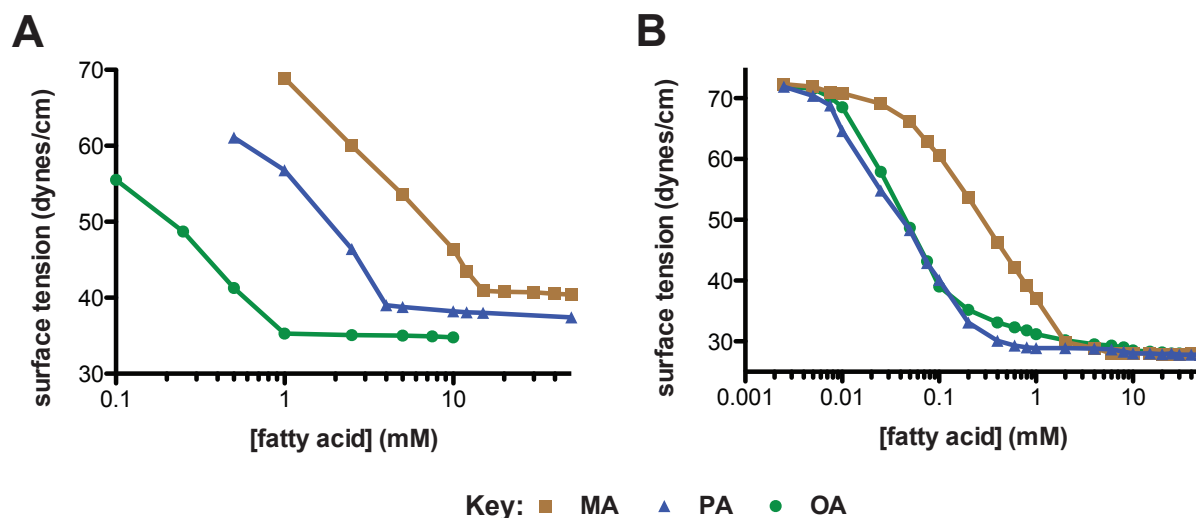


**Figure S1:** Surface tension of fatty acid solutions at pH 10.5 (A) and 8.5 (B). Surface tension measurements were taken by the Noüy ring method. MA, myristoleate (C14:1); PA, palmitoleate (C16:1), OA, oleate (C18:1).

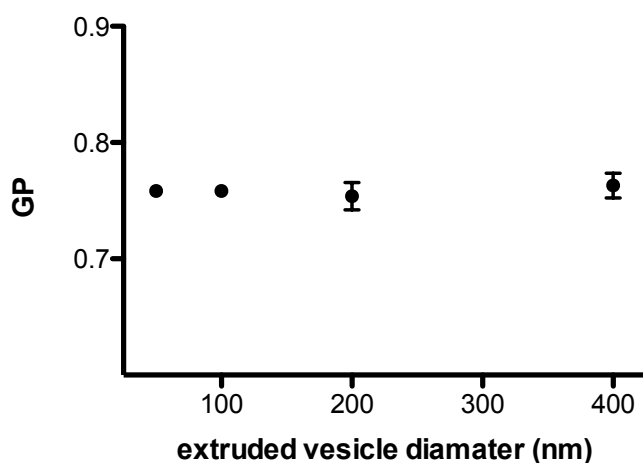


**Figure S2:** Dependence of Laurdan GP on the extruded vesicle size. 10 mM oleate at pH 8.5 was extruded using the filters with pore sizes of the given diameter. GP is independent of extruded diameter and thus is independent of vesicle size at these ranges.

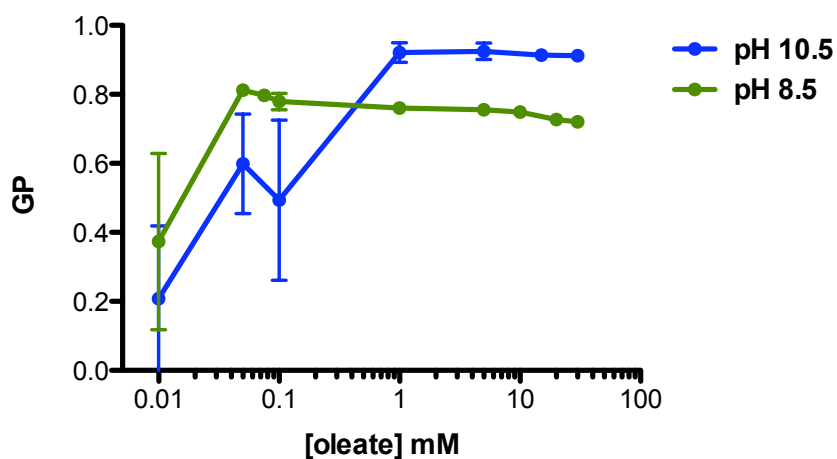


**Figure S3:** Concentration dependence of Laurdan GP in oleate solutions during the monomer-aggregate transition. Solutions below the critical concentrations (1 mM at pH 10.5, 20  $\mu$ M at pH 8.5) are characterized by noisy Laurdan emission with low GP, likely reflecting the insolubility of the dye in the absence of hydrophobic aggregates. Upon aggregation, Laurdan partitions into the aggregates and samples their composition.

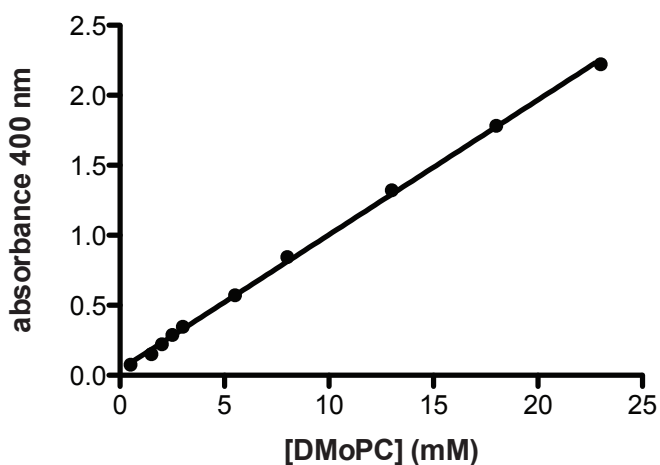


**Figure S4:** Turbidity of 50 nm (dimyristoleoyl phosphocholine) phospholipid vesicles scales linearly with concentration.

*concentration*

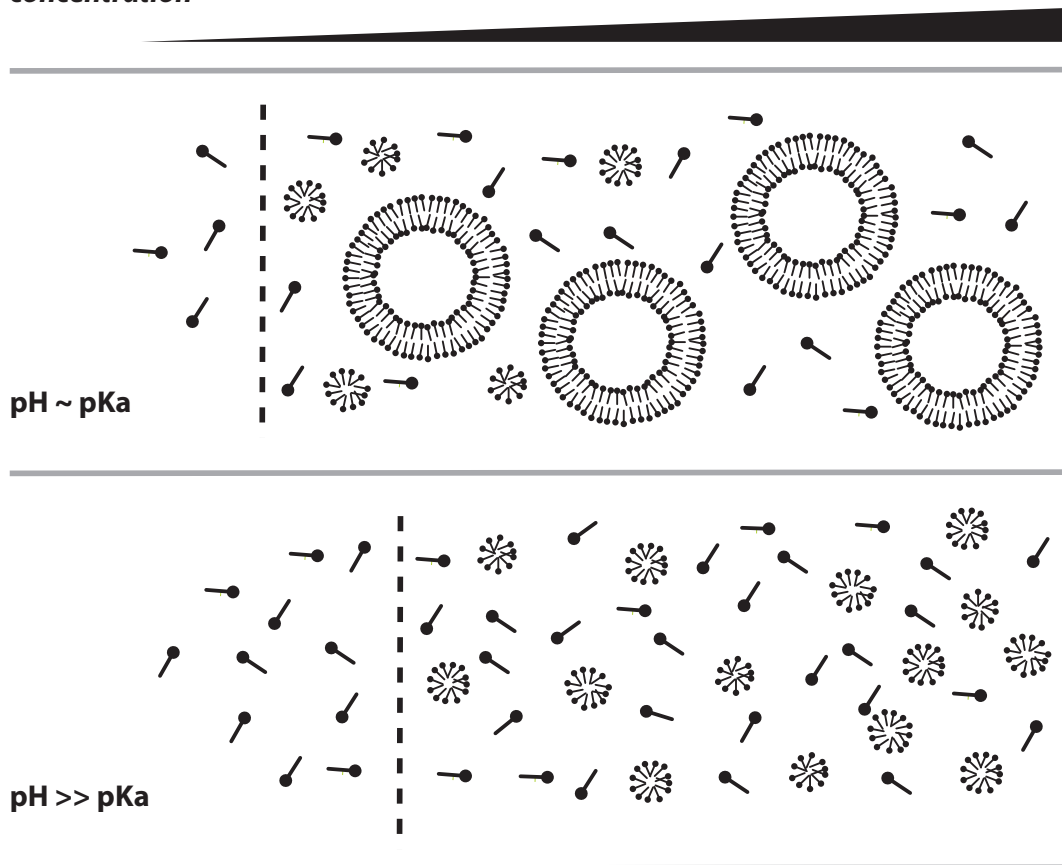


**Figure S5:** Model for fatty acid phase behavior. Solutions feature a pseudophase separation from monomers to aggregates, characterized by a cac (dashed line) that is dependent on pH. In addition, vesicle solutions feature a concentration-dependent vesicle-micelle equilibrium, with higher concentrations favoring the larger vesicle aggregates.

## Materials and Methods

**Lipid solutions:** Fatty acids were obtained from Nu-chek and phospholipids from Avanti Polar Lipids. Laurdan, NBD-PE (N-(7-Nitrobenz-2-Oxa-1,3-Diazol-4-yl)-1,2-Dihexadecanoyl-sn-Glycero-3-Phosphoethanolamine) and Rhodamine-DHPE (Rhodamine B 1,2-Dihexadecanoyl-sn-Glycero-3-Phosphoethanolamine) were obtained from Invitrogen. All other reagents were from Sigma-Aldrich. Fatty acid vesicle solutions were prepared by mixing the fatty acids (as neat oil) in 0.2 M bicine buffer titrated with NaOH to pH 8.5, unless otherwise noted. This was followed by vigorous vortexing and tumbling overnight. Micelle solutions were prepared by the dissolving the fatty acid in water titrated with sodium hydroxide to pH 10.5, unless otherwise noted. Phospholipid vesicles were prepared by thin film rehydration of chloroform solutions. Laurdan was incorporated into the solutions as a concentrated stock in ethanol either before addition of buffer. FRET dyes were incorporated into fatty acid solutions by addition in chloroform to the neat oil, followed by rotary evaporation. Large, multilamellar vesicles were prepared with 2 mM 8-Hydroxypyrene-1,3,6-trisulfonic acid (HPTS), a water soluble dye for imaging, in the buffer and were isolated via extrusion through a 5  $\mu$  filter followed by dialysis against a 1  $\mu$  filter, as previously described [32]. All other vesicle solutions were extruded 11 times through 100 nm filters with an Avanti mini extruder. 50 nm vesicles were prepared with an additional 11 passes through a 50 nm filter.

**Surface tension measurements:** Surface tensions were measured by the Noüy ring method on a Fisher Scientific Surface Tensiometer 21. Samples (5 ml) were prepared by serially diluting a



concentrated (100 mM) vesicle/micelle stock and then allowed to equilibrate for at least 24 hours before measuring. All measurements were taken at 21° C. Monomer concentrations were calculated from surface tension plots using the Langmuir-Szyszkowski equation:

$$\sigma_0 - \sigma = RT\Gamma_{max} \log \left( \frac{c}{K} + 1 \right)$$

where  $\sigma$  is the measured surface tension,  $\sigma_0$  is the surface tension with no surfactant (72.8 dynes/cm),  $K$  is the equilibrium constant for surface adsorption,  $\Gamma_{max}$  is the maximum surface excess, and  $c$  is the monomer concentration. Therefore,

$$c = K \left( e^{\frac{\sigma_0 - \sigma}{RT\Gamma_{max}}} - 1 \right)$$

We obtained  $\Gamma_{max}$  from the maximum slope of the surface tension vs.  $\log$ ([fatty acid]) plot according to the Gibbs isotherm:

$$\Gamma = - \frac{1}{RT} \frac{\partial \sigma}{\partial \log c}$$

Lastly,  $K$  was obtained by solving for  $c$  in the linear region below the cmc/cac.

**Light scattering measurements:** Light scattering intensities of oleate and palmitoleate solutions were measured on a Precision Detectors dynamic light scatterer. Absorbance readings of myristoleic acid solutions were taken on an Amerisham Ultrospec 3100 UV/Vis spectrophotometer. All measurements were taken at 21° C.

**Laurdan measurements:** Steady state fluorescence readings were performed on a Varian Cary Eclipse fluorimeter. General Polarization values were calculated as a unit-less ratio:

$$GP = \frac{I_{500} - I_{430}}{I_{500} + I_{430}}$$

where  $I_{500}$  and  $I_{430}$  are the emission at 500 nm and 430 nm, respectively, upon excitation at 364 nm. We note that this is opposite in sign of the commonly used form of GP for Laurdan in phospholipid membranes. This is because of the generally larger red shift of Laurdan in fatty acid aggregates as compared to phospholipid membranes. All measurements were taken at 21° C.

**Partition coefficients:** Micelle to vesicle partition coefficients were derived from measured Laurdan intensities by equating GP as a weighted average of micelle and vesicle emissions and partitions. Characteristic vesicle ( $I_{500}^v, I_{430}^v$ ) and micelle ( $I_{500}^m, I_{430}^m$ ) Laurdan intensities for each fatty acid were measured at pH 8.5 and 10.5, respectively, and a concentration of either 30 mM (oleate, palmitoleate) or 50 mM (myristoleate). The micelle/vesicle partition was calculating by solving for  $X_m$  (micelle aggregation fraction) and  $X_v$  (vesicle aggregation fraction) in the following:

$$GP = \frac{X_m(I_{500}^m - I_{430}^m) + X_v(I_{500}^v - I_{430}^v)}{X_m(I_{500}^m + I_{430}^m) + X_v(I_{500}^v + I_{430}^v)}$$

$$X_m + X_v = 1$$

where  $GP$  is the measured Laurdan polarization for the given sample. We note that this approach carries several assumptions: 1) the only existing aggregates are micelles or vesicles, with representative sampling of Laurdan between them minimal contribution from the monomer phase 2) Laurdan emission ratios at high concentrations (30 or 50 mM) at pH 8.5 or pH 10.5 approximate that in a pure vesicle or pure micelle solution. The latter assumption is limited by of the excess light scattering of more concentrated vesicle solutions and the differing pKas of the fatty acids, which likely result in a micelle:vesicle ratio of  $> 0$  at pH 8.5 and the reference concentrations used. Partition coefficients as therefore expressed as ‘apparent  $X_m/X_v$ ’, which are relative to the solution standard used.

Micelle/vesicle partitions were also derived from absorbance at 400 nm ( $Abs_{400}^c$ ). The vesicle fraction was calculated as proportional to the normalized absorbance per concentration above the cac (2 mM for myristoleate). The micelle fraction was assumed to be the difference between this and the normalized vesicle absorbance at 50 mM ( $Abs_{400}^v$ ), assuming  $X_v \sim 1$  at 50 mM.

Therefore,

$$X_v = k * \frac{Abs_{400}^c}{c - cac}$$

$$X_m = k * \left( Abs_{400}^v - \frac{Abs_{400}^c}{c - cac} \right)$$

$$X_m/X_v = \left( Abs_{400}^v - \frac{Abs_{400}^c}{c - cac} \right) / \frac{Abs_{400}^c}{c - cac}$$

where k is the inverse of the absorption per unit concentration of 50 nm myristoleate vesicles and c is the solution concentration. This derivation involves the same assumptions used as for the Laurdan partition coefficients and is therefore comparable.

**Vesicle growth:** Growth and shrinkage of 100 nm myristoleate vesicles was monitored as previously described [12, 18]. Briefly, 10 mM myristoleate vesicles were prepared with equal fractions of Rhodamine-DHPE and NBD-DHPE at a concentration of 0.2 mol % relative to total lipids. During experiments, FRET was recorded on a Cary Eclipse fluorimeter (excitation 430 nm) by quantifying FRET efficiency,  $F_\varepsilon$ :

$$F_\varepsilon = 1 - \frac{E_D}{E_{D,\infty}}$$

where  $E_D$  is the emission of the donor (530 nm) and  $E_{D,\infty}$  the emission of the donor at infinite dilution, which was measured via addition of 1% Triton X100 at the end of the experiment. All

values were adjusted for changes in volume. FRET efficiency was equated to surface area using a standard curve of 10 mM myrisoleate with varying concentrations of FRET dyes. Growth of large vesicles was observed on Nikon TE2000-S inverted microscope using a 60X ELWD objective. All measurements were taken at 21° C.

**Solution evaporation:** Vesicle solutions (5 mM in 400  $\mu$ L 0.1 M Na<sup>+</sup> bicine) were agitated via stir bar (150 RPM) in opaque 5 mL glass vials at 35° C. Agitation was used to keep solutions homogenous and prevent films from forming on the side of the vials. This method led to an evaporation rate of approximately 10  $\mu$ L/hour. Identical experiments were also performed without evaporation (using capped vials) to confirm that there was no measurable bleaching and/or dye degradation in timescales up to 40 hours. Predicted relative surface area (SA) as a function of final concentration (c) was derived from the quadratic curve fit of the apparent  $X_m/X_v$  as a function of concentration in Figure 4B using the following:

$$SA(c) = \left[ \left( \frac{X_m}{X_m} \right)_{5mM} - \left( \frac{X_m}{X_m} \right)_c \right] + 1$$

Where  $\left( \frac{X_m}{X_m} \right)_{5mM}$  is the micelle-vesicle partition at 5 mM (initial concentration) and  $\left( \frac{X_m}{X_m} \right)_c$  is the micelle-vesicle partition at the final concentration.

## References

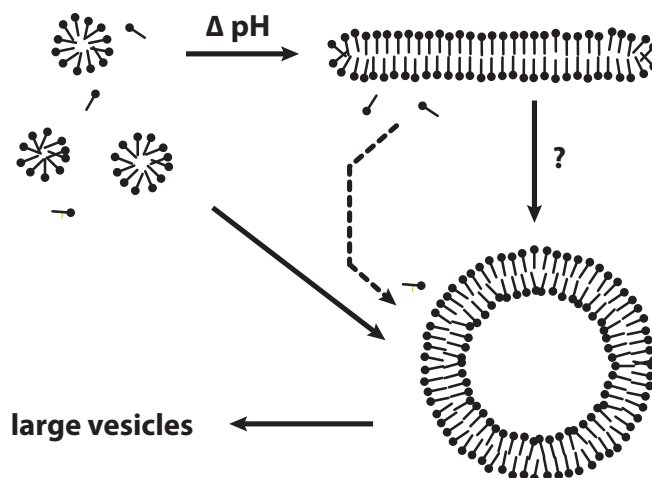
1. Gebicki, J.M. and M. Hicks, *Ufasomes are stable particles surrounded by unsaturated fatty acid membranes*. Nature, 1973. **243**(5404): p. 232-4.
2. Hargreaves, W.R. and D.W. Deamer, *Liposomes from ionic, single-chain amphiphiles*. Biochemistry, 1978. **17**(18): p. 3759-3768.
3. Rushdi, A.I. and B.R. Simoneit, *Lipid formation by aqueous Fischer-Tropsch-type synthesis over a temperature range of 100 to 400 degrees C*. Orig Life Evol Biosph, 2001. **31**(1-2): p. 103-18.
4. Simoneit, B.R.T., *Prebiotic organic synthesis under hydrothermal conditions: an overview*. Advances in Space Research, 2004. **33**(1): p. 88-94.
5. Yuen, G.U. and K.A. Kvenvolden, *Monocarboxylic Acids in Murray and Murchison Carbonaceous Meteorites*. Nature, 1973. **246**(5431): p. 301-303.
6. Deamer, D.W., *Boundary structures are formed by organic components of the Murchison carbonaceous chondrite*. Nature, 1985. **317**(6040): p. 792-794.
7. Hanczyc, M.M., S.M. Fujikawa, and J.W. Szostak, *Experimental models of primitive cellular compartments: encapsulation, growth, and division*. Science, 2003. **302**(5645): p. 618-22.
8. Mansy, S.S., et al., *Template-directed synthesis of a genetic polymer in a model protocell*. Nature, 2008. **454**(7200): p. 122-5.
9. Mansy, S.S. and J.W. Szostak, *Thermostability of model protocell membranes*. Proceedings of the National Academy of Sciences of the United States of America, 2008. **105**(36): p. 13351-5.
10. Zhu, T.F. and J.W. Szostak, *Coupled Growth and Division of Model Protocell Membranes*. J Am Chem Soc, 2009. **131**(15): p. 5705-5713.
11. Chen, I.A., R.W. Roberts, and J.W. Szostak, *The emergence of competition between model protocells*. Science, 2004. **305**(5689): p. 1474-6.
12. Budin, I. and J.W. Szostak, *Physical effects underlying the transition from primitive to modern cell membranes*. Proceedings of the National Academy of Sciences of the United States of America, 2011. **108**(13): p. 5249-54.
13. Cistola, D.P., et al., *Ionization and phase behavior of fatty acids in water: application of the Gibbs phase rule*. Biochemistry, 1988. **27**(6): p. 1881-8.

14. Haines, T.H., *Anionic lipid headgroups as a proton-conducting pathway along the surface of membranes: a hypothesis*. Proceedings of the National Academy of Sciences, 1983. **80**(1): p. 160-164.
15. Dejanović, B., et al., *An ESR characterization of micelles and vesicles formed in aqueous decanoic acid/sodium decanoate systems using different spin labels*. Chemistry and physics of lipids, 2008. **156**(1,2): p. 17-25.
16. Fukuda, H., et al., *Electron Spin Resonance Study of the pH-Induced Transformation of Micelles to Vesicles in an Aqueous Oleic Acid/Oleate System*. Langmuir, 2001. **17**(14): p. 4223-4231.
17. Böchliger, E., et al., *Matrix Effect in the Size Distribution of Fatty Acid Vesicles*. The Journal of Physical Chemistry B, 1998. **102**(50): p. 10383-10390.
18. Chen, I.A. and J.W. Szostak, *A kinetic study of the growth of fatty acid vesicles*. Biophys J, 2004. **87**(2): p. 988-98.
19. Budin, I., R.J. Bruckner, and J.W. Szostak, *Formation of protocell-like vesicles in a thermal diffusion column*. Journal of the American Chemical Society, 2009. **131**(28): p. 9628-9.
20. Budin, I. and J.W. Szostak, *Expanding roles for diverse physical phenomena during the origin of life*. Annual review of biophysics, 2010. **39**: p. 245-63.
21. Parasassi, T., Krasnowska, E.K., Bagatolli, L., Gratton, E., *Laurdan and Prodan as Polarity-Sensitive Fluorescent Membrane Probes*. Journal of Fluorescence, 1998. **8**(4): p. 1998.
22. Harris, F.M., K.B. Best, and J.D. Bell, *Use of laurdan fluorescence intensity and polarization to distinguish between changes in membrane fluidity and phospholipid order*. Biochimica et Biophysica Acta (BBA) - Biomembranes, 2002. **1565**(1): p. 123-128.
23. Bruckner, R.J., et al., *Flip-Flop-Induced Relaxation of Bending Energy: Implications for Membrane Remodeling*. Biophysical journal, 2009. **97**(12): p. 3113-3122.
24. Parasassi, T., et al., *Quantitation of lipid phases in phospholipid vesicles by the generalized polarization of Laurdan fluorescence*. Biophysical journal, 1991. **60**(1): p. 179-189.
25. Clint, J.H., *Surfactant Aggregation* 1992, Glasgow and London: Blackie.
26. HUANG, et al., *Formation and coexistence of the micelles and vesicles in mixed solution of cationic and anionic surfactant*. Vol. 273. 1995, Heidelberg, ALLEMAGNE: Springer.

27. Israelachvili, J.N., D.J. Mitchell, and B.W. Ninham, *Theory of self-assembly of hydrocarbon amphiphiles into micelles and bilayers*. Journal of the Chemical Society, Faraday Transactions 2: Molecular and Chemical Physics, 1976. **72**: p. 1525-1568.
28. Nelson, K.E., et al., *Concentration by evaporation and the prebiotic synthesis of cytosine*. Orig Life Evol Biosph, 2001. **31**(3): p. 221-9.
29. Zanchetta, G., et al., *Phase separation and liquid crystallization of complementary sequences in mixtures of nanoDNA oligomers*. Proc Natl Acad Sci U S A, 2008. **105**(4): p. 1111-7.
30. Baaske, P., et al., *Extreme accumulation of nucleotides in simulated hydrothermal pore systems*. Proceedings of the National Academy of Sciences of the United States of America, 2007. **104**(22): p. 9346-51.
31. Monnard, P.A., A. Kanavarioti, and D.W. Deamer, *Eutectic phase polymerization of activated ribonucleotide mixtures yields quasi-equimolar incorporation of purine and pyrimidine nucleobases*. J Am Chem Soc, 2003. **125**(45): p. 13734-40.
32. Zhu, T.F. and J.W. Szostak, *Coupled growth and division of model protocell membranes*. Journal of the American Chemical Society, 2009. **131**(15): p. 5705-13.
33. Zhu, T.F. and J.W. Szostak, *Preparation of large monodisperse vesicles*. PLoS One, 2009. **4**(4): p. e5009.

## Appendix: Structural kinetics of the micelle to vesicle transition

Itay Budin, Anik Debnath, and Jack W. Szostak



A major advantage of fluorescence-based structural assays over other tools is their time resolution, which allows them to kinetically track molecular processes. We thus applied the probe Laurdan, introduced in chapter 4 to discern between micelles and vesicles, to study the structural transition between these two states upon immediate pH drop. This process has been extensively studied, yet the mechanisms involved remain unclear. Vesicle assembly, as read out from changes in turbidity, is generally slow (minutes to hours). Assembly features sigmoidal kinetics and can be catalyzed by the presence of pre-existing vesicles [1] or mineral surfaces [2], which eliminate the initial lag. However, assays for micelle aggregation, such as changes in dynamic light scattering and the formation of pyrene excimers [3], indicate much faster timescales (< seconds). These differing timescales are shown in Figure 1.



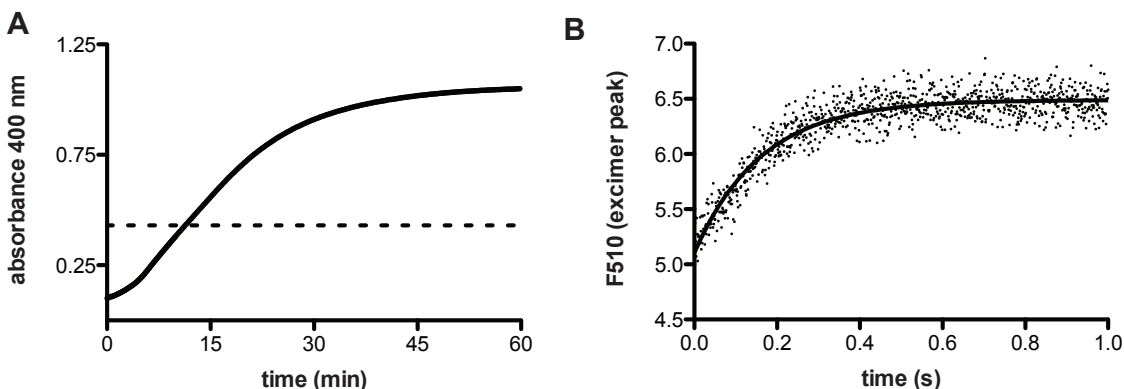


**Figure 1:** Differing timescales of the micelle to vesicle transition upon pH drop. (A) Vesicle assembly by turbidity readings shows slow sigmoidal kinetics. Dashed line indicates the turbidity of the final sample extruded to 50 nm, showing that this reading does not discern between de novo vesicle formation and the subsequent growth of those vesicles. (B) Micelle aggregation by a pyrene-excimer assay shows rapid kinetics. Pyrene, solubilized statistically as monomers in micelles, undergoes a spectrum shift in the presence of larger aggregates, which allow multiple pyrenes to associate (‘excimers’). This assay is similar to that used in reference 3. Both experiments run at 21° C with 10 mM oleate, 0.2 M bicine pH 8.5 (final concentrations); micelles initially kept at pH 11 via titration with NaOH.

We tracked the change in the GP of Laurdan in oleate micelles (pH 11) upon rapid mixing with buffer (pH 8.5). We observed an initial rapid drop in GP to a value below that for vesicles, followed by a slow recovery to the characteristic vesicle GP. The timescales of these two phases largely match those of micelle aggregation and vesicle assembly, respectively. When micelles were added to a three-fold excess of pre-formed vesicles, we only observed a single-exponential decay to the vesicle GP value. The timescale of this decay was consistent with timescales for membrane growth via micelle addition [3].

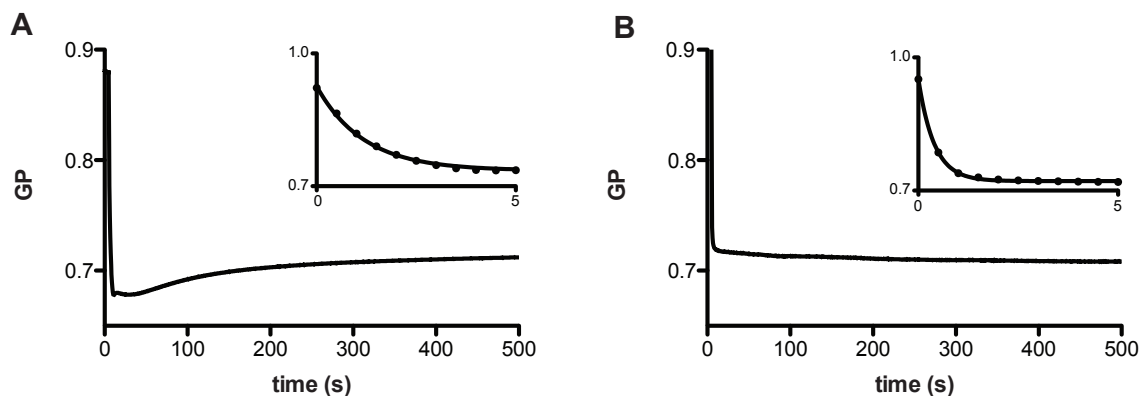


**Figure 2:** The micelle to vesicle transition tracked by Laurdan. (A) Upon dilution in buffer, micelles undergo two structural transitions. An initial rapid drop in Generalized Polarization (insert,  $k \sim 1 \text{ s}^{-1}$ ), followed by a slow ascent ( $k \sim 0.01 \text{ s}^{-1}$ ) to the characteristic vesicle GP value. (B) Upon dilution in buffer containing pre-formed vesicles (3-fold excess), micelles undergo a single, rapid drop in GP (insert,  $k \sim 2 \text{ s}^{-1}$ ) to the characteristic vesicle GP value. Both experiments run at  $21^\circ \text{ C}$  with 10 mM oleate micelles, 0.2 M bicine pH 8.5 (final concentrations); micelles initially kept at pH 11 via titration with NaOH.

These results present two intriguing questions, which we are actively exploring:

1) What is the structure of the intermediate aggregate between micelles and vesicles? The GP value of this structure(s) is below that for the mature fatty acid membrane, suggesting that it is more ordered than its corresponding membrane. I hypothesize that this reflects a planar intermediate, e.g. a disk-like micelle or membrane patch. Similar metastable state has been documented in other lipid systems by x-ray and neutron scattering [4-6]. Increased ordering could be a result of line tension from exposed bilayer edges, which could drive tighter packing of the structure in order to minimize interfacial energy.

2) By what process does the intermediate aggregate mature into vesicles? This step is rate-limiting for vesicle assembly and presumably faces kinetic barriers in order to account for long timescales. If we assume the presence of a disc-like intermediate, then its growth to a critical size is likely needed before the structure can ‘fold up’ into a vesicle, thereby eliminating its edge energy. One possibility is that growth could occur via Ostwald ripening driven by this very same line tensions. Two observations support this hypothesis. First, the rate for the recovery in GP (the second phase) does not scale with micelle concentration. This is inconsistent with any first order process of molecular aggregation. Second, we have observed that the incorporation of phospholipids, even in very small amounts (e.g. 2%) inhibit vesicle assembly, yet allow for the initial micellar aggregation. This has been previously observed in our lab [7] and is perplexing since bilayers are a much more energetically favorable state for phospholipids than micelles. An appealing explanation lies in the insolubility of phospholipids and the ability of insoluble components to retard Ostwald ripening [8].

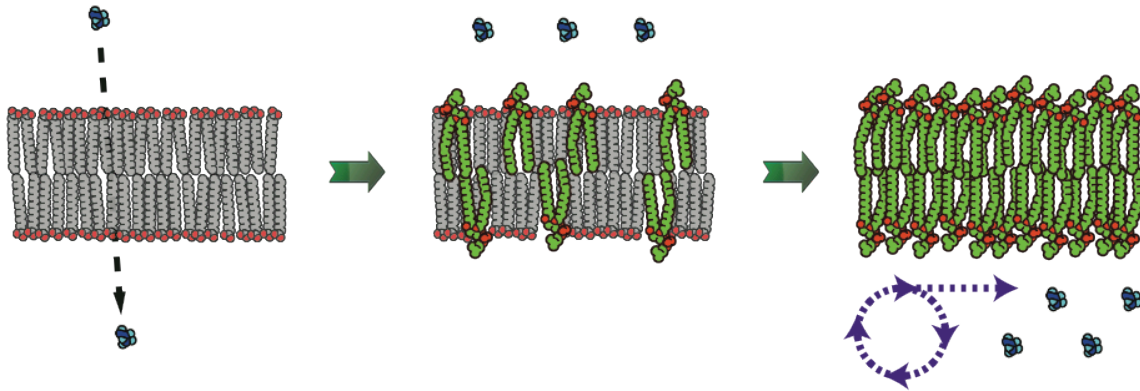
In summary, initial data has led us to a hypothesis that the micelles assemble into vesicles via a planar aggregate intermediate, whose growth via Ostwald ripening is rate limiting for this process. Further experiments will be performed to test this model and further characterize this transition. The ability of phospholipids to arrest this process is especially promising, as it might allow for the use of less ambiguous structural tools that otherwise suffer from poor time resolution, e.g. electron microscopy.

## References

1. Rasi, S., F. Mavelli, and P.L. Luisi, *Matrix effect in oleate micelles-vesicles transformation*. Orig Life Evol Biosph, 2004. **34**(1-2): p. 215-24.
2. Hanczyc, M.M., S.S. Mansy, and J.W. Szostak, *Mineral surface directed membrane assembly*. Orig Life Evol Biosph, 2007. **37**(1): p. 67-82.
3. Chen, I.A. and J.W. Szostak, *A kinetic study of the growth of fatty acid vesicles*. Biophys J, 2004. **87**(2): p. 988-98.
4. Weiss, T.M., et al., *Dynamics of the Self-Assembly of Unilamellar Vesicles*. Physical Review Letters, 2005. **94**(3): p. 038303.
5. Egelhaaf, S.U. and P. Schurtenberger, *Micelle-to-Vesicle Transition: A Time-Resolved Structural Study*. Physical Review Letters, 1999. **82**(13): p. 2804-2807.
6. Leng, J., S.U. Egelhaaf, and M.E. Cates, *Kinetics of the Micelle-to-Vesicle Transition: Aqueous Lecithin-Bile Salt Mixtures*. Biophysical journal, 2003. **85**(3): p. 1624-1646.
7. Fujikawa, S.M., I.A. Chen, and J.W. Szostak, *Shrink-Wrap Vesicles*. Langmuir, 2005. **21**(26): p. 12124-12129.
8. Taylor, P., *Ostwald ripening in emulsions*. Advances in Colloid and Interface Science, 1998. **75**(2): p. 107-163.

## Physical effects underlying the adoption of phospholipid membranes by early cells

Itay Budin and Jack W. Szostak



*Note: A version of the following was published in the Proceedings of the National Academy of Sciences.*

**Abstract:** To understand the emergence of Darwinian evolution it is necessary to identify physical mechanisms that enabled primitive cells to compete with one another. While all modern cell membranes are composed primarily of diacyl or dialkyl glycerol phospholipids, the first cell membranes are thought to have self-assembled from simple, single-chain lipids synthesized in the environment. We asked what selective advantage could have driven the transition from primitive to modern membranes, especially during early stages characterized by low levels of membrane phospholipid. Here we demonstrate that surprisingly low levels of phospholipids can drive protocell membrane growth during competition for single-chain lipids. Growth results from the decreasing fatty acid efflux from membranes with increasing phospholipid content. The ability to synthesize phospholipids from single-chain substrates would have therefore been highly advantageous for early cells competing for a limited supply of lipids. We show that the resulting increase in membrane phospholipid content would have led to a cascade of new

selective pressures for the evolution of metabolic and transport machinery to overcome the reduced membrane permeability of diacyl lipid membranes. The evolution of phospholipid membranes could thus have been a deterministic outcome of intrinsic physical processes and a key driving force for early cellular evolution.

## **Introduction**

The first cell membranes are likely to have formed from simple, single-chain lipids such as short-chain fatty acids and their derivatives, that were present in the prebiotic environment (1, 2). Membranes composed of such amphiphiles are permeable to polar nutrients such as nucleotides (3) and feature the dynamic properties necessary for spontaneous growth and division (2, 4). The high permeability of fatty acid-based membranes is consistent with a heterotrophic model for early cells, in which chemical building blocks are synthesized in the environment and passively diffuse across the cell membrane to participate in replication. All modern cells synthesize phospholipids (or sulfolipids in rare exceptions (5, 6)) with two hydrophobic chains as their primary membrane lipids. Phospholipid membranes prevent the rapid permeation of ions and polar molecules, allowing modern cells to retain internally synthesized metabolites and to control all import and export. The evolution of phospholipid membranes must have therefore mirrored the emergence of metabolic and transport machinery during early cellular evolution.

This transition from single-chain lipids to phospholipids had to be gradual, both to allow for the co-evolution of metabolic and transport machinery and because of the initial inefficiency of nascent catalysts (e.g. ribozymes). Hence, the selective advantage associated with phospholipid

synthesis had to apply to small differences in phospholipid content in order to drive this transition. What selective advantage could be conferred by the low levels of phospholipid that must have been present at the beginning of this process? Our laboratory has previously demonstrated that populations of fatty acid vesicles, representing primitive cellular compartments (protocells), are able to compete directly with each other via the exchange of fatty acid monomers (7). These exchange processes allow some vesicles to grow at the expense of others, e.g. RNA-induced osmotic swelling causes vesicles to grow by incorporating fatty acids from empty vesicles. Here we asked whether low levels of phospholipids, potentially synthesized by genomically encoded catalysts (e.g. ribozymes), could also drive competitive growth and therefore provide a clear selective pressure for the evolution of modern cell membranes. We were motivated by previous experiments suggesting that phospholipid-containing micelles can alter the fatty acid equilibrium between vesicles and micelles (8) and that pure phosphatidylcholine vesicles disrupt neighboring oleate vesicles (9).

## **Results**

### **Phospholipid-driven growth of fatty acid vesicles**

To address the hypothesis that phospholipids could drive competition between protocells we asked whether mixed fatty acid/phospholipid vesicles grow upon mixing with pure fatty acid vesicles. To monitor surface area change, we measured the Förster resonance energy transfer (FRET) between donors and acceptor fluorophores included at a fixed initial concentration in the bilayer. This assay quantitatively measures surface area by relating the decrease (or increase) in FRET to a change in fluorophore concentration (2, 7). We first asked whether 100 nm oleate

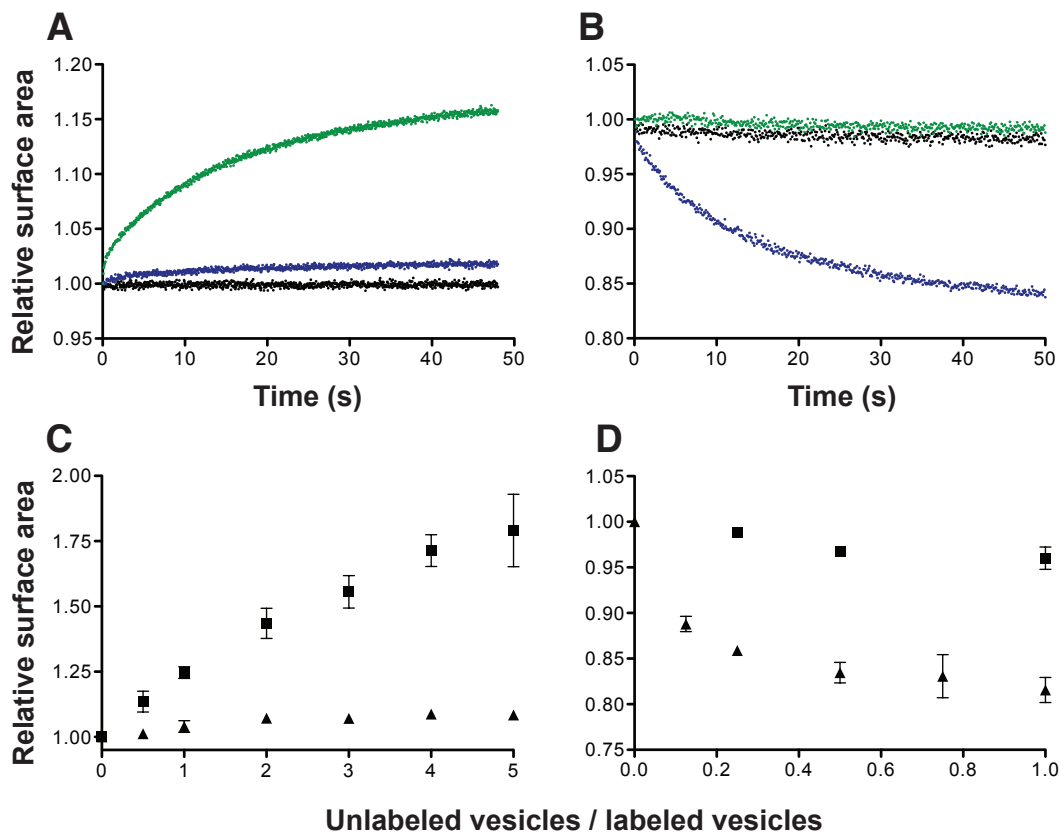


**Fig. 1.** Phospholipids drive competition between fatty acid vesicles. (*A-B*) Competition between vesicles was monitored by a FRET-based real time surface area assay. Growth of FRET-labeled 90:10 oleate:DOPA vesicles (*A*) and shrinkage of FRET-dye labeled oleate vesicles (*B*) when mixed 1:1 with buffer (black), unlabeled oleate vesicles (green), or unlabeled 90:10 oleate:DOPA vesicles (blue). (*C-D*) The dependence of vesicle growth or shrinkage on vesicle stoichiometry. Final growth after equilibrium of FRET-labeled 90:10 oleate:DOPA vesicles (*C*) and shrinkage of FRET-labeled oleate vesicles (*D*) when mixed with varying amounts of unlabeled oleate (■) or unlabeled 90:10 oleate:DOPA (▲) vesicles. Error bars indicate S.E.M. (N = 3).



vesicles containing 10 mol % di-oleoyl-phosphatidic acid (DOPA) grow upon mixing with 1 equivalent of pure oleate vesicles (Fig. 1A). After mixing, a ~16% increase in the surface area of the phospholipid-containing vesicles was observed ( $k \sim 0.1 \text{ s}^{-1}$ ). Mixing with either buffer or vesicles of the same composition did not lead to growth. We also observed the corresponding shrinkage of pure oleate vesicles upon mixing with vesicles containing 10 mol % DOPA (Fig. 1B), but not upon mixing with buffer or with additional oleate vesicles.

The emergence of a catalytically functional polymer from a population of random sequences would have been a rare stochastic event. Within a population of protocells, the first cell containing a phospholipid synthase catalyst would have been surrounded by a vast excess of protocells that could not synthesize phospholipids. We therefore considered the effect of the ratio of phospholipid-containing vesicles to pure fatty acid vesicles on the magnitude of the observed growth. We found that the amount of growth increased continuously as the ratio of fatty acid donor vesicles to phospholipid-containing acceptor vesicles increased (Fig. 1C). Indeed, the extent of growth appears to be limited only by the eventual dilution of initial phospholipid content. As a result, early phospholipid synthesizing cells would be expected to grow continuously, at the expense of neighboring vesicles, at a rate controlled by the rate at which they could synthesize phospholipid.

We next asked whether phospholipid-driven growth could facilitate vesicle division, as has been demonstrated for the growth of large multilamellar vesicles following fatty acid micelle addition (4). We prepared large (~4  $\mu$ ) multilamellar oleate vesicles containing 10 mol % DOPA and an encapsulated soluble dye (Fig. 2A). Upon mixing with a large excess of unlabelled oleate

vesicles, rapid growth was observed (Fig. 2B). Remarkably, growth proceeded by the same pathway as previously observed (4) following the rapid addition of excess fatty acid micelles: the extrusion of a thin tubular tail from the vesicle, followed by the transformation of the original spherical vesicle into a long, narrow filamentous vesicle (Fig. 3D). The cause of this shape change is the lag between surface area growth and volume growth, which is osmotically limited by the slowly permeating buffer in the medium (Fig. S1). When a mild shear force was applied to these filamentous structures by gentle agitation, efficient vesicle division was observed (Fig. 3C). This pathway allows for spontaneous protocell division without the need for pre-existing cellular machinery but is inaccessible by osmotically-driven competition, which leads to the growth of swollen and therefore spherical vesicles. We obtained similar results in experiments using a more prebiotically plausible lipid mixture of 2:1 decanoic acid: decanol and 10 mol % of di-decanoyl-phosphatidic acid (DDPA) (Fig. S2). This mixture of short saturated single-chain amphiphiles mimics the major products of the abiotic Fischer-Tropsch-Type synthesis (10) and lipids extracted from the Murchison meteorite (11).

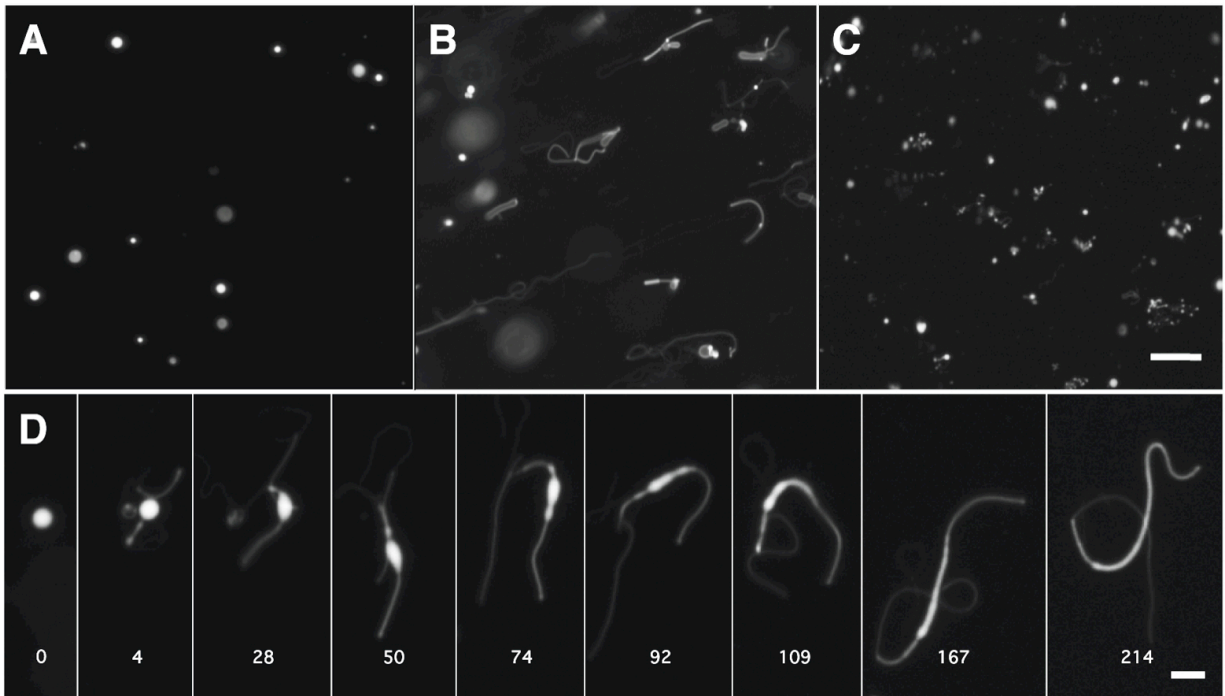


**Fig. 2.** Phospholipid-driven growth leads to a filamentous shape transition and vesicle division. (A) Large, multilamellar 90:10 oleate:DOPA vesicles, labeled with an encapsulated soluble dye, are initially spherical. (B) Upon mixing with a 100-fold excess of unlabelled oleate vesicles, the mixed vesicles rapidly grow into long, filamentous vesicles. (C) The fragile filamentous vesicles then readily divide into small daughter vesicles upon the application of gentle shear forces (see Methods) onto the sample. Scale bar, 30  $\mu\text{m}$ . (D) Time course showing the shape transformation of a labeled 90:10 oleate:DOPA vesicle upon addition of unlabeled oleate vesicles. Time in seconds; scale bar, 5  $\mu\text{m}$ .

### Mechanism of competitive growth

Monomer desorption is the rate limiting step in the exchange of fatty acids between vesicles (12). We therefore hypothesized that phospholipids drive competitive growth by reducing the efflux of fatty acids leaving the membrane while keeping the influx of fatty acids unchanged. In principle, two effects could decrease the flux of fatty acids desorbing from a membrane: first, a decreased

fatty acid off-rate in the presence of phospholipids, and second, a decrease in the net efflux from the membrane due to the reduced fraction of the membrane surface area occupied by fatty acids.

To ask whether phospholipids decrease fatty acid off-rates, we measured oleate desorption rates from mixed bilayer membranes using a stopped-flow fluorescence assay (13). We measured fatty acid desorption rates by monitoring the drop in fluorescence over time of a pH-sensitive dye encapsulated within phospholipid reporter vesicles. The decrease in fluorescence is caused by the adsorption of fatty acids into the reporter vesicle membrane, followed by flip-flop across the bilayer in a protonated form, and subsequent proton release on the interior face of the reporter vesicle (Fig. S3). We found that oleate desorption was progressively slowed by increasing DOPA content in the donor vesicles, so that desorption from a pure fatty acid bilayer was 3-fold faster than desorption from an almost pure phospholipid bilayer (Fig. 3A). This latter rate is consistent with previously measured (13) oleate desorption rates from phospholipid bilayers. Assuming that adsorption is unaffected, reducing the off-rate of fatty acids would then drive both growth of the phospholipid-containing vesicles and shrinkage of the pure fatty acid vesicles (supporting online text). The effect of phospholipid on the oleate desorption rate is sufficient to explain the magnitude of growth that we observed in competition experiments: 10 mol % DOPA inhibited oleate desorption by 22%, corresponding to an expected surface area change of 14% at equilibrium (experimental: 16%) in 1:1 competition experiments (e.g. Fig. 1A). The free energy values for oleate dissociation derived from these rates were linearly dependent on phospholipid content (Fig. S4), indicating that a non-cooperative phospholipid-fatty acid interaction was responsible for the observed effects.

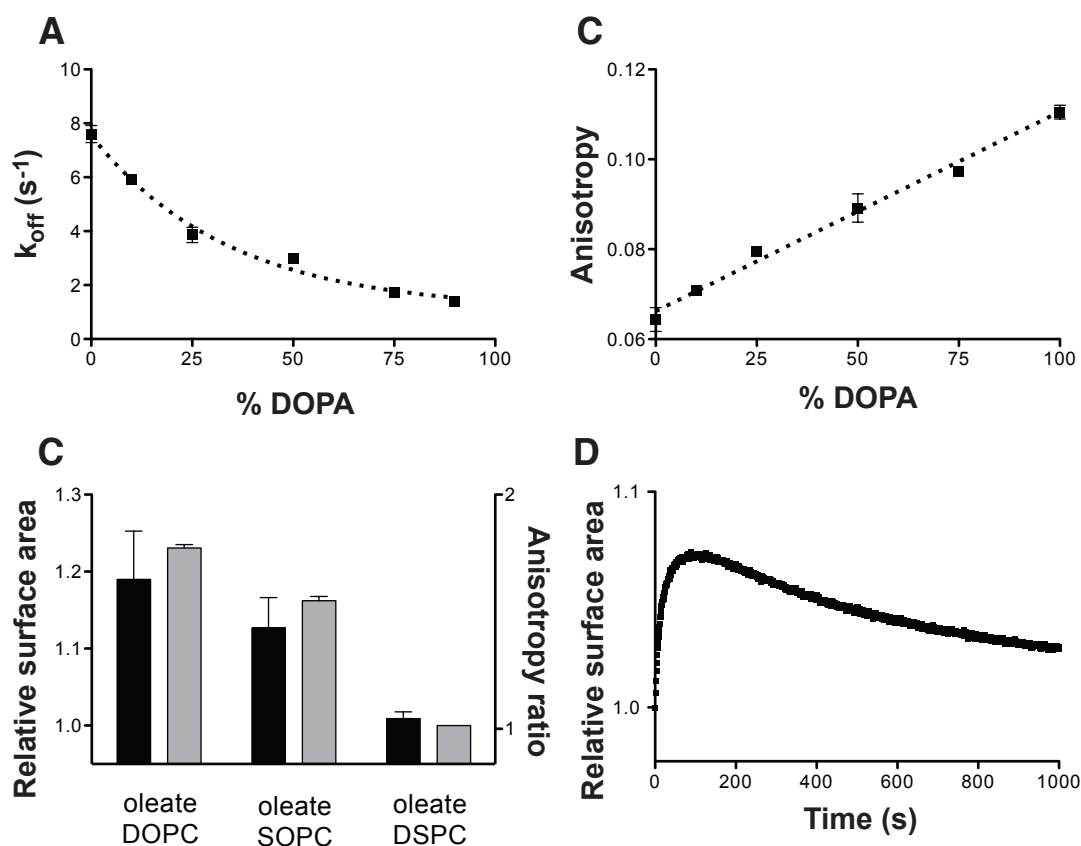


**Fig. 3.** Mechanisms of phospholipid-driven growth. (A) The desorption rate of oleate in mixed oleate/DOPA vesicles as a function of DOPA content. Increasing phospholipid content slows oleate desorption, leading to growth of phospholipid-enriched vesicles. (B) The steady-state anisotropy of DPH in oleate/DOPA vesicles as a function of DOPA content. Bilayer packing order increases linearly with increasing fraction of the diacyl lipid. Dashed line indicates linear regression fit,  $R^2 = 0.98$ . (C) The extent of growth of FRET labeled 90:10 oleate:DSPC vesicles when mixed 1:1 with the given 90:10 vesicle composition (black bars, left axis) correlates with the ratio of the membrane fluidity between oleate/DSPC bilayers and those of the given composition as measured by DPH anisotropy (grey bars, right axis). DOPC, di-oleoyl-phosphocholine (C18:1); SOPC, 1-stearoyl-2-oleoyl-phosphocholine (C18:0/C18:1). (D) Growth of FRET-labeled 90:10 oleate:NA vesicles when mixed 1:1 with unlabeled oleate vesicles. Growth proceeds in the first 60 seconds, followed by a slow relaxation due to the equilibration of the slowly exchanging NA fraction. Error bars indicate S.E.M. (N = 3).

To characterize the structural basis for the phospholipid-driven decrease in desorption rate we measured the effectiveness of a variety of phospholipids. The oleate desorption rate was mildly dependent on phospholipid head group structure (Fig. S5A), consistent with the potential of the head group to hydrogen bond with fatty acids in the bilayer (14, 15). We observed a stronger effect by varying the acyl chain composition of the phospholipid; saturated acyl chains inhibited desorption more efficiently than phospholipids with unsaturated or branched chains (Fig. S5B). Saturated acyl chains, lacking cis double bonds, permit increased inter-acyl chain van der Waals interactions and thus form more ordered membranes (16). This led us to hypothesize that diacyl lipids slow fatty acid desorption by increasing the acyl chain order in the bilayer. Since more closely packed acyl chains are expected to have a higher affinity for each other, an increase in bilayer order would slow monomer desorption, as has been observed for the desorption of cholesterol (17) and phospholipids (18). To test this hypothesis, we measured the steady state fluorescence anisotropy of the fluorophore 1,6-diphenyl-1,3,5-hexatriene (DPH), a reporter of the microviscosity of the bilayer interior (19). As expected, oleate membranes exhibited significantly lower anisotropy than DOPA membranes, indicating that monoacyl membranes are less ordered and more fluid than their corresponding diacyl membranes (Fig. 3B). The anisotropy of mixed membranes was linearly dependent on the diacyl lipid content, an observation consistent with the desorption rates in mixed membranes. The anisotropy of mixed membranes containing acyl chain analogues (Fig. S6) also correlated with the rate of oleate desorption in these mixtures (Fig. S5B). To confirm that lower fluidity can independently drive growth we measured the change in surface area of oleate vesicles containing 10 mol % of di-stearoyl-phosphocholine (DSPC), a saturated chain phospholipid, after mixing with oleate vesicles

containing equal amounts of unsaturated PCs (Fig. 3C, black bars). The DSPC-containing vesicles grew at the expense of vesicles containing unsaturated PCs, with the magnitude of growth in agreement with the ratio of their fluidity measurements via DPH anisotropy (Fig. 3C, gray bars). Since both saturated and unsaturated PCs are essentially insoluble in water, the growth of the membranes containing DSPC cannot be due to a dilution effect, but must instead reflect the increased order that the phospholipids introduce to the fatty acid bilayer.

In addition to the desorption effect described above, competition could also be driven by the entropically favored dilution of the insoluble phospholipid fraction in the fatty acid membrane. Mechanistically, this mode of growth occurs because only the fraction of the vesicle surface area composed of fatty acids can contribute to monomer efflux, while the entire surface area permits fatty acid influx, leading to a net influx (growth) in the presence of pure fatty acid vesicles. To test this mechanism independently of off-rate effects, we screened for lipids with low solubility that do not alter the fluidity of oleate membranes. Nervonic acid (NA), a 24 carbon unsaturated fatty acid, is stable in oleate vesicles as a minor fraction without affecting bilayer fluidity (Fig. S7) but has a longer residence time than oleate due to its longer chain length. When oleate vesicles containing 10 mol % NA were mixed with pure oleate vesicle, we observed an initial period of growth, as in the case of the phospholipid-containing vesicles. However, this growth phase was followed by a slow loss of the added surface area as the NA equilibrated between the two vesicle populations. Since the off-rate of a lipid from a bilayer is dependent on the number of carbon atoms in its acyl chain(s), a very long chain monoacyl lipid that remains in the bilayer indefinitely would be sufficient to drive growth. However, there is no prebiotic route to such

species, while diacyl lipid synthesis is a simple chemical means of producing insoluble lipids via the linkage of two, short acyl chains (20, 21).

We have identified two distinct mechanisms by which phospholipids can drive competitive growth at the expense of pure fatty acid vesicles. Because both the rate of fatty acid desorption (Fig. 3A) and the surface fraction of insoluble phospholipid scale throughout the binary mixture range (0-100 mol %), competition for fatty acids and related molecules should be driven by any difference in phospholipid content between vesicles. Consistent with this prediction, we observed growth of oleate vesicles containing 75 mol % DOPA upon mixing with vesicles containing 25 mol % DOPA (Fig. S8). Early cells that were capable of synthesizing more phospholipid could therefore have grown at the expense of other cells that synthesized less phospholipid. This would have led to an evolutionary arms race (22) driving increasing diacyl lipid content in early cell membranes.

### **Effect of increasing phospholipid content on membrane permeability**

What would have been the consequences of such an inexorable transition from monoacyl to diacyl lipid membranes? If high membrane permeability was necessary for early heterotrophic cells to take in chemical building blocks from the environment, changes in lipid composition that affect membrane permeability would have imposed new selective pressures. Previous work (3) has shown that the permeability of membranes composed of short-chain (C10-14) fatty acids is significantly higher than that of long-chain (C16-C18) phospholipids. However, it is unclear if this effect is because of an intrinsic physical difference between single-chain and diacyl lipid bilayers or because of the reduced bilayer thickness of short chain lipids (23).



Here we considered the dependence of phospholipid content on solute permeation in a homogeneous C10 membrane system, as acyl chains of this length are accessible by prebiotic chemistry (10). The permeation of the sugar ribose to decanoic acid-based membranes (4:1:1 decanoic acid: decanol: glycerol monodecanoate, DA:DOH:GMD) was strongly inhibited by increasing proportions of di-decanoyl-phosphatidic acid (DDPA) as measured by a real time vesicle swelling assay (24) (Fig. 4A). Similarly, the permeation of 5'-imidazole-activated dAMP (ImpdA), a model prebiotic building block for template copying (25), was 6-fold slower in DDPA membranes compared to monoacyl membranes (Fig. 4B). The increased permeability of single-chain membranes is explained by their intrinsically higher fluidity (lower order) compared to diacyl lipid membranes (Fig. 3B), as permeability is correlated with bilayer fluidity (26). Because this increased order also inhibits fatty acid desorption, enhanced competition proficiency is intrinsically coupled to a reduction in membrane permeability.

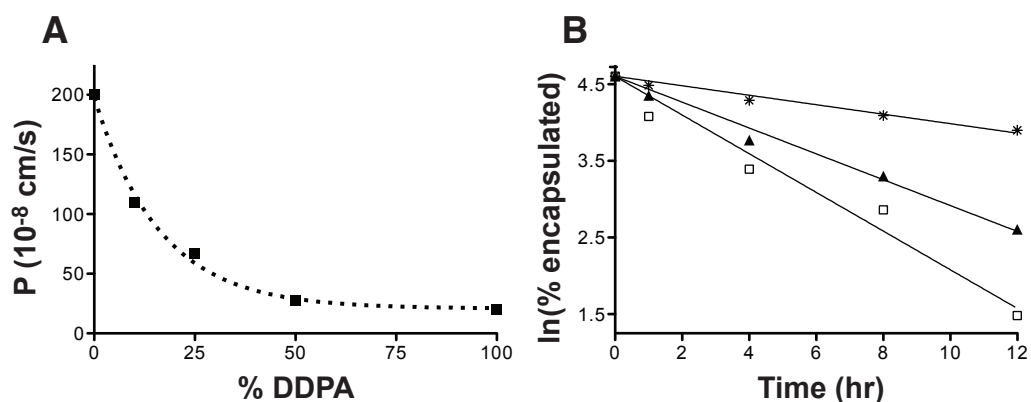


**Fig. 4.** Phospholipids inhibit solute permeation through fatty acid-based membranes. (A) Permeability of C10 membranes (4:1:1 DA:DOH:GMD) to ribose as a function of DDPA content as measured by a stopped-flow relaxation assay. (B) Leakage of encapsulated ImpdA from C10 vesicles as measured by scintillation counting of dialysis buffer aliquots. Membrane compositions: (□) 4:1:1 DA:DOH:GMD, (▲) 4:1:1 DA:DOH:GMD with 25 mol % DDPA, and (\*) DDPA.

## Discussion

The experiments presented here demonstrate that the synthesis of diacyl phospholipids would have been highly beneficial for early protocells featuring membranes composed of fatty acids and their derivatives. The chemical pathway from fatty acids to the simplest phospholipid, phosphatidic acid, occurs via successive acyl- and phospho-transfer reactions. While the intermediates in this pathway, glycerol monoesters and lysophospholipids, stabilize fatty acid bilayers to divalent cations (15) and varying pH (27), they exchange rapidly between bilayers (28) and thus would not stay localized to a single cell. Thus, there is no selective advantage for a genomically encoded catalyst that would enable internal synthesis of these intermediates, even

though an environmental source of such lipids would be beneficial. In contrast, diacyl lipids, such as phospholipids, are firmly anchored to the membrane ( $t_{1/2} \sim$  hours to days (28, 29)) due to their decreased solubility. Therefore, the synthesis of phosphatidic acid by the acylation of a lysophospholipid with an activated fatty acid is the first step in this pathway for which a genomically encoded catalyst would confer a selective advantage. An acyltransferase ribozyme that catalyzes this reaction, analogous to the protein acyltransferases ubiquitous in phospholipid synthesis, would therefore be sufficient to drive protocell growth and could have been selected for during early cellular evolution. Once such acyltransferases had evolved, there would have been a selective advantage for the synthesis of phospholipid precursors, as they would remain associated with their host cell via incorporation into diacyl lipids.

We have argued that phospholipid-driven competition could have led early cells into an evolutionary arms race leading to steadily increasing diacyl lipid content in their membranes. We have also shown that such a transition in membrane composition would have come at the expense of membrane permeability. Cells adopting increasingly phospholipid membranes would have therefore been effectively sealing themselves off from previously available nutrients in their environment. What selective pressures would such a predicament impose on early, heterotrophic cells? One possibility is that membrane transporters, a hallmark of modern cells, would have emerged as a means for overcoming low membrane permeability. While protein channels and pumps are complex molecular assemblies, early transporters could have formed from short peptides (30) or nucleic acid assemblies (31, 32), perhaps in complexes with cationic lipids. Additionally, cells could have evolved the ability to synthesize their own building blocks from simpler, more permeable substrates (metabolism) (Fig. 5). Early catalysts, such as the phospho-

and acyltransferases proposed here for phospholipid synthesis, could have been adapted for metabolic tasks such as sugar catabolism and peptide synthesis (33), respectively. The emergence of phospholipid membranes would also have allowed early cells to utilize ion gradients (30), which rapidly decay in fatty acid membranes (34), and to explore new environmental niches characterized by lower monoacyl lipid concentrations. Hence, early changes in cell membrane composition and permeability, driven by the simple physical phenomena demonstrated here, could have been an important driver of the evolution of metabolism and membrane transport machinery.

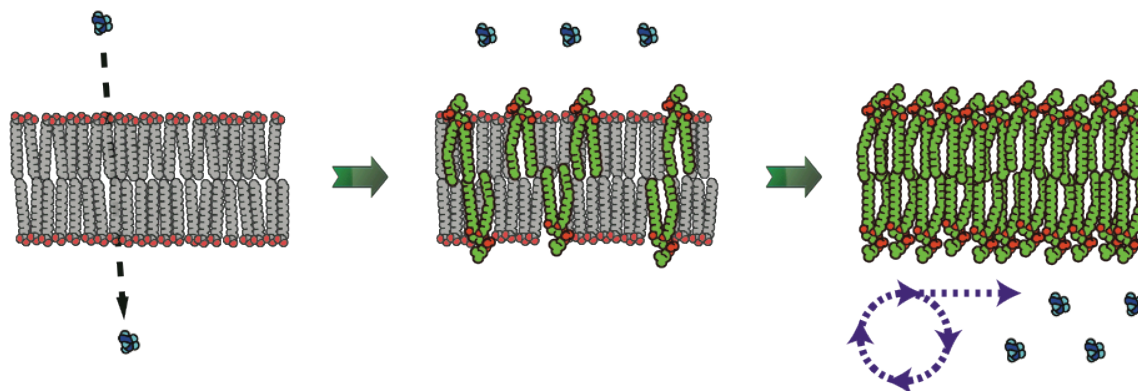


**Fig. 5.** Schematic for membrane-driven cellular evolution. The gradual transition from highly permeable primitive membranes (left) to phospholipid membranes (right) is driven by the selective growth advantage provided by increasing phospholipid content in the membrane. In turn, this imposes a selective pressure for the emergence of internalized metabolism to counter the reduced permeability of diacyl lipid membranes.

## Methods

**Materials.** Phospholipids and diacyl glycerol were obtained from Avanti Polar Lipids. Single chain lipids (fatty acids, fatty alcohols, and glycerol monoesters) were obtained from Nu-chek

Prep. Rhodamine DHPE (Rhodamine B 1,2-dihexadecanoyl-*sn*-glycero-3-phosphoethanolamine) and NBD-PE (*N*-(7-nitrobenz-2-oxa-1,3-diazol-4-yl)-1,2-dihexadecanoyl-*sn*-glycero-3-phosphoethanolamine) were obtained from Invitrogen. <sup>3</sup>H-ImpdA was prepared by activation of 2,8-<sup>3</sup>H dAMP (Moravek Biochemicals) with carbonyldiimidazole (CDI) (35). Briefly, dAMP was desalted on a spin-column (Dowex, Dow Chemicals), dried, and reacted with 5 equivalents of CDI in 75:25 DMSO:DMF containing 3 equivalents of triethylamine. The imidazolide was purified by reverse-phase HPLC on a C18 column (Alltech) equilibrated with 20 mM triethylammonium bicarbonate pH 7.8, 2% acetonitrile and eluted with a 0-7% gradient of acetonitrile. All other reagents were obtained from Sigma-Aldrich.

**Vesicle preparation.** Phospholipid vesicles were prepared by thin film hydration from chloroform stock solutions. Fatty acid and mixed vesicles were prepared by dispersing the neat oil in buffer. For mixed vesicles, the phospholipid stock solution was first added to the oil and solvent evaporated. All vesicle solutions were incubated for > 12 hours under gentle agitation. Unilamellar vesicles were prepared by extrusion 11 times through 100 nm pore-size polycarbonate membranes in an Avanti mini-extruder. All extruded vesicles were used between 4 and 24 hours after extrusion. Solutes to be encapsulated were included in the hydration/dispersion buffer, and extrusion was preceded by 5-10 cycles of freeze-thaw. Unencapsulated solutes were removed by gel filtration (Sephacrose-4B) or dialysis. For microscopy experiments, large, monodisperse vesicles were prepared by extrusion through 5  $\mu$ m pore-size membranes followed by repeated dialysis against 3  $\mu$ m pore-size membranes as previously described (4). Alternatively, for experiments using DDPA or high DOPA content, dialysis was substituted with repeated pipetting against 3  $\mu$ m pore-size membranes, which act as

large-pore sieves. For single-chain lipid mixtures, all gel filtration and dialysis buffers contained the appropriate lipid mixture at concentrations above the critical aggregation concentration; 100  $\mu$ M for oleate mixtures and 30 mM for decanoic acid mixtures. Unless otherwise noted, vesicles were prepared in 0.2 M Na<sup>+</sup>-bicine pH 8.5.

**Microscopy.** Vesicles to be used for imaging were prepared with 2 mM encapsulated HPTS, unless otherwise noted. For competition experiments, labeled vesicles were quickly mixed with extruded, unlabeled vesicles and pipetted into a disposable hemocytometer (Incyto) or home-made flow cell for imaging. For vesicle division, shear force was applied either by blowing compressed air onto a drop of vesicle-containing solution or by gently pressing on the top of the imaging chamber. Images were taken on an inverted epifluorescence microscope (Nikon TE2000S) with extra long working distance objective lenses. The illumination source was a metal halide lamp equipped with appropriate optical filters for fluorescence imaging and neutral density filters to minimise photobleaching. Images were recorded on a CCD camera (Hamamatsu) and processed using Phylum software. Experiments were performed at 23° C.

**Competition measurements.** The surface area of 100 nm vesicles was monitored by FRET as previously described (2, 7). Labeled vesicles were prepared with a 1:1 ratio of Rhodamine-DHPE and NDB-PE at 0.2 mol % (for oleate vesicles) or 0.4 mol % (for oleate/DOPA vesicles). For kinetic experiments, the ratio of acceptor to donor emission was recorded on a stopped-flow spectrofluorimeter (Applied Photophysics SX.18MV-R). For steady-state measurements, the FRET signal was calculated as the ratio of donor emission before and after the addition of 1% Triton X-100, measured on an in-line fluorimeter (Varian). Measurements were converted to

relative surface area using standard curves of FRET signal vs. dye concentration. Total lipid concentrations were kept below 3 mM to avoid scattering artifacts. All experiments were performed in 0.2 M Na<sup>+</sup>-bicine at pH 8.5, 1 mM EDTA at 23° C.

**Desorption measurements.** Fatty acid desorption rates were measured as previously described (13). Unless otherwise noted, vesicles were prepared with 0.25 mM (final concentration) of the fatty acid and were mixed with reporter vesicles (1 mM 1-palmitoyl-2-oleoyl-phosphocholine) encapsulating 0.5 mM HPTS (8-hydroxypyrene-1,3,6-trisulfonic acid) in a stopped-flow spectrometer. The decline in the pH-sensitive HPTS emission at 510 nm ( $\lambda_{\text{ex}}$  460 nm) was fitted to a first order exponential decay. Traces were taken as the average from 5 independent runs. All experiments were performed in 0.2 M Na<sup>+</sup>-bicine pH 8.5, 1 mM EDTA at 23° C.

**Anisotropy measurements.** DPH was added to 100 nm vesicles as a 1% v/v concentrated ethanol stock, followed by a > 1 hr incubation. Steady-state anisotropy measurements were taken as described (19) on a Cary Eclipse (Varian) spectrophotometer with a manual polarizer accessory. Anisotropy was calculated as a unit-less ratio defined as  $R = \frac{I_{\parallel} - I_{\perp}}{I_{\parallel} + 2I_{\perp}}$ , where  $I$  is the emission intensity at 430 nm ( $\lambda_{\text{ex}}$  360 nm) parallel ( $I_{\parallel}$ ) or perpendicular ( $I_{\perp}$ ) to the direction of polarization of the excitation source. Measurements were taken at 23° C.

**Permeability measurements.** Ribose permeability was measured by the shrink-swell assay (24). Vesicles containing 10 mM encapsulated calcein were mixed with buffer containing 0.7 M ribose in a stopped-flow spectrofluorimeter. Fluorescence intensity ( $\lambda_{\text{em}}$  540-560 nm,  $\lambda_{\text{ex}}$  470 nm) initially declined rapidly due to water efflux, then slowly relaxed back to the initial value due to

ribose (and water) influx. Solute permeability was calculated from the relaxation rate. Bicine permeability was measured similarly on an in-line fluorimeter. Nucleotide permeability was measured by monitoring leakage of 2,8-<sup>3</sup>H-ImpdA from 100 nm vesicles. After encapsulation, vesicles were loaded into 65 kDa MWCO dialysis tubes and leakage monitored by scintillation counting of dialysis buffer aliquots (36). Except for bicine permeability, all experiments were performed in 0.1 M POPSO (piperazine-1,4-bis(2-hydroxy-propanesulfonic acid)) pH 8.2 at 30° C. This buffer was chosen for its low permeability, even at elevated temperatures, which allowed us to specifically monitor ribose influx during shrink-swell experiments.

**Acknowledgments.** We thank R. Bruckner, A. Ricardo, S. Tobé, T. Zhu and C. Blain for discussions and S. Tobé for assistance with nucleotide permeability experiments. This work was supported by a grant from the NASA Exobiology Program (EXB02-0031-0018) to J.W.S. J.W.S. is an Investigator of the Howard Hughes Medical Institute.

Author contributions: I.B. and J.W.S. designed the research; I.B. performed research; I.B. and J.W.S analyzed the data and wrote the paper.

The authors declare no conflict of interest.

## References

1. Hargreaves WR, Deamer DW (1978) Liposomes from ionic, single-chain amphiphiles. *Biochemistry* 17:3759-3768.



2. Hanczyz MM, Fujikawa SM, Szostak JW (2003) Experimental models of primitive cellular compartmentalization: encapsulation, growth, and division. *Science* 302:618-622.
3. Mansy SS, *et al* (2008) Template-directed synthesis of a genetic polymer in a model protocell. *Nature* 454:122-125.
4. Zhu TF, Szostak JW (2009) Coupled growth and division of model protocell membranes. *J. Am. Chem. Soc.* 131:5705-5713.
5. Haines TH (1973) Halogen- and Sulfur-Containing Lipids of *Ochromonas*. *Ann. Rev. of Microbio.* 27:403-412.
6. Van Mooy BAS, *et al* (2009) Phytoplankton in the ocean use non-phosphorus lipids in response to phosphorus scarcity. *Nature* 258:69-72.
7. Chen IA, Roberts RW, Szostak JW (2004) The emergence of competition between model protocells. *Science* 305:1474-1476.
8. Cheng Z, Luisi PL (2003) Coexistence and mutual competition of vesicles with different size distributions. *J. Phys. Chem. B* 107:10940-10945.
9. Fujikawa SM, Chen IA, Szostak JW (2005) Shrink-wrap vesicles. *Langmuir* 21:12124-12129.
10. Rushdi AI, Simoneit BRT (2001) Lipid formation by aqueous Fischer-Tropsch-type synthesis over a temperature range of 100 to 400° C. *Orig. Life Evol. Biosph.* 31:103-118.
11. Deamer DW, Pashley RM (1989) Amphiphilic components of the Murchison carbonaceous chondrite: Surface properties and membrane formation. *Origins Life Evol. Biosph.* 19:21-38.
12. Simard JR, Pillai BK, Hamilton JA (2008) Fatty acid flip-flop in model membrane is faster than desorption into the aqueous phase. *Biochemistry* 47:9081-9089.
13. Zhang G, Kamp F, Hamilton JA (1996) Dissociation of long and very long chain fatty acids from phospholipid bilayers. *Biochemistry* 35:16055-16060.
14. Cistola DP, Hamilton JA, Jackson D, Small DM (1988) Ionization and phase behavior of fatty acids in water: application of the Gibbs phase rule. *Biochemistry* 27:1881-1888.
15. Monnard PA, Apel CL, Kanavarioti A, Deamer DW (2002) Influence of ionic inorganic solutes on self-assembly and polymerization processes related to early forms of life: implications for a prebiotic aqueous medium. *Astrobiology* 2:139-152.
16. Seelig A, Seelig J (1977) Effect of a single cis double bond on the structure of a phospholipid bilayer. *Biochemistry* 16:45-50.

17. Lund-Katz S, Laboda HM, McLean LR, Phillips MC (1988) Influence of molecular packing and phospholipid type on rates of cholesterol exchange. *Biochemistry* 27:3416-3423.
18. Silvius JR, Leventis R (1993) Spontaneous interbilayer transfer of phospholipids: dependence on acyl chain composition. *Biochemistry* 32:13318-13326.
19. Van Blitterswijk WJ, van Hoeven RP, van der Meer BW (1981) Lipid structural order parameters (reciprocal of fluidity) in biomembranes derived from steady-state fluorescence polarization measurements. *Bio. Et Biophys. Acta* 644:323-332.
20. Hargreaves WR, Mulvihill SJ, Deamer DW (1977) Synthesis of phospholipids and membranes in prebiotic conditions. *Nature* 266:78-80.
21. Epps DE, Sherwood E, Eichberg J, Oro J (1978) Cyanamide mediated synthesis under plausible primitive earth conditions: The Synthesis of Phosphatidic Acids. *J. Mol. Evol.* 11:279-292.
22. Dawkins R, Krebs JR (1979) Arms races between and within species. *Proc. R. Soc. Lond. B.* 205:489-511.
23. Paula S, Volkov AG, Van Hoek AN, Haines TH, Deamer DW (1996) Permeation of protons, potassium ions, and small polar molecules through phospholipid bilayers as a function of membrane thickness. *Biophys. J.* 70:339-348.
24. Sacerdote MG, Szostak JW (2005) Semipermeable lipid bilayers exhibit diastereoselectivity favoring ribose. *Proc. Natl Acad. Sci. USA* 102:6004-6008.
25. Orgel LE (2004) Prebiotic chemistry and the origin of the RNA world. *Crit. Rev. Biochem. Mol. Biol.* 39:99-123.
26. Lande MB, Donovan JM, Zeidel ML (1995) The relationship between membrane fluidity and permeabilities to water, solutes, ammonia, and protons. *J. Gen. Physiol.* 106:67-84.
27. Apel CL, Deamer DW (2005) The formation of glycerol monodecanoate by dehydration/condensation reaction: increasing the chemical complexity of amphiphiles on the early earth. *Orig. Life Evol. Biosph.* 35:323-332 (2005).
28. McLean LR, Phillips MC (1984) Kinetics of phosphatidylcholine and lysophosphatidylcholine exchange between unilamellar vesicles. *Biochemistry* 23:4624-4630.
29. Abreu MSC, Moreno MJ, Vaz WLC (2004) Kinetics and thermodynamics of association of a phospholipid derivative with lipid bilayers in liquid-disordered and liquid-ordered phases. *Biophys. J.* 87:353-365.

30. Pohorille A, Deamer D (2009) Self-assembly and function of primitive cell membranes. *Research in Microbiology* 160:449-456.
31. Kaucher MS, Harrell WA, Davis JT (2006) A unimolecular G-quadruplex that functions as a synthetic transmembrane Na<sup>+</sup> transporter. *J. Am. Chem. Soc.* 128:38-39.
32. Janas T, Janas T, Yarus M (2004) A membrane transporter for tryptophan composed of RNA. *RNA* 10:1541-1549.
33. Li N, Huang G (2005) Ribozyme-catalyzed aminoacylation from CoA thioesters. *Biochemistry* 44:4582-4590.
34. Chen IA, Szostak JW (2004) Membrane growth can generate a pH gradient in fatty acid vesicles. *Proc. Natl. Acad. Sci. USA* 101:7965-7970.
35. Hoard DE, Ott DG (1965) Conversion of mono- and oligodeoxyribonucleotides to 5'-triphosphates. *J. Am. Chem. Soc.* 87:1785-1788.
36. Chakrabarti AC, Breaker RR, Joyce GF, Deamer DW (1994) Production of RNA by a polymerase protein encapsulated within phospholipid vesicles. *J. Mol. Evol.* 39:555-559.

## Supporting Methods

### Alternate phospholipid synthesis pathways

While our experiments are based on the structure of diacyl phospholipids, archaeal dialkyl phospholipids are quite different (S1). The building blocks of archaeal phospholipid synthesis are pyrophosphate-activated isoprenoids, which are added sequentially to a glycerol phosphate backbone via ether linkages. The ubiquity of isoprenoid synthesis in biology (S3) and the suspected thermophilicity (S2) of the last common ancestor suggest a possible role for archaeal phospholipids early in cellular evolution. However, there are no obvious abiotic pathways for isoprenoid synthesis. Fischer-Tropsch reactions yield straight chain alkanes as their major product (S4), suggesting a metabolic origin (S5, S6) for isoprenoid lipid chains. Nonetheless, the physical phenomena we have described are also likely to apply to branched, dialkyl lipid systems, provided that there is a similar difference in fluidity between monoalkyl and dialkyl membranes.

### Calculation of expected growth from desorption rates

Assuming equal adsorption rates for vesicles of different compositions, the partition coefficient ( $P$ ) of fatty acid monomers between two vesicle populations (A and B) should be inversely proportional to their corresponding desorption rates:  $P = \frac{k_B^{off}}{k_A^{off}}$ . This partition coefficient equals

the ratio of the final surface areas ( $SA$ ) of A and B, so that  $P = \frac{1 + \Delta SA_A}{1 + \Delta SA_B}$ . Since the growth of

one population must equal the shrinkage of the other,  $P = \frac{1 + \Delta SA}{1 - \Delta SA}$  and  $\Delta SA = \frac{P - 1}{P + 1}$ .

### Calculation of free energy of bilayer association from measured desorption rates

The standard free energy of a lipid in a bilayer can be calculated as  $\Delta G^\circ = -RT \ln K_{eq}$ , where  $K_{eq}$  is the equilibrium partition coefficient and is equal to the ratio of on and off rates from the bilayer:  $K_{eq} = \frac{k_{on}}{k_{off}}$ . If we assume the on rate is constant with varying phospholipid content,  $K_{eq}$

can be expressed in terms of the off rate and equilibrium constants of pure oleic acid:

$K_{eq} = K_{OA} \left( \frac{k_{off}^{OA}}{k_{off}} \right)$ . The partition coefficient of oleate can be calculated from its measured critical

aggregation concentration (cac) ( $\sim 50 \mu\text{M}$ , measured by light scattering of serial dilutions (S7))

via its standard free energy (S8):  $\Delta G^\circ_{OA} = RT \ln cac$ , where cac is expressed in mole fraction of

solvent; therefore,  $K_{OA} = \frac{1}{cac_{OA}}$  and  $K_{eq} = \frac{k_{off}^{OA}}{k_{off} * cac_{OA}}$ . The standard free energy for oleate given

a measured desorption rate is thus:  $\Delta G^\circ = -RT \ln \left( \frac{1}{cac_{OA}} \frac{k_{off}^{OA}}{k_{off}} \right)$ , where  $k_{off}$  is the measured

desorption rate for oleate in the mixture.

## Supporting Figures

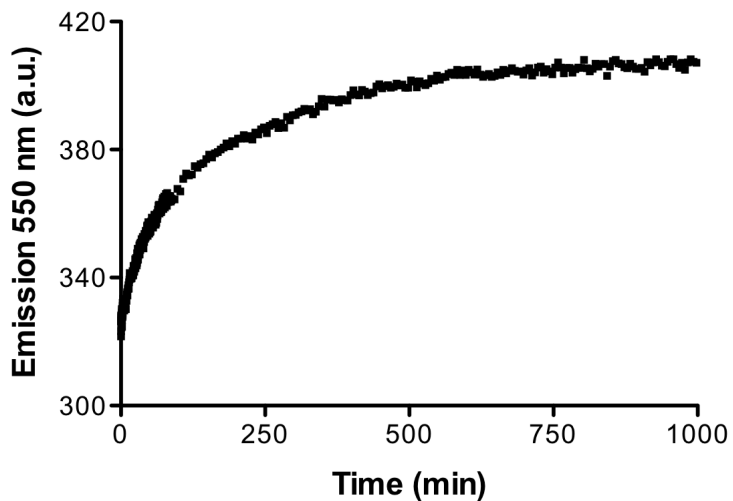


**Fig. S1.** Bicine permeability is slow in fatty acid-based membranes. 100 nm 2:1:1 DA:DOH:GMD vesicles were prepared in 0.2 M bicine and diluted in a hypertonic solution of 0.5 M bicine. The recovery of encapsulated calcein fluorescence at 550 nm ( $\lambda_{\text{ex}}$  470 nm) within several hours reflects the permeation of bicine across the membrane, returning the vesicles to their initial spherical shape. Other, longer chain-length membrane compositions used in this study exhibited significantly slower bicine permeation.

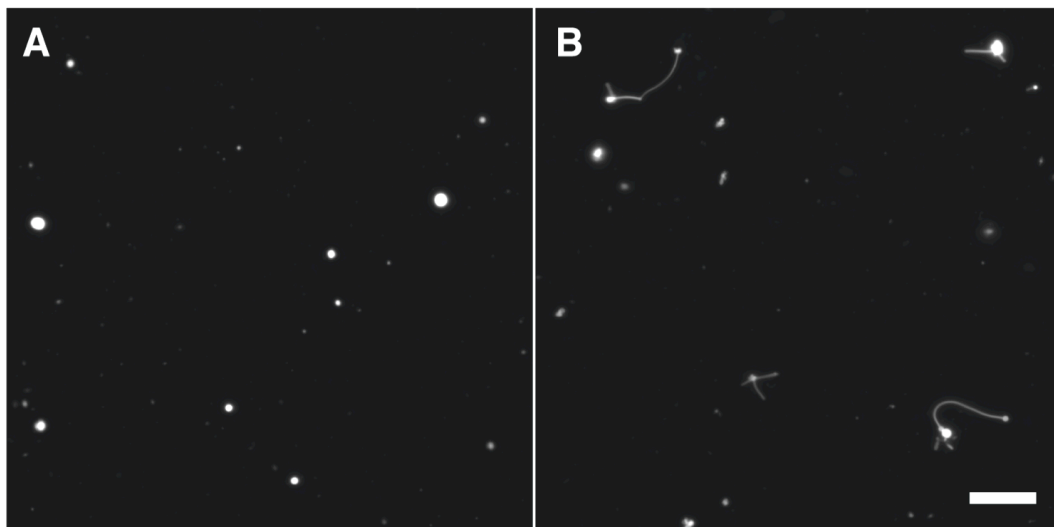


**Fig. S2.** Phospholipid-driven growth of vesicles composed of short, saturated chain lipids. (A) Large, multilamellar 6:3:1 DA:DOH:DDPA vesicles, labeled with 0.1 mol % Rhodamine DHPE, are initially spherical. (B) Upon mixing with a 5-fold excess of unlabeled 2:1 DA:DOH vesicles, the labeled vesicles grow via the protrusion of thin, tubular tails. Higher amounts of unlabeled vesicles or continual phospholipid synthesis would result in the further vesicle elongation into tubular filaments. Image taken 5 minutes after mixing. Scale bar, 30  $\mu\text{m}$ .

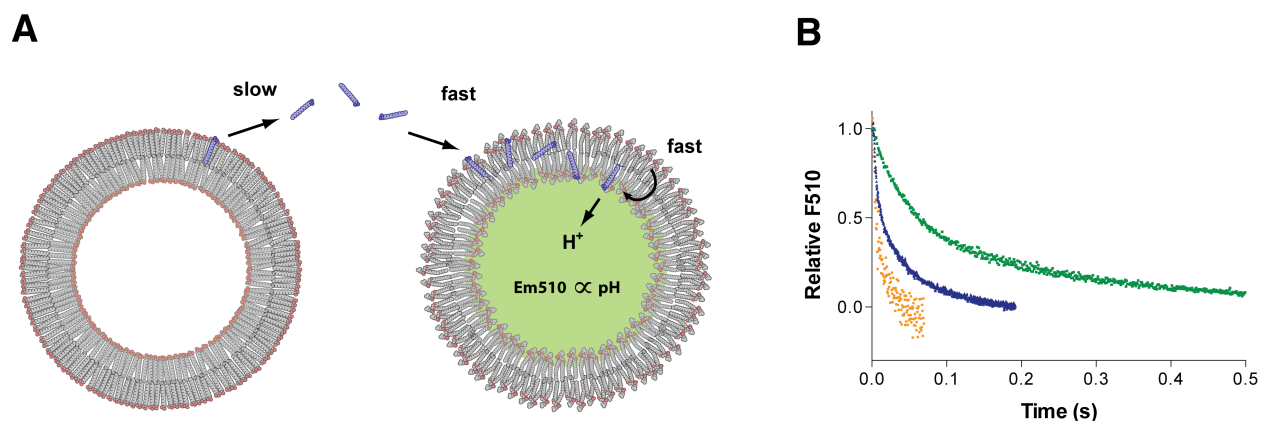


**Fig. S3.** Measuring fatty acid desorption rates. (A) Schematic for the assay used to measure fatty acid desorption rates. Fatty acid containing vesicles (left) are mixed with phospholipid reporter vesicles (right). The slow desorption of monomers from fatty acid vesicles is followed by their rapid adsorption into phospholipid reporter vesicles, flip-flop, ionization and therefore acidification of the interior of the reporter vesicle. The resulting decrease in fluorescence of the encapsulated pH-sensitive dye HPTS is used to monitor monomer desorption from fatty acid vesicles. (B) Chain length dependence of the rate of monomer desorption from fatty acid membranes. Desorption rate depends on the chain length of the fatty acid: green, oleic acid (C18:1),  $k \sim 7.3 \text{ s}^{-1}$ ; blue, palmitoleic acid (C16:1),  $k \sim 34 \text{ s}^{-1}$ ; orange, myristoleic acid (C14:1),  $k \sim 102 \text{ s}^{-1}$ . Palmitoleic acid and myristoleic acid were mixed at concentrations of 1 mM and 5 mM, respectively, because of the high critical aggregation concentration of these lipids.



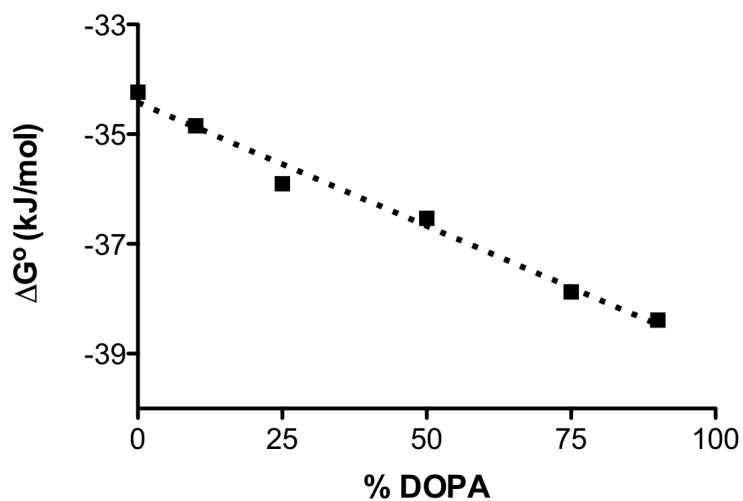


**Fig. S4.** Free energy of oleate association with mixed oleate/DOPA membranes. Standard free energy of bilayer association relative to solution was calculated (supporting online text) using measured oleate desorption rates (Fig. 3A) and the critical aggregation concentration of oleic acid ( $\sim 50 \mu\text{M}$ ). Dashed line indicates linear regression,  $R^2 = 0.99$ .

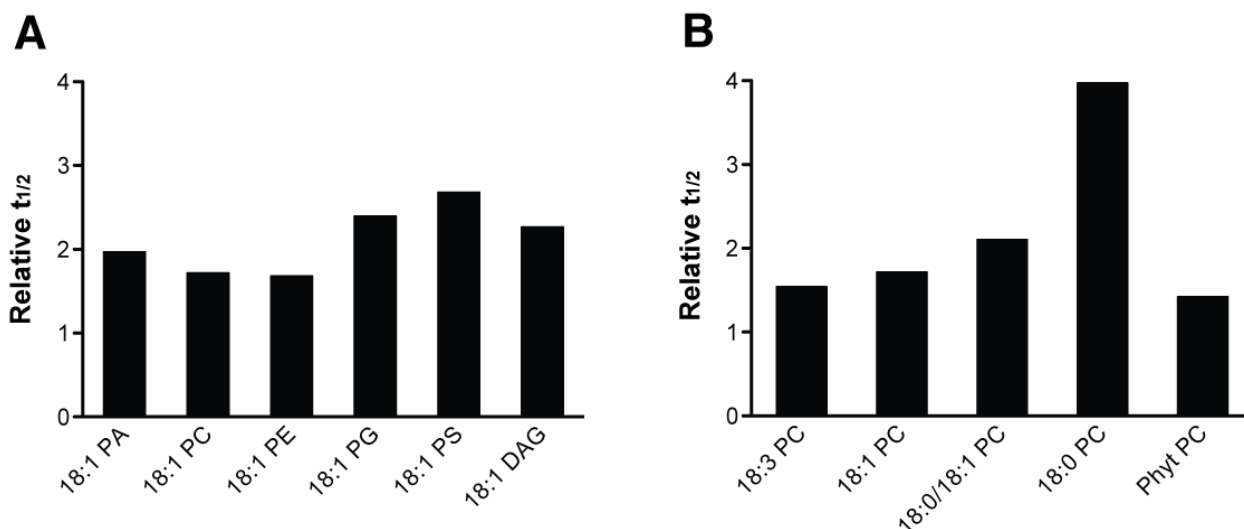


**Fig. S5.** The effect of phospholipid head group and acyl chains on oleate desorption rates in mixed membranes. (A) The half times of oleate desorption from vesicles containing 25 mol % of the given C18:1 phospholipid, normalized to that in pure oleate membranes. The inhibition of desorption correlates with the hydrogen bonding potential of the phospholipid head groups (e.g. hydroxyls for glycerol, carboxyl, and amine for serine). PA, phosphatidic acid; PC, phosphatidylcholine; PE, phosphatidylethanolamine; PG, phosphatidylglycerol; PS, phosphatidylserine; DAG, diacyl glycerol. (B) The half times of oleate desorption from vesicles containing 25 mol % of the given phosphatidylcholine acyl analogue, normalized to that in pure oleate membranes. Saturated phospholipids, which form ordered bilayers, more strongly inhibited desorption than unsaturated phospholipids, which form disordered bilayers, or branched phospholipids (Phyt PC), which interfere with straight-chain acyl packing. Phyt, di-O-phytanyl, a C20 isoprenoid chain lipid.

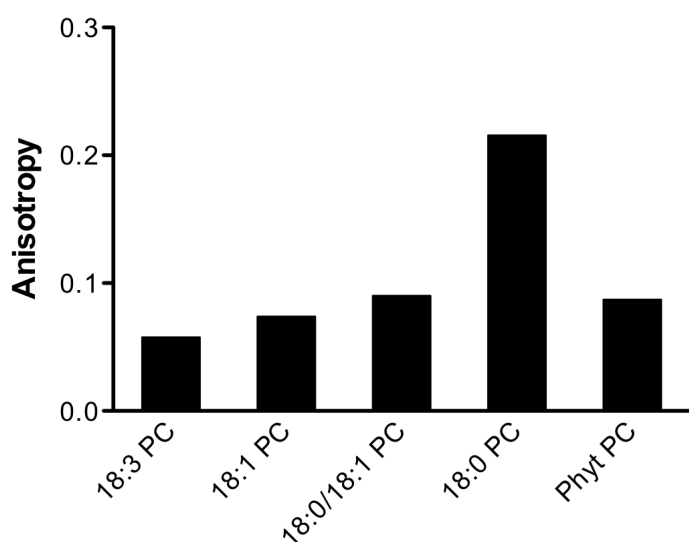


**Fig. S6.** Anisotropy of mixed membranes containing phospholipids with different acyl chains. The steady-state anisotropy of DPH (0.2 mol %) was measured in oleate vesicles containing 25 mol % of the indicated phosphatidylcholine. Increased anisotropy indicates a more ordered, less fluid bilayer interior, and correlates well with the measured oleate desorption rates from these membranes (Fig. 3A). Phyt, di-O-phytanyl-phosphatidylcholine, a C20 isoprenoid chain lipid.

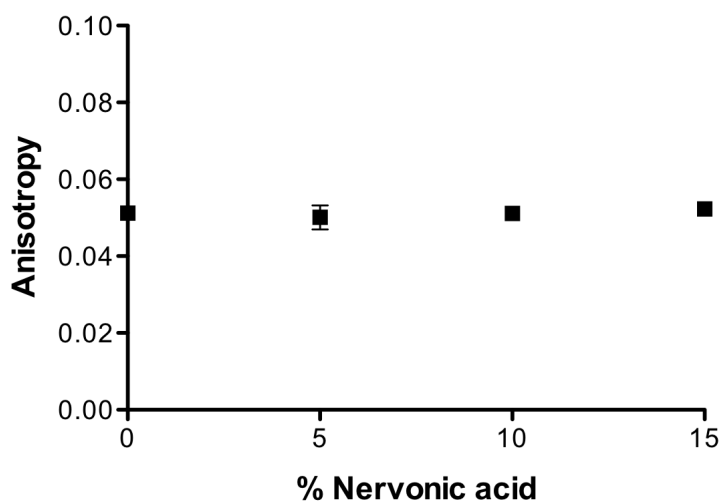


**Fig. S7.** Steady-state DPH anisotropy of oleate (C18:1) membranes containing nervonic acid (NA) (C24:1). Membrane fluidity is unaffected at 5-15 mol % NA, despite the longer chain length and lower solubility of NA. Error bars indicate S.E.M. (N=3).

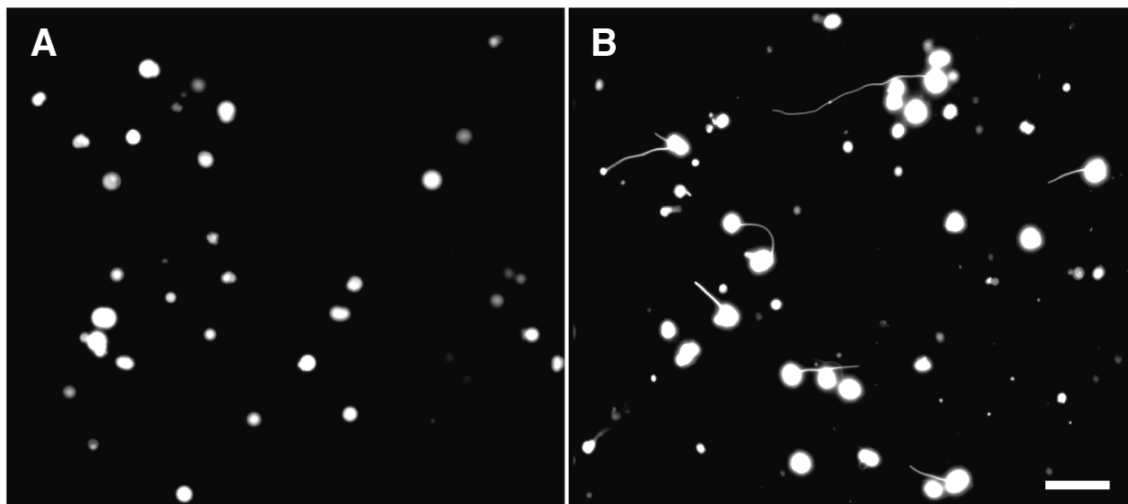


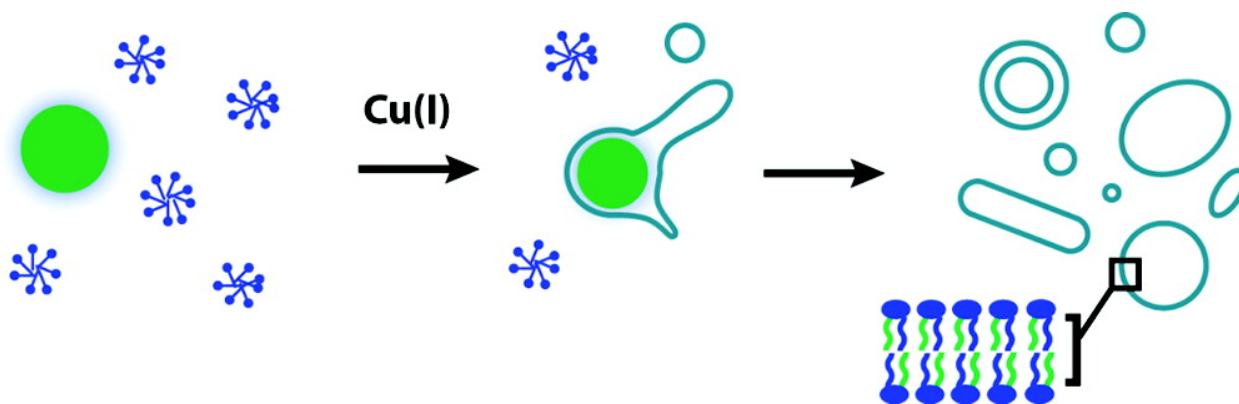
**Fig. S8.** Growth of phospholipid-enriched mixed vesicles. (A) Large, multilamellar 25:75 oleate:DOPA vesicles, labeled with 0.1 mol % Rhodamine DHPE, are initially spherical. (B) Upon mixing a 10-fold excess of unlabeled 75:25 oleate:DOPA vesicles, the phospholipid-enriched vesicles grow via the protrusion of thin, tubular tails. Growth is limited by the dilution of the initial phospholipid content, but would be continuous in the case of phospholipid-synthesizing protocells. Image taken 5 minutes after mixing. Scale bar, 30  $\mu\text{m}$ .

## References

- S1. Koga Y, Morii H (2007) Biosynthesis of ether-type polar lipids in archaea and evolutionary considerations. *Micro. Mol. Bio. Rev.* 71:97-120.
- S2. Benner SA, Ellington AD, Tauer A (1989) Modern metabolism as a palimpsest of the RNA world. *Proc. Natl. Acad. Sci. USA* 86:7054-7058.
- S3. Ciccarelli FD, *et al.* (2006) Toward automatic reconstruction of a highly resolved tree of life. *Science* 311:1283-1287.
- S4. Mccollom TM, Ritter G, Simoneit RT (1999) Lipid synthesis under hydrothermal conditions by Fischer-Tropsch-type reactions. *Orig. Life Evol. Biosph.* 29:153-166.
- S5. Scott IA (1997) How were porphyrins and lipids synthesized in the RNA world? *Tet. Lett.* 38:4961-4964.
- S6. Ryu Y, Scott IA (2003) Efficient one-step synthesis of isoprenoid conjugates of nucleoside 5'-diphosphates. *Org. Lett.* 5:4713-4715.
- S7. Chen IA, Szostak JW (2004) Membrane growth can generate a pH gradient in fatty acid vesicles. *Proc. Natl Acad. Sci. USA* 101:7965-7970.
- S8. Israelachvili JN, Mitchell DJ, Ninham BW (1976) Theory of self-assembly of hydrocarbon amphiphiles into micells and bilayers. *J. Chem. Soc., Faraday Trans. 2* 72:1525-1568.

## Membrane assembly driven by a biomimetic coupling reaction

Itay Budin and Neal Devaraj



*Note: a version of the following was published in the Journal of the American Chemical Society.*

**Abstract:** One of the major goals of synthetic biology is the development of non-natural cellular systems. In this work, we describe a catalytic biomimetic coupling reaction capable of driving the de novo self-assembly of phospholipid membranes. Our system features a coppercatalyzed azide–alkyne cycloaddition that results in the formation of a triazole-containing phospholipid analogue. Concomitant assembly of membranes occurs spontaneously, not requiring preexisting membranes to house catalysts or precursors. The substitution of efficient synthetic reactions for key biochemical processes may offer a general route toward synthetic biological systems.

### Introduction

Designing synthetic substitutes for evolved biochemical processes is a strategy toward developing artificial cellular systems (1). Here we describe a catalytic biomimetic coupling reaction capable of driving the de novo self-assembly of phospholipid membranes, organizing

structures ubiquitous to all cells. In bacteria and eukaryotes, membrane assembly results from acyl transfer reactions that couple single-chain amphiphiles into membrane-forming phospholipids (Figure 1A). These reactions are catalyzed *in vivo* by enzyme complexes, which, along with the machinery involved in fatty acid activation, ensure the specificity of phospholipid synthesis (2). We envisioned mimicking this biological system by using a synthetic catalytic coupling reaction. We chose the copper-catalyzed azide–alkyne cycloaddition because of its robustness in water, the solvent necessary for bilayer assembly through the hydrophobic effect (3). The reaction also benefits from high selectivity and a nearly nonexistent background in the absence of catalyst, features that are reminiscent of biochemical processes.

## Results

To mimic phospholipid synthesis, we designed substrates to replace the native precursors of the common phospholipid 1-palmitoyl-2-oleoyl-*sn*-glycero-3-phosphocholine (POPC): an oleyl azide in lieu of oleic acid and an alkyne analogue of the lysophospholipid 1-palmitoyl-*sn*-glycero-3-phosphocholine (Figure 1B). The cycloaddition product resembles POPC, with the exception of a triazole linker. As expected, neither the azide nor the alkyne formed membranes in aqueous solution. However, the purified triazole product, when hydrated, readily formed large membrane vesicles that were visible under fluorescence microscopy (Figure 2A). Steady-state anisotropy measurements with the membrane fluidity probe diphenylhexatriene (DPH) (4) indicated the triazole-containing membranes to be well-ordered with fluidity (Figure 2B) and chain melting temperatures [Figure S1 in the Supporting Information (SI)] comparable to those of native POPC membranes.

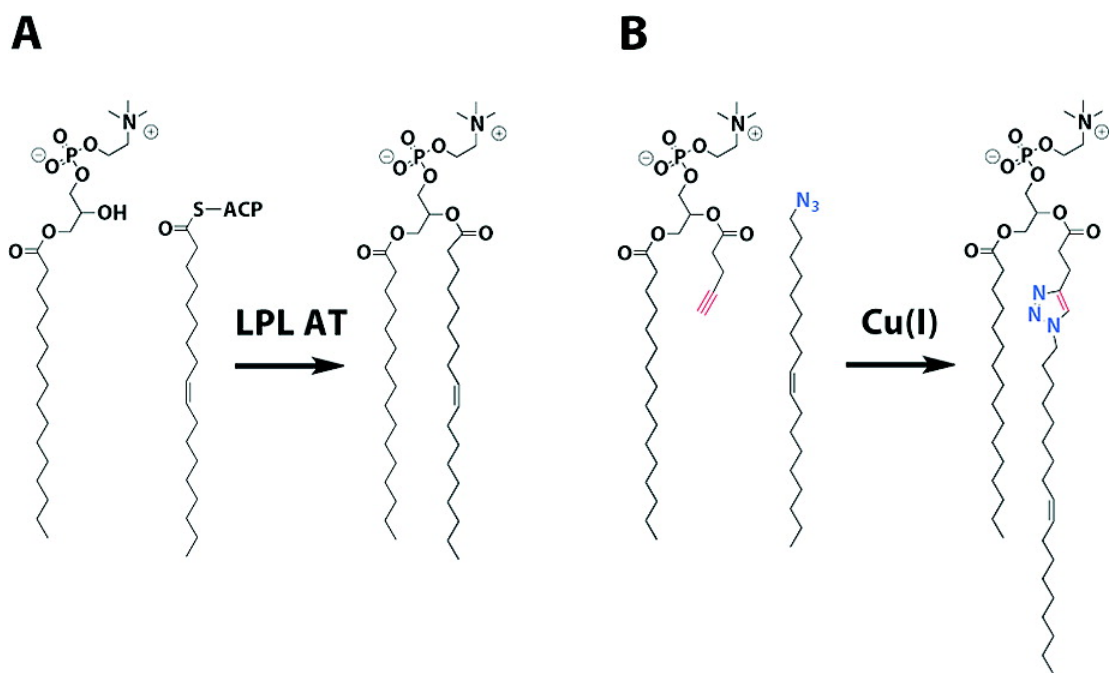


**Figure 1.** Biomimetic synthesis of phospholipid membranes. (A) Native phospholipid synthesis relies on acyl transfer reactions between lysophospholipids and thioester-activated fatty acids that are catalyzed by membrane-associated enzymes. (B) This process is mimicked by copper-catalyzed cycloaddition of an alkyne lysolipid substitute and oleyl azide. The resulting triazole is an analogue of the natural phospholipid POPC. Abbreviations: LPL AT, lysophospholipid acyltransferase; ACP, acyl carrier protein.



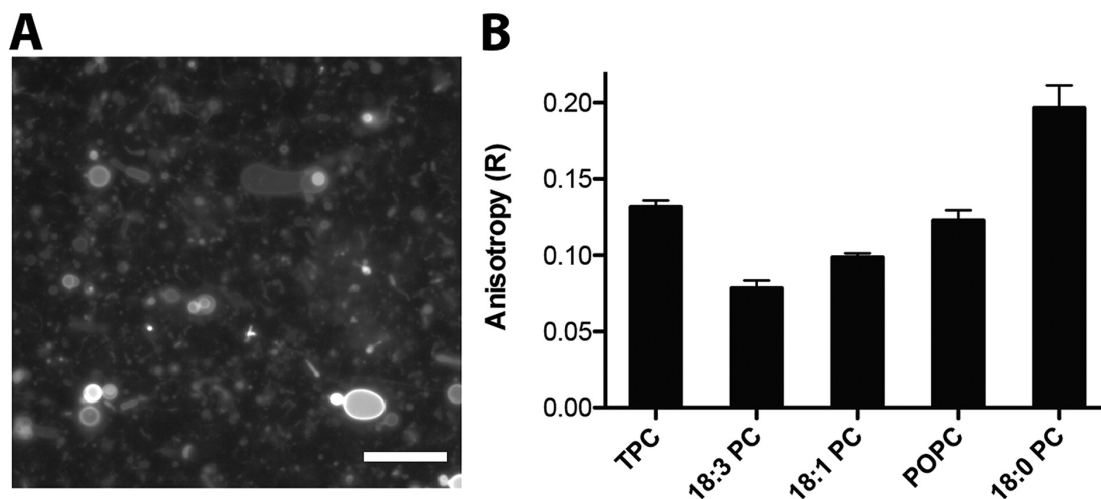


**Figure 2.** Characterization of triazole phospholipid vesicles. (A) Fluorescence microscopy of membrane-containing vesicles formed by hydrating a thin film of triazole phospholipid (TPC). Membranes were stained using 10  $\mu$ M Rh-DHPE dye. The scale bar denotes 15  $\mu$ m. (B) Steady-state anisotropy of DPH in membranes formed from TPC compared with those from native phosphocholines with the indicated acyl chains. The unitless anisotropy ratio (R) is a measure of the acyl packing of the bilayer, with higher values indicating a more ordered membrane (see Methods in the SI).

Because of the triazole coupling reaction's aqueous compatibility, we hypothesized that we could use it to drive spontaneous membrane assembly in situ. Membrane assembly has been observed as a result of pH changes (5), solvent exchanges (6), and application of electric fields (7). Here it is driven by covalent bond formation, which both lowers the solubility of the substrates (Figure S2) and switches the aggregate state from micelles to bilayers. After adding catalytic copper to an aqueous emulsion of oleyl azide oil and the alkyne surfactant, we observed the formation of large vesicle structures, both spherical and tubular, on the periphery of the oleyl azide oil droplets (Figure 3). After 24 h, with no further agitation of the solution, the oil droplets were largely consumed, and fields of large ( $> \mu$ m) heterogeneous vesicles remained. Time-lapse

fluorescence microscopy revealed that the vesicles budded off from the oil droplet as tubules (Movie S1) in a manner similar to thin-film hydration. Though our initial experiments were carried out in either distilled water or HEPES buffer, we observed similar results in numerous physiologically relevant buffers, a solvent tolerance that is typical of such triazole coupling reactions. To confirm that the resulting structures were membrane compartments, we included a polar fluorophore, 8-hydroxypyrene-1,3,6-trisulfonic acid (HPTS), in the reaction buffer and observed encapsulation with fluorescence microscopy (Figure S3A) and size-exclusion chromatography (Figure S3B). Neither membrane self-assembly nor encapsulation were observed in the absence of the copper catalyst.

To determine whether membrane formation coincided with the synthesis of the triazole phospholipid, we analyzed the reaction over time using combined liquid chromatography, mass spectrometry, and evaporative light scattering detection (ELSD) measurements (Figure 4). The addition of the copper catalyst led to triazole formation within minutes, and this process progressed to near completion over a period of 20 h, correlating well with vesicle formation.

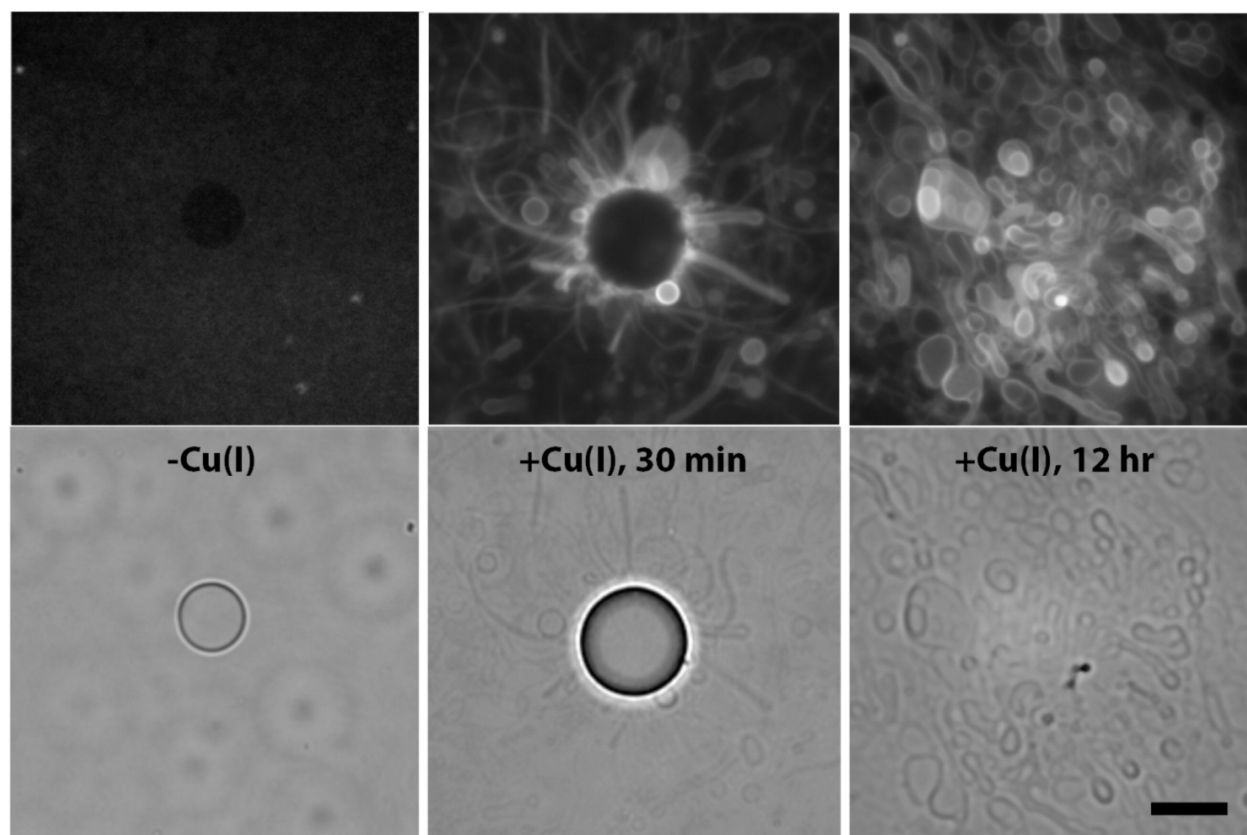


**Figure 3.** Spontaneous vesicle assembly driven by triazole phospholipid synthesis. An aqueous emulsion of oleyl azide (5 mM) and alkyne lysolipid (5 mM) imaged without catalyst (left), 30 min after addition of catalyst (0.25 mM) (middle), and 12 h after addition of catalyst (right). The upper panels are fluorescence micrographs of vesicles obtained using a membrane dye (Rh-DHPE, 2  $\mu$ M); the bottom panels show the corresponding phase-contrast images. Before addition of the catalyst, only the emulsion oil droplets were visible, and phospholipid membranes were not present. Shortly after addition of copper, several vesicle and tubular structures were observed, a large number of which appeared at the periphery of the azide oil droplets. After 12 h, the oil droplets were consumed and replaced with large fields of vesicles. The scale bar denotes 10  $\mu$ m.

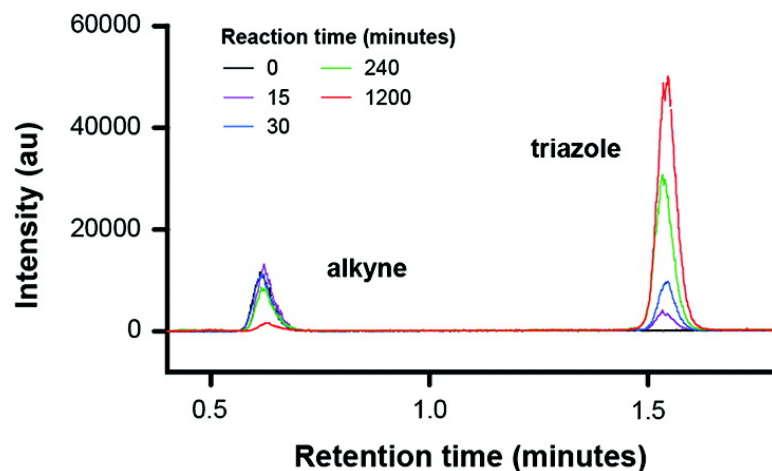


**Figure 4.** HPLC/ELSD traces monitoring the progress of the cycloaddition reaction. The time scale of alkyne lysolipid consumption and triazole phospholipid formation was consistent with that observed for vesicle self-assembly. The alkyne lysolipid and triazole phospholipid retention times were verified by mass spectrometry and the use of known standards.

Our observations of vesicle assembly support a model in which the reaction takes place primarily at the interface of the insoluble oleyl azide emulsion droplets and the isotropic alkyne lysolipid analogues, which exist as micelles in the aqueous solvent (Figure 5). However, we cannot rule out the possibility that the reaction also occurs in mixed azide/alkyne micelles. Controlling the interface between the azide and alkyne, either through use of carrier agents or fluidics, may prove to be a route to controlling membrane assembly in this system.

Despite its simplicity, our unnatural approach to phospholipid synthesis shares key characteristics with evolved enzymatic reactions, including 1. hydrolytically stable substrates, which are unreactive in the absence of catalyst; 2. robust and highly specific product formation in the presence of a multiturnover catalyst; and 3. compatibility with aqueous solvents, which leads to organization of the product into bilayer membranes. These features are in contrast to traditional synthetic reactions, which utilize highly reactive substrates and are challenged by

reaction specificity and solvent compatibility, with water often acting as a competing nucleophile. Notably, our method provides an advantage over enzymatic systems: natural lipid acyltransferases are primarily membrane-bound, requiring pre-existing membranes to function, and are thus unlikely to be useful for de novo membrane assembly. Furthermore, previous attempts to reconstitute acyltransferase enzyme activity using activated natural precursors have met with poor results, likely because of the complexity of the enzymes and inherent difficulties of reconstitution in synthetic systems (8). In contrast, our approach uses highly selective azide/alkyne reactive groups and an exceedingly simple hydrated copper ion as the catalyst. The minimal nature of our approach will likely lend itself to further elaboration, as we envision incorporating this system into a fully synthetic cell. We are also exploring practical applications of triazole membrane assembly, for instance in packaging and delivering therapeutics, improving transfection efficiencies, reconstituting functional membrane proteins, and performing confined biochemical reactions.

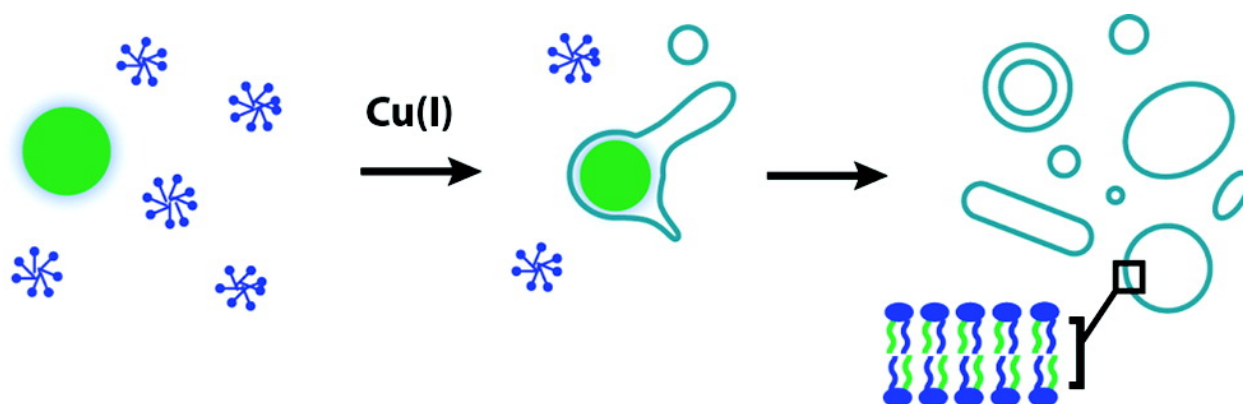


**Figure 5.** Model of membrane assembly. Reactive azide oil droplets (green) interact with alkyne lipid micelles in solution (blue) to form an emulsion. After addition of the copper catalyst, the cycloaddition begins to take place, primarily at the interface between the oil droplets and the aqueous solution. The reaction results in the formation of phospholipid membranes at the substrate interface. Over time, the oil droplets are consumed and replaced with spherical and tubular vesicles composed of phospholipid membranes.

## References

1. Szostak, J. W.; Bartel, D. P.; Luisi, P. L. *Nature* 2001, 409, 387– 390.
2. Shindou, H.; Shimizu, T. *J. Biol. Chem.* 2009, 284, 1– 5.
3. Rostovtsev, V. V.; Green, L. G.; Fokin, V. V.; Sharpless, K. B. *Angew. Chem., Int. Ed.* 2002, 41, 2596– 2599.
4. Van Blitterswijk, W. J.; Van Hoeven, R. P.; Van der Meer, B. W. *Biochim. Biophys. Acta* 1981, 644, 323– 332.
5. Walde, P.; Wick, R.; Frest, M.; Mangone, A.; Luisi, P. L. *J. Am. Chem. Soc.* 1994, 116, 11649– 11654.
6. Pautot, S.; Frisken, B. J.; Cheng, J. X.; Xie, X. S.; Weitz, D. A. *Langmuir* 2003, 19, 10281– 10287.
7. Angelova, M. I.; Dimitrov, D. S. *Faraday Discuss. Chem. Soc.* 1986, 81, 303– 311.
8. Schmidl, P. K.; Schurtenberger, P.; Luisi, P. L. *J. Am. Chem. Soc.* 1991, 113, 8127–8130.

## Supporting Information

A QuickTime movie showing membrane tubule formation from an azide droplet during the reaction is available at the following:

[http://pubs.acs.org/doi/suppl/10.1021/ja2076873/suppl\\_file/ja2076873\\_si\\_002.qt](http://pubs.acs.org/doi/suppl/10.1021/ja2076873/suppl_file/ja2076873_si_002.qt)

## Methods

### Synthesis of alkyne lysolipid (3-(palmitoyloxy)-2-(pent-4-ynoyloxy)propyl (2-(trimethylammonio)ethyl) phosphate)

70 mg of 1-palmitoyl-2-hydroxy-*sn*-glycero-3-phosphocholine (Avanti) was dissolved in 10 mL methylene chloride. To this was added 70 mg of 4-pentynoic acid, 140 mg of 1,3-diisopropylcarbodiimide and 25 mg of 4-(dimethylamino)pyridine. The solution was stirred overnight, filtered and the solvent removed by rotary evaporation. The product was isolated by column chromatography (CHCl<sub>3</sub>/MeOH/H<sub>2</sub>O) as a white solid. Yield 70%. <sup>1</sup>HNMR (400 MHz CDCl<sub>3</sub>): δ 5.25-5.2 (m, 1H), 4.4-4.3 (m, 3H), 4.2-4.1 (m, 2H), 4.05-4.0 (m, 1H) 3.95-3.9 (m, 2H), 3.4 (s, 9H), 2.6-2.4 (m, 4H), 2.35-2.25 (t, 2H), 2.05 (t, 1H), 1.6-1.5 (m, 2H), 1.35-1.2 (m, 24H), 0.9-0.8 (t, 3H). [M+H]<sup>+</sup> calculated mass 576.36 found mass 576.48

### Synthesis of oleyl azide ((*Z*)-1-azidooctadec-9-ene)

Oleyl azide was synthesized using an adaptation of a previously reported procedure<sup>(1)</sup>. 150 mg of oleyl bromide (*Z*)-1-bromooctadec-9-ene (Sigma) was dissolved in 1 mL anhydrous dimethylformamide and reacted overnight under nitrogen at 85°C with 100 mg sodium azide.

After the reaction, 5 mL water was added and the organic phase extracted using methylene chloride. After drying with MgSO<sub>4</sub>, the solvent was removed by rotary evaporation and the product isolated by column chromatography as a pale yellow oil. Yield 80%. <sup>1</sup>HNMR (400 MHz CDCl<sub>3</sub>): δ 5.4-5.3 (m, 2H), 3.3-3.2 (t, 2H), 2.1-1.95 (m, 4H), 1.7-1.5 (m, 2H) 1.4-1.2 (m, 22H), 0.9 (t, 3H).

**Synthesis of triazole phospholipid ((Z)-3-(heptadecanoyloxy)-2-((3-(1-(octadec-9-en-1-yl)-1H-1,2,3-triazol-4-yl)propanoyl)oxy)propyl (2-(trimethylammonio)ethyl) phosphate)**

13 mg of oleyl azide and 24 mg of alkyne lipid were dissolved in 2:1 dimethylformamide:water and stirred for 48 hours in the presence of a copper wire. The solvent was evaporated and the resulting triazole isolated by column chromatography as a white powder. Yield 65%. <sup>1</sup>HNMR (400 MHz CDCl<sub>3</sub>): δ 7.5 (s, 1H), 5.4-5.3 (m, 2H) 5.25-5.2 (m, 1H), 4.5-4.25 (m, 5H), 4.2-4.1 (m, 1H), 4.05-4.0 (m, 2H) 3.9-3.8 (m, 2H), 3.4 (s, 9H), 3 (m, 2H), 2.8-2.7 (m, 2H), 2.6-1.0 (56H), 0.9-0.8 (t, 6H). [M+H]<sup>+</sup> calc mass 869.64 found mass 869.73

**Membrane Assembly**

To 100 μL of either distilled water or appropriate buffer, 0.15 mg of oleyl azide and 0.3 mg alkyne phospholipid were added followed by 0.1 mg of sodium ascorbate and 6 μg of copper sulfate. The mixture was agitated overnight. Control experiments were prepared identically with the absence of copper catalyst.

**Encapsulation Experiments**

A 1 mM solution of 8-Hydroxypyrene-1,3,6-trisulfonic acid (HPTS) was made in 10 mM



HEPES buffer. This solution was then used as the buffer for membrane assembly as described above. After overnight agitation, a vesicle sample was diluted 10 fold in buffer and observed using fluorescence microscopy (Figure S1A). Alternatively, the reaction mixture was separated via size exclusion chromatography (Sepharose 4B) and a fraction collector (Gilson). HPTS fluorescence (excitation 460 nm, emission 510 nm) was measured using a plate reader (Figure S1B, green). A control experiment lacking the copper catalyst was run similarly (Figure S1B, blue).

### **LC-MS of product formation**

Membrane assembly was performed in distilled water as described above. A 5  $\mu$ L sample was taken at various time points before and after addition of copper catalyst. This sample was diluted with 20  $\mu$ L acetonitrile and analyzed using an analytical LC/MS with an Evaporative Light Scattering Detector from Waters Co. (Milford, MA), operated by Fractionlynx 4.0 or Masslynx software with Waters Xterra columns (C8) at a flow rate of 0.3 mL/min. For all LC/MS runs, solvent A consisted of water with 0.1% formic acid and solvent B of acetonitrile with 0.1% formic acid.

### **Anisotropy Measurements**

Diphenylhexatriene (5  $\mu$ M final concentration) was added to 100 nm extruded vesicles (2 mM phospholipid) as a 1% vol/vol concentrated ethanol stock, followed by an overnight incubation. Steady-state anisotropy was measured on a Cary Eclipse (Varian) spectrophotometer with a manual polarizer accessory and peltier temperature controller. Anisotropy (R) was calculated as a unit-less ratio (2) calculated as  $(I_{\parallel} - I_{\perp}) / (I_{\parallel} + 2 * I_{\perp})$ , where  $I_{\parallel}$  and  $I_{\perp}$  are the emission

intensities at 430 nm (excitation 360 nm) parallel and perpendicular, respectively, to the direction of polarization of the excitation source. Measurements were taken at 23 °C, unless otherwise noted

## Supporting Figures

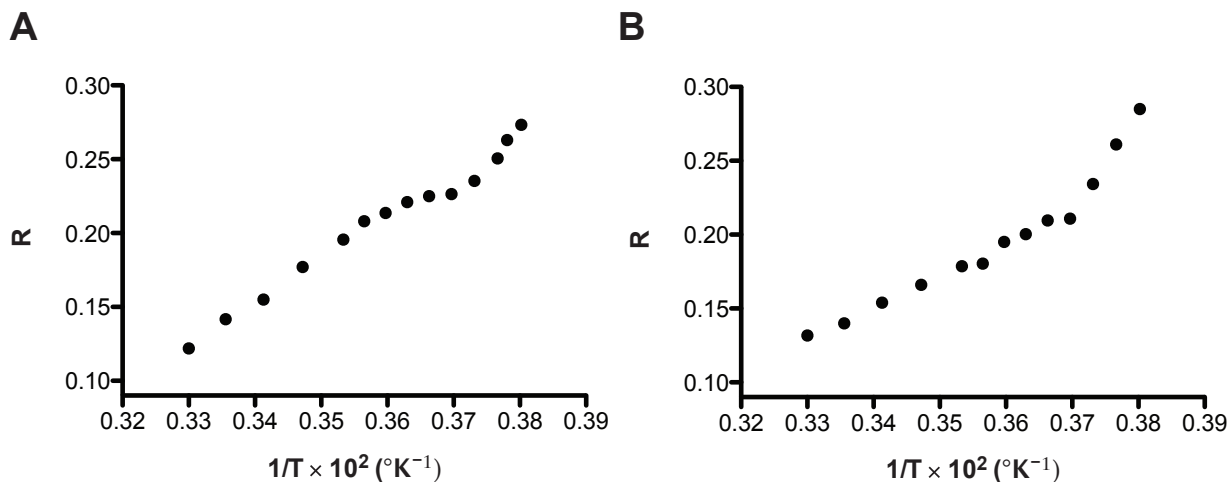


**Figure S1.** Chain melting temperature of triazole phospholipid. DPH anisotropy as a function of temperature shows discontinuities signifying acyl melting temperatures for (A) Triazole phospholipid and (B) POPC membranes.

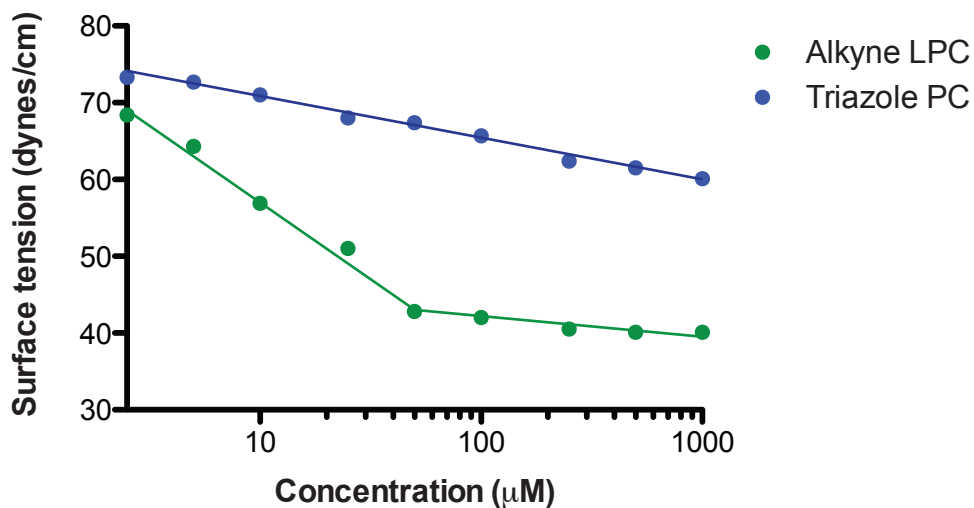


**Figure S2.** Aqueous solubilities of alkyne substrate and triazole product. Surface tension of lipid solutions was measured by the Nüoy method; plateau in LPC surface tension indicates micellar aggregation.

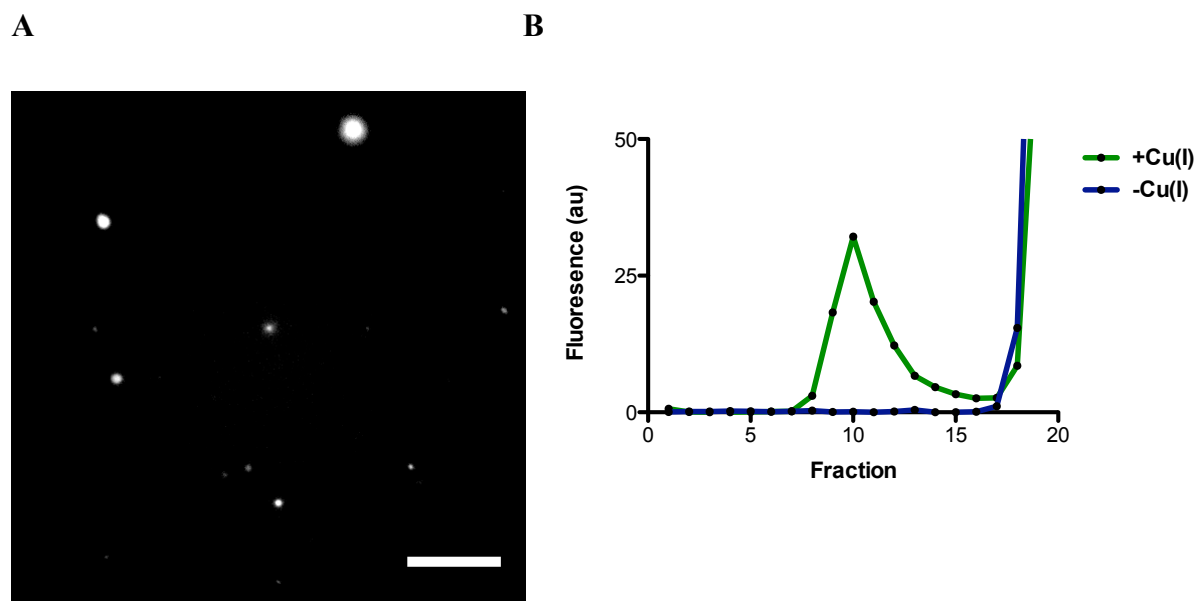


**Figure S3.** Encapsulation of polar fluorescent dye (8-Hydroxypyrene-1,3,6-trisulfonic acid) in triazole phospholipid membrane vesicles. A) Fluorescence microscopy of dye encapsulated in vesicles formed during copper-catalyzed reaction. Scale bar denotes 15  $\mu$ . B) Fluorescence intensity versus collected fraction after size-exclusion chromatography of vesicle formed in the presence (green line) and absence (blue line) of the copper catalyst. All experiments were performed in 10 mM HEPES buffer.

## References

1. J. P. Collman, N. K. Devaraj, C. E. Chidsey, *Langmuir* **20**, 1051 (2004).
2. W. J. Van Blitterswijk, R. P. Van Hoeven, B. W. Van der Meer, *Biochim Biophys Acta* **644**, 323 (1981).